

SEISMIC GEOMORPHOLOGY OF CONTINENTAL MARGIN EVOLUTION IN THE
LATE CRETACEOUS TO NEogene OF THE BROWSE BASIN,
NORTHWEST AUSTRALIA

by

ZhuangxiaoXue Liu

A thesis submitted to the Faculty and the Board of Trustees of the Colorado School of Mines in partial fulfillment of the requirements for the degree of Master of Science (Geology).

Golden, Colorado

Date _____

Signed: _____

Zhuangxiao Xu Liu

Signed: _____

Dr. Lesli J. Wood

Thesis Advisor

Golden, Colorado

Date _____

Signed: _____

Dr. M. Stephen Enders

Department Head

Department of Geology and Geological Engineering

ABSTRACT

Recent discoveries in the Browse Basin of Northwest offshore Australia provide the impetus for data abundance and interest in evaluating the temporal and spatial changes in slope morphology and sediment movements from shelf to slope.

Northwest Shelf of Australia was characterized by clastic margin development from the end of Cretaceous to the end of the Oligocene. The margin became carbonate dominated post Oligocene. These differences are reflected in the margins clinoform morphology. Carbonate margin of Browse Basin has a concave profile, reflecting its development as a rimmed margin basin. Water depths of siliciclastic margin from topset to toesets are more than 1000m, the clinoform show a low progradation rate and a relatively high aggradation rate. Very little difference in toeset slopes can be seen in between these two margin types, the majority of difference is seen in the clinoform foresets. Slope gullies are well developed during Eocene-Oligocene time, showing both spatial and temporal variability across the margin. The gullies migrate northwestward through time, and slightly lateral migrate from southwest to northeast along seismic cross-section line profiles. They reveal a bi-model distribution of gully morphometrics, gullies on western and central slope exhibit larger dimensions than the gullies on the eastern slope. This change in gully morphologies corresponds to the thickness change of Tpal-Tolig interval which two thick located in the western and central region of the study area, respectively. The spatial and temporal variability of the gully morphologies indicates two sources located to the southern region of the study area.

TABLE OF CONTENTS

ABSTRACT	iii
LIST OF FIGURES.....	vi
LIST OF TABLES.....	xii
ACKNOWLEDGEMENTS	xiii
CHAPTER 1 INTRODUCTION AND BACKGROUND.....	1
1.1 Defining the Continental Margin	1
1.2 Geological Background	3
1.3 Terminology	8
1.3.1 Slope Gullies.....	8
1.3.2 Channels.....	8
1.3.3 Submarine Canyon vs. Incised Valley.....	9
1.3.4 Rimmed and Non-rimmed Carbonate Margins.....	9
1.3.5 Strata Terminations: Onlap, Downlap and Truncation.....	10
1.4 Dataset.....	11
1.5 Methodology.....	13
CHAPTER 2 STRATIGRAPHIC EVOLUTION OF THE BROWSE BASIN.....	16
2.1 Introduction	16
2.2 Key Surface Interpretation.....	19
2.3 Sequence Set Interpretation.....	28
2.3.1 Sequence Set 1: Campanian to Paleocene	30

2.3.2 Sequence Set 2: Eocene to Early Oligocene	32
2.3.3 Sequence Set 3: Late Oligocene to Early Miocene	35
CHAPTER 3 CONTRASTING CLASTIC TO CARBONATE CLINOFORMING MARGINS OF THE BROWSE BASIN	38
3.1 Introduction and Methodology	38
3.2 Classification of Siliciclastic Margin	39
3.3 Classification of Carbonate Margin	44
CHAPTER 4 MORPHOLOGY OF SLOPE GULLIES	51
4.1 Morphology of Slope Gullies	51
4.2 Observations	52
4.3 Interpretation	66
CHAPTER 5 DISCUSSIONS AND CONCLUSIONS.....	70
5.1 Model for theDepositional System.....	70
5.2 Continental Slope Evolution	71
5.3 Slope Gully Complexes	73
5.4 Conclusions.....	80
REFERENCES.....	82
APPENDIX A.....	87

LIST OF FIGURES

Figure 1.1 Diagram showing the geomorphology of a generic continental margin. The exact nature of the continental slope and its mergence with the most basinal continental rise as a function of margin type (clastic vs carbonate) is a topic of this study.....	3
Figure 1.2 Map of northwest Australia, showing the Bonaparte, Browse, offshore Canning and Carnarvon basins. The Poseidon 3D seismic survey is outlined in red within the Browse Basin, and the location is also shown on Figure 1.4. Wells are shown in green, other 3D seismic data sets not used in this study are shown as green boxes. Continental Australia is shown in white.....	4
Figure 1.3 Tectonostratigraphic summary diagram. Modified after AGSO timescale (Young and Laurie, 1996); sea level curve (Haq et al., 1988; Greenlee and Lehmann, 1993); stratigraphic column (AGSO Browse Basin Project Team, 1997).....	5
Figure 1.4 Regional structural element map showing the location of the Poseidon 3D seismic survey (dashed red box). Location of Figure 1.4 is shown on Figure 1.2. Location of the 3D seismic (red outline), is shown in Figure 1.2. Kronos-1 well is shown. Modified after Brincat et al., 2003.	7
Figure 1.5 Sketches of rimmed margins and non-rimmed margins. A) Showing the reef growth on the rimmed margin. Rimmed margins are characterized by flat tops, linear trends of the shelf edge and a sharp shelf break. This type of carbonate margin has a relatively steeper gradient slope foreset compared to non-rimmed margins. B) Non-rimmed carbonate margins generally lack a protecting reef at the shelf edge to act as an energy barrier. This type of carbonate margin is easily reworked by storm and high-energy processes. The break between shelf and slope is a relatively broad area compared to the abrupt shelf edge of rimmed carbonate margins. Modified from Read, 1985.	10
Figure 1.6 Sketches of strata terminations. A) Onlap is a relationship in which initially horizontal strata terminate against an initially inclined surface, or the initially inclined strata terminate progressively updip against a surface of greater initial inclination; B) Downlap is a relationship that seismic reflections of inclined strata terminate downdip against an surface. C) Truncation is the termination below a surface, it represents the relationship that the strata is eroded by the post-depositional erosional or structural effects. Modified from Mitchum Jr, 1977.	11

Figure 1.7 Map showing location of the Kronos-1 well and seismic profiles discussed in the text. The purple line outlines the extent of the 3D. The blue circle shows the area of no data.....	13
Figure 1.8 Interval velocity tie to the well log and lithology at the Kronos-1 well. Key surfaces (see text for nomenclature) are noted in the log as listed in the well-completion report (ConocoPhillips, 2011). Location of Kronos-1 well is shown in Figure 1.7.....	15
Figure 2.1 Interpreted seismic line showing the six interpreted sequence boundaries within the study area; the Kecamp, Tbase, Tpal, Tolig, Temio and Tmmio, from the deepest to the shallowest. Three sequence sets are defined as the boundaries between them mark major process changes in the basin. Representative strata terminations (red arrows) along each mapped surface are shown on the profile. Location of seismic line is shown on Figure 1.7 (A-A'). Location of Figure 2.13 is indicated by black arrow.....	17
Figure 2.2 Seismic inline 2419 showing the correlation of inline 2419 and Kronos-1 well. Kronos-1 well is marked by red line on this figure, Location of Kronos-1 well and the seismic profile (F-F') are shown in Figure 1.7. Six key surfaces are shown on the seismic profile.....	18
Figure 2.3 Chart showing the correlation from the regional horizons mapped as part of this study and their seismic character (shown on the left).....	20
Figure 2.4 Time structure contour map for Kecamp, showing the structural high of this horizon in the southeast portion of the data area, and relief dives to the northwest. Relief on the upper continental slope is low ranging from 2600 m at the eastern shelf edge to 2800 ms before deepening dramatically to the west to nearly 3300 ms. Location of Figure 2.5 is shown on this figure (M-M').....	21
Figure 2.5 Seismic Crossline 2360 showing submarine canyon incision along the horizon Kecamp. The width of the canyon can extend to 10km. Location of seismic line is shown on Figure 2.4. The younger strata above horizon Kecamp show bidirectional onlapping against both sides of the canyon, and multiple late stage channels fill the upper part of the canyon. The average width of these channels is 600m, and the average depth of them is approximately 40ms	22
Figure 2.6 Time structure map for horizon Tbase. Tbase has a similar trend to Kecamp, it shows relatively low relief from shelf to slope compared to Temio and Tmmio. The structural high in the east-northeast.....	23
Figure 2.7 Time structure contour map for Tpal, showing a gently steep shelf and upper slope, representing a low angle continental margin.....	24

Figure 2.8 Time structure map for horizon Tolig, reflecting a moderately steep slope compared to older margins, but continuing to display a gradual transition between shelf and slope.	26
Figure 2.9 Time structure map for Temio, showing a sharp steepening of dip from the shelf to the continental slope.	27
Figure 2.10 Time stucture map for Tmmio. The shelf break, marked at the dramatic change in structural dips, continues to migrate west-northwest as the margin progrades.	28
Figure 2.11 Isochron map for sequence set 1, bounded by Tpal and Kecamp. This map shows that the southeast area of the seismic data contains the thickest strata between horizon Kecamp and horizon Tpal. The unit does show a gradual thinning to the northwest from approximately 450 ms to 50 ms. A 60 km ² (7.5 km x 8 km), 250 ms thick unit is present at the central area of the southernmost portion of the dataset, and a northwestward oriented incision is clearly present in the data.....	31
Figure 2.12 The isochron map for sequence set 2 indicates that throughout this interval, the thickest area is over the central part of the seismic data. The unit thickens from southeast to center from 300 ms to 600 ms and then thins to the northwest to approximately 100 ms , the northeast portion has a relatively thinner thickness as 400 ms compared to the center.....	33
Figure 2.13 Sweetness attribute map showing gullies along the Tpal surface. These channel incisions are prolific at the base of sequence set 2 and they frequently cut down into the Cretaceous Puffin Formation.....	36
Figure 2.14The sequence set 3 isochron map shows that interval thickens northwestward from approximately ~400 ms to ~800 ms, then thins to ~200 ms from the central region to the westernmost area. The shelf edge migrates northwestward within this sequence set.....	37
Figure 3.1 Two types of siliciclastic shelf margins, modified after Carvajal et al., 2009. A) showing clinoform growth in moderately deep water basins (<1000 m water depth), and B) showing clinoform growth in very deep water basins (>1000 m water depth).	40
Figure 3.2 Western dip-oriented (southeast-northwest) seismic profile showing the shelf-edge positions (orange dots) relative to times, as well as the profile of siliciclastic slope, sequence boundaries are shown in their defined colors. Location of the profile is shown in Figure 1.7 (A-A').	45

- Figure 3.3 Central dip-oriented (southeast-northwest) seismic profile showing the shelf-edge positions relative to times, as well as the profile of siliciclastic slope. Location of the profile is shown in Figure 1.7 (B-B') ... 46
- Figure 3.4 Eastern dip-oriented (southeast-northwest) seismic profile showing the shelf-edge positions relative to times, as well as the profile of siliciclastic slope. Location of the profile is shown in Figure 1.7 (C-C')... 47
- Figure 3.5 Classification of carbonate slopes and the corresponding mathematical expressions. A) Rimmed margins always exhibit slopes with concave profile, the descriptive expression is exponential, an example from Western Great Bahama Bank is observed (Adams and Kenter, 2014). B) Sigmoidal profile and the corresponding Gaussian expression is common of the non-rimmed margins, the example is the Great Australia Bight (James and Christopher, 1991). C) Carbonate margins that include slope shedding always show planar profile, the example of this type of carbonate margin has been found in Proterozoic carbonate platform, Namibia (Adams and Kenter, 2014)..... 48
- Figure 3.6 Seismic lines extracted from the 3D seismic data set of the Browse Basin study area and used to examine temporal and spatial changes in margin shape. Western profile 3.6A and central profile 3.6B of the study area show an exponential curvature of the carbonate margin, reflecting its development as Rimmed Margin basin. The eastern profile 3.6C has a slight concave or straight curvature, suggests it developed as a Non-rimmed Margin basin. Location of the profiles are shown in Figure 1.7 50
- Figure 4.1 Seismic cross-section line 1318 extracted from the sweetness cube showing the location of four attribute slices; A, B, C and D used to identify and measure the shape, size and orientation of slope gully channels in the lower, middle and upper portions of the Tpal-Tolig sequence set 2. Location of unconformity Tpal and Tolig is marked on the profile. Location of this seismic profile is shown in Figure 1.7 53
- Figure 4.2 Sweetness attribute map A. A) Uninterpreted attribute map A. B) Interpreted attribute map A showing the paleogeomorphology and gully development for the lowermost 1/3 of the Tpal-Tolig interval. A total of 27 slope gullies are observed on this surface. From southwest to northeast portion, each gully is numbered in order from 1 to 27. The red line (X-X') marks the location of the seismic profile in Figure 4.4. In this map, blues represent low sweetness and reds represent high sweetness..... 55
- Figure 4.3 Scatter diagram showing the dimensions of the slope gullies on attribute map A. Two groups of gullies are recognized. Gully 1-16 are relatively wider, deeper and longer in contrast to gully 17-27. The

- depth and width keeps a positive relationship as the depths increase while widths increase..... 56
- Figure 4.4 Seismic random cross-section line, location is shown in Figure 4.2 and 4.5 (X-X'). Gullies imaged in Map A are shown in orange and gullies imaged in Map B are shown in red. Individual gullies appear to stack vertically (orange) or laterally (red) in to gully complexes with thicknesses of up to 450 m (200 ms). Gully migration at Map B time is towards the northeast. 58
- Figure 4.5 Sweetness attribute map B showing the paleogeomorphology and gully development for the middle 1/3 of the Tpal-Tolig interval. A total of six slope gullies are observed on this surface. From southwest to northeast portion, each gully is numbered in order from 1 to 6. The red line (X-X') marks the location of the seismic profile in Figure 4.4. In this map, blues represent low sweetness and reds represent high sweetness. 59
- Figure 4.6 Scatter diagram showing that gullies along attribute map B remain constant dimensions at the range of 700-850 m wide, 110-145 m (45-60 ms) deep and approximately 10-20 km long. Widths and depths for these six gullies show much less variation than gullies found in the older portions of this interval..... 60
- Figure 4.7 Sweetness attribute map C showing the paleogeomorphology and gully development for the uppermost 1/3 of the Tpal-Tolig interval. A total of 15 slope gullies are observed on this surface. From southwest to northeast portion, each gully is numbered in order from 1 to 15. The red line (Y-Y') marks the location of the seismic profile in Figure 9. Blues represent low sweetness and reds represent high sweetness. 62
- Figure 4.8 Scatter diagram showing dimensions of the gullies along attribute map C. Widths, depths and lengths are approximately 450-650 m, 70-115 m (35-55 ms), 3-8 km, respectively (Table 4.3). Southern gullies (gullies 1-5) are wider than northern gullies (gullies 6-15). Depth vary little, but a trend toward decrease in depth can be observed from gully 1 to gully 15..... 64
- Figure 4.9 Seismic cross-section random line. Location is shown in figure 4.7 (Y-Y'). Gullies imaged in Map C are shown in black line traces. Individual gullies appear to stack vertically in to gully complexes with thicknesses of up to 420 m (200) ms. There is a slight migration toward the northeast..... 65
- Figure 4.10 Sweetness attribute map D showing the paleogeomorphology and gully development for the topmost horizon of the Tpal-Tolig interval. A t

otal of 12 slope gullies are observed on this surface. From southwest to northeast portion, each gully is numbered in order from 1 to 12. The red line (Z-Z') marks the location of the seismic profile in figure 4.12. Blues represent low sweetness and reds represent high sweetness..... 66

Figure 4.11 Scatter diagram showing the dimensions of the gullies along attribute map D. They are 550-1000 m wide, 90-200 m (40-95 ms) deep and 8-14 km long. Gully 6 and 7 have larger width and depth than the other ten gullies. The dimensions of gully 6 and 7 can reach up to 1000 m wide and over 200 m (90 ms) deep. Gully 1-5 and 8-12 show similar dimensions from scatter diagram..... 67

Figure 4.12 Seismic cross-section line 3418. Location is shown in figure 4.10. Gullies imaged in Map D are shown in black line traces. Individual gullies appear to stack vertically in to gully complexes with thicknesses of up to 315 m (150 ms). There is a slight migration toward the northeast..... 68

Figure 5.1 Schematic of A) Slope gully systems and measured parameters from this study, and B) channel belt measures and nomenclature used by Jobe et al. (2016). Figure modified from Jobe et al., 2016. 74

Figure 5.2 Series of graphs showing absolute measures in meters along the Y-axis and the 10%, 50% and 90% probability measures (P=probability) for A. fluvial, submarine and slope gully channel widths, B. fluvial, submarine and slope gully channel thicknesses, C. fluvial and submarine channel belts and gully complex widths, D. fluvial and submarine channel belt and gully complex thicknesses, E. ratio of fluvial and submarine channel to channel belt widths, and the ratio of gully to gully complex widths, F. the ratio of fluvial and submarine channel to channel belt thicknesses, and the ratio of gully to gully complex thicknesses, and G. the aspect ratio of fluvial and submarine channel belt width to thickness and the aspect ratio of gully complex width to thickness. (Figure modified after Jobe et al., 2016)..... 75

Figure 5.3 Normalized channel belt and gully complex dimension cross-plot. The cross-plot is divided into two parts by a diagonal line. The upper part of the figure represents the vertical accretion dominant systems, while the data below this line indicates that the systems are dominated by lateral accretion..... 79

Figure 5.4 Series of paleogeographic renderings showing a strong south to north current along the western margin of Australia throughout the Neogene (<http://www.acer-acre.ca/the-components-of-the-earth-system>)..... 80

LIST OF TABLES

Table 2.1 Summary of the main geological characteristics associated with each sequence sets.....	29
Table 3.1 Measured depth, true vertical depth from SRD, two-way vertical time and average interval velocity for sequence sets 1, 2 and 3.....	42
Table 3.2 Aggradation rate (A) and progradation rate (P) of siliciclastic dominated margin in study area. P. refers to progradation, while A. refers to aggradation.....	43
Table 4.1 Table showing measured depth, true vertical depth, two-way vertical time and average interval velocity of surface Tpal, Tolig and boundaries which separate the lower part, middle part and upper part of Tpal-Tolig unit.....	52
Table 4.2 Summary of the slope gully dimensions coleted fomr Map A. Average interval velocity aoolied in this calcylation is 4527.3 m/s.....	57
Table 4.3 Summary of the slope gully dimensions on attribute map B. Average interval velocity used in this calculation is 4781.6 m/s.....	61
Table 4.4 Summary of the slope gully dimensions on attribute map C. Average interval velocity used in this calculation is 4169.8 m/s.....	63
Table 4.5 Summary of the slope gully dimensions on attribute map D. Average interval velocity applied in this calculation is 4169.8 m/s.....	68
Table 5.1 Slope gully dimensions for each sub-interval of Sequence Set 2 Tpal-Tolig.....	76
Table A.1 List showing relationship between measured depth, true vertical depth, two-way time and interval velocity from Kronos-1 well. The list is sorted from shallowest depth to deepest depth within the target interval in this study (ConocoPhillips , 2011)	87

ACKNOWLEDGEMENTS

I would first like to show my deepest gratitude to my supervisor, Dr. Lesli Wood, a respectable scholar, who has provided with valuable guidance in every stage of my project and writing of this thesis, support and help me throughout my graduate study. Without her enlightening instruction, impressive kindness and patience, I could not have completed my thesis. Her keen and vigorous academic observation enlightens me not only in this thesis but also in my future study. I would like to thank my thesis committee members Mary Carr and Bruce Trudgill, for their suggestions and edits to make this thesis better. I would also like to thank Dallas Dunlap for offering me the data of the Browse Basin.

I would like to thank Hirofumi Kobayashi, Kenya Ono, Oscar Vazquez for helping me with the Petrel procedure and all the technical questions. Thank you Hang Deng, Hehe Chen, Jianqiao Wang, Haipeng Li, Jingqi Xu, and Pengfei Hou, the Ph.D. students at Colorado School of Mines spending so much time teaching me and answering my questions.

I would like to thank my parents, friends and graduate students in SAnD, supporting me and pushing me with my research.

I feel so lucky to have all of you here at Colorado School of Mines and in my life.

CHAPTER 1

INTRODUCTION AND BACKGROUND

The deepwater research community has shown increasing interest in understanding how sediments are transferred from shelf edge to toe of slope settings (Courp and Monaco, 1990). Recent discoveries in the Browse Basin of northwest offshore Australia provide abundant data for investigating such temporal and spatial changes in sediment movements occurring over a margin that is transitioning from clastic- to carbonate-dominated. Seismic geomorphologic interpretation of a large (5000 km²) 3D seismic data volume was integrated with available well data (Kronos-1) and an Arc-GIS database of key previous observations mined from publications in the Browse Basin area, to assess temporal and spatial changes in sediment routing from shelf to basin, as well as changes in shelf to slope morphology that occurred as the margin transitioned from clastic- to carbonate-dominated. In addition, the late Cretaceous (super-greenhouse) to Miocene time period contains some dramatic changes in basin conditions that are likely reflected in the basin's stratal evolution.

1.1 Defining the Continental Margin

The primary goals of this study are to characterize the seismic geomorphologic features of the Northwest Australian continental margin of the Browse Basin. Continental margins are an important region of the ocean floor, as they typically mark the edge of the continental crust. The continental margin is distinguished by three features: the continental shelf, the continental slope, and the continental rise (Garrison,

2012). This study will focus primarily on the changes occurring over the continental shelf and slope transition.

The continental shelf of Northwest Australia is the submerged part of the larger subaerially exposed continent of Australia. It is gently inclined seaward at a slope less than 1° . The width of the Australian continental shelf can be as much as 80 km (50 miles), however within the study area the shelf is 35 km wide at its maximum water depth of 700 meters. The boundary between shelf and continental slope is termed the "shelf break". Shelf edge deltas are important architectures developed near the shelf break (Steel et al., 2003), and examining changes in shelf deltaic deposition and its relationship to continental slope channel development is one of the primary targets in this research.

The continental slope lying basinward of the shelf break is a much steeper geomorphologic zone than the shelf. The modern continental slope dips northwest and ranges in water depth from 700 m at the shelf break to 1000 m where the continental slope merges with the continental rise. This zone of convergence is often referred to as the "toe of slope". The continental rise can be quite wide and transitions basinward into the abyssal plain (Figure 1.1). In this study, we hypothesize that the nature of the continental slope (morphology, facies associations, degree of slope channelization) will vary as the margin transitions from clastic-dominated to carbonate-dominated.

The northwest margin of Australia has evolved from a rift basin to a passive margin basin (AGSO Browse Basin Project Team, 1997). The interval of this study is from Upper Cretaceous strata to Neogene strata, all of which formed during the passive margin phase of the basin's evolution.

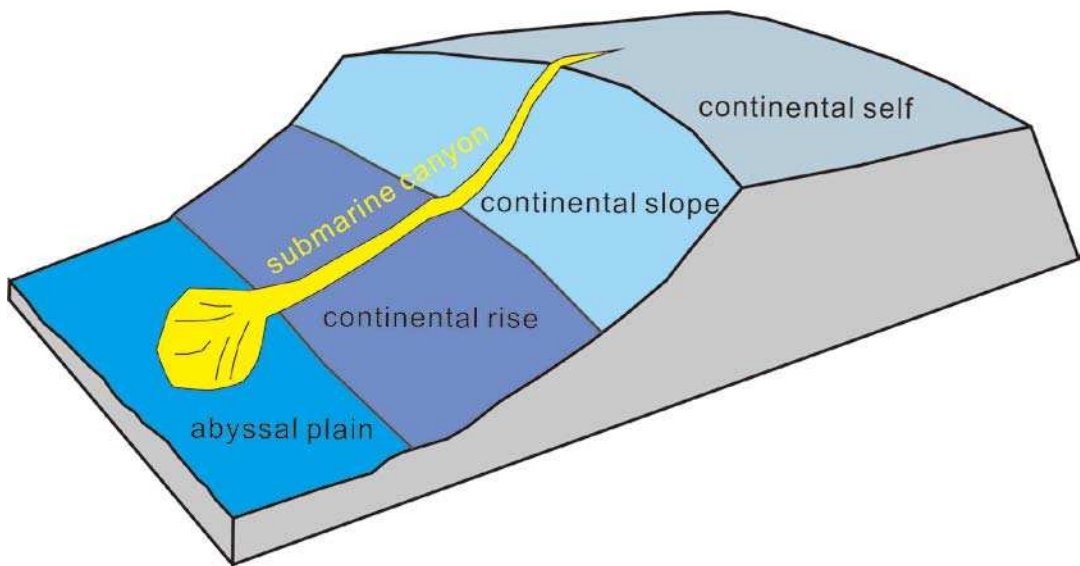


Figure 1.1 Diagram showing the geomorphology of a generic continental margin. The exact nature of the continental slope and its mergence with the most basinal continental rise as a function of margin type (clastic vs carbonate) is a topic of this study.

Key questions to be addressed in this study include:

- 1.) What is the genetic structural and stratigraphic evolution of the study area from Late Cretaceous to Miocene?
- 2.) What is the geomorphologic difference between clastic-dominated margins during Late Cretaceous to Oligocene and the carbonate-dominated margins during Oligocene to Miocene?
- 3.) How do slope channel morphologies develop in response to changes in sediment supply and marine conditions?

1.2 Geological Background

The Browse Basin offers an excellent laboratory to address the questions noted in the Introduction for the following reasons: 1. The basin has undergone both clastic-dominant and carbonate-dominant phases of its evolution during a relatively short time frame. 2. A chronostratigraphic and sequence framework is well established across the

study area by previous workers (Marshall and Lang, 2013; Laitrakull et al., 2011). 3. The basin has an abundance of high quality 3D seismic that images the stratigraphic section of interest, as well as a well penetration with good quality logs, and sedimentologic and biostratigraphic data through the interval of interest. Velocity data from the Kronos-1 well are also used to convert time thicknesses to true thicknesses, as we investigated the spatial and temporal changes in slope gully geometries,

Although we are only examining a small region of the Browse Basin margin, the entire margin is 2800 km long, 900 km wide, and contains a maximum thickness of Cenozoic and younger strata of at least 10 km (Marshall and Lang, 2013). The northwest region, including the Bonaparte, Browse, offshore Canning and Carnarvon basins (Figure 1.2), is a world-class oil and gas province. Our focus is a portion of the Browse Basin strata from late Cretaceous to the Miocene (Figure 1.3).

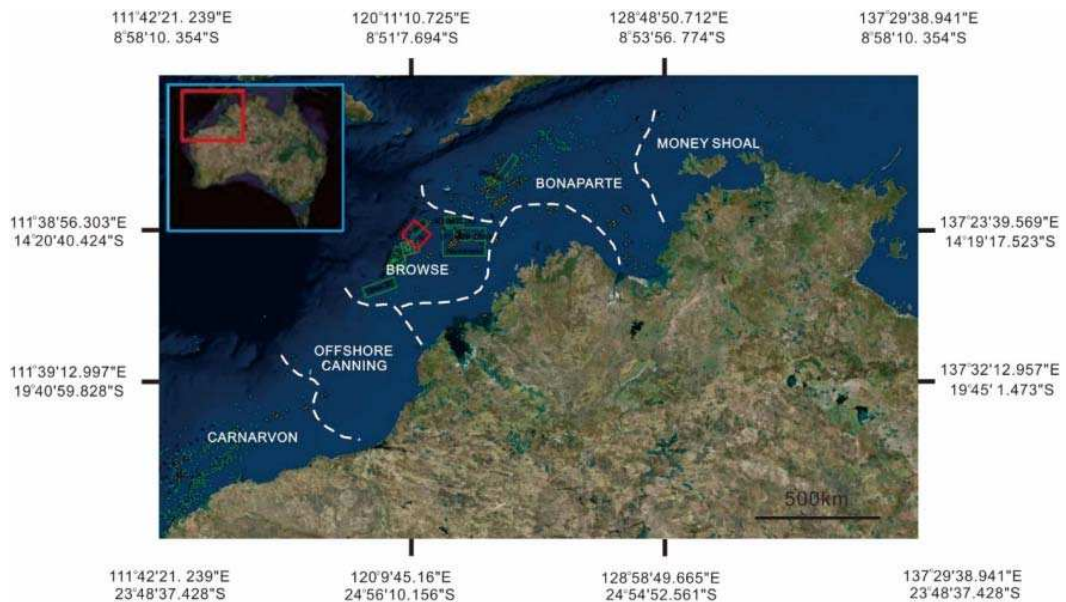


Figure 1.2 Map of northwest Australia, showing the Bonaparte, Browse, offshore Canning and Carnarvon basins. The Poseidon 3D seismic survey is outlined in red within the Browse Basin, and the location is also shown on Figure 1.4. Wells are shown in green, other 3D seismic data sets not used in this study are shown as green boxes. Continental Australia is shown in white.

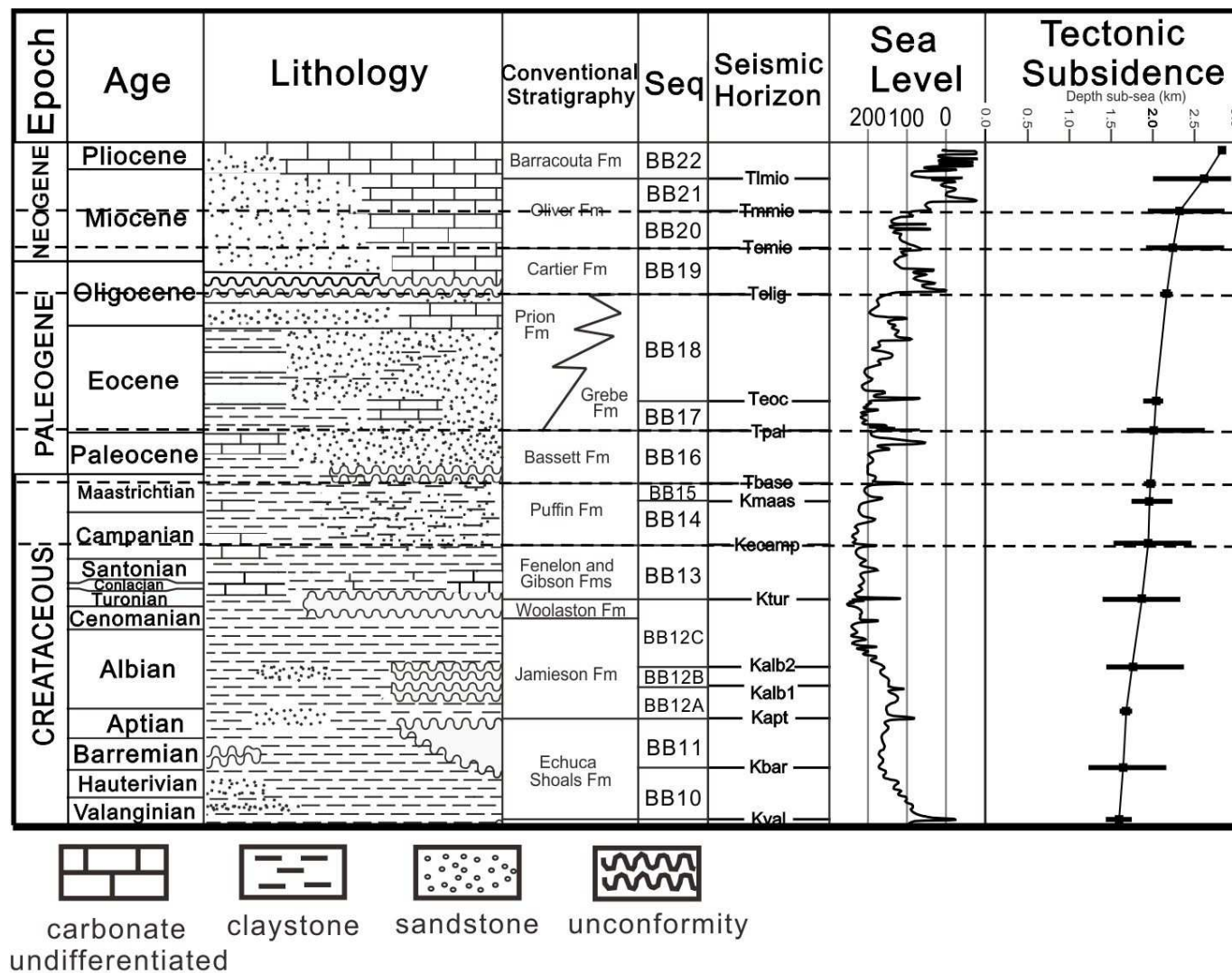


Figure 1.3 Tectonostratigraphic summary diagram. Modified after AGSO timescale (Young and Laurie, 1996); sea level curve (Haq et al., 1988; Greenlee and Lehmann, 1993); stratigraphic column (AGSO Browse Basin Project Team, 1997).

Browse Basin is a large, offshore basin composed of several sub-basins (Figure 1.4). The offshore part of the Browse Basin covers an area of approximately 140,000 km². Structurally the study area is located entirely in the offshore Timor Sea region off the coast of northwestern Australia and sits beside the Scott Plateau to the west. The basin is bounded by the Kimberley Block, Yampi Shelf and Ashmore Platform (Figure 1.4) (Australia Geological Survey Organization, 1993). A total of 22 sequences ranging in age from Devonian to Pliocene have been defined from well and seismic data in Browse Basin by previous researchers (AGSO Browse Basin Project Team, 1997). In this study, we focus on sequence BB14–BB20 (Figure 1.3). Six surfaces are mapped in the seismic all contained within the BB14-BB20 sequence interval. They are, from the oldest to the youngest, the Kecamp, Tbase, Tpal, Tolig, Temio and Tmmio horizons (Figure 1.3).

Sequence BB14-BB20 is composed of Late Cretaceous through Neogene strata. The Late Cretaceous strata are widespread deposits of marine siltstone and claystone. These strata are separated from the overlying Paleogene strata by a significant regional unconformity at ~ 65.5 Ma (AGSO Browse Basin Project Team, 1997). Post unconformity strata is composed of a relatively thick, Paleocene to early Eocene mass flow sandstone. Following this deposition and to the end of the Eocene, clastic sedimentation decreased and carbonate sediments were deposited, with carbonate sedimentation continuing throughout Cenozoic (Australia Geological Survey Organization, 1993).

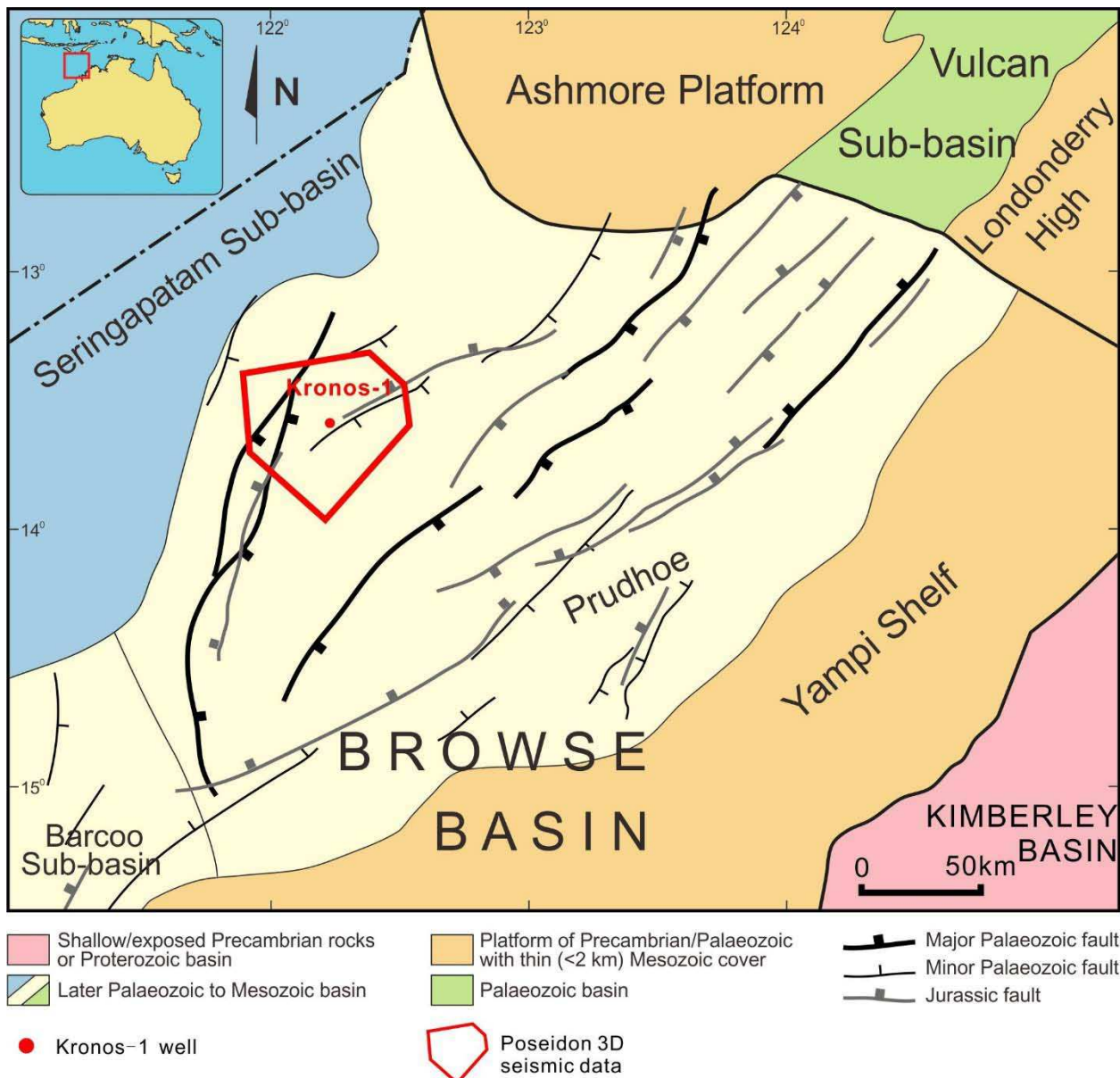


Figure 1.4 Regional structural element map showing the location of the Poseidon 3D seismic survey (dashed red box). Location of Figure 1.4 is shown on Figure 1.2. Location of the 3D seismic (red outline), is shown in Figure 1.2. Kronos-1 well is shown. Modified after Brincat et al., 2003.

1.3 Terminology

1.3.1 Slope Gullies

Gullies are channelized architectures with steep sides and low sinuosity. Slope gullies are commonly observed occurring in the upper portion of continental margin marine slopes that are fed by deltas, as well as those with no fluvial input (Field et al., 1999; Lonergan et al., 2013). Slope gullies may originate at the shelf edge or originate hundreds of meters basinward from the shelf edge (Shumaker et al., 2016). They show dimensions that are smaller than the typical submarine canyons ranging from tens to hundreds of meters wide and tens of meters deep (Field et al., 1999; Chiocci and Normark, 1992; Micallef and Mountjoy, 2011; Lonergan et al., 2013; Shumaker et al., 2016). They are often evenly spaced along submarine slopes and steep areas of the seafloor, but terminate over relatively short distances at the toe of the slope. Gullies are important indicators of sediment transport from the outer shelf to the continental slope and the deep basin, and are an important component of the evolution of continental margins (Syvitski et al., 1996; Micallef and Mountjoy, 2011).

1.3.2 Channels

Channels are a common element in deep-marine and fluvial settings (Arnott, 2010; Bridge and Tye, 2000). They are a negative topographical element that forms by erosion and can transport sediments along a long pathway (Arnott, 2010). Channels tend to extend for longer distances than slope gullies. Submarine channels can exhibit either low sinuosity or high sinuosity, and are generally smaller than submarine canyons (Cardenas, 2009). They commonly show levee and point bar morphologies, which are lacking slope gullies (Shepard and Emery, 1973; Shepard, 1981).

1.3.3 Submarine Canyon vs. Incised Valley

Both submarine canyons and incised valleys are long-lived conduits for basinward transport of sediments. Canyon and valley dimensions are typically larger than those of slope gullies or submarine channels, with the canyons and valleys showing depths of up to 2500 m and width's of 10's of kms (Normark and Carlson, 2003; Arnott, 2010). Unlike leveed channels, canyons and valleys show no associated levee morphology (Shepard and Emery, 1973; Shepard, 1981). Canyons are dominated by bypass, whereas deepwater valleys often show an abundance of depositional architectures, including channels, levees, and lateral lobes.

1.3.4 Rimmed and Non-rimmed Carbonate Margins

Rimmed carbonate margins (Figure 1.5A) are shallow continental margin located platforms that have reef growth (Read, 1982). The reef buildups on these rimmed margins provide protections from open ocean processes, and restrict circulation along the margin (Read, 1982). Rimmed margins are characterized by stratigraphically flat tops, linear trends along the shelf edge and a sharp transition from carbonate shelf to slope (Adams and Kenter, 2014; Read, 1982; Read, 1985). This type of carbonate margin has a relatively steeper gradient slope foreset compared to non-rimmed carbonate margin (Adams and Kenter, 2014; Hine and Mullins, 1983).

Non-rimmed carbonate margins (Figure 1.5B) are characterized by gently, seaward-dipping surfaces. They generally lack a protecting reef at the shelf edge to act as an energy barrier (Adams and Kenter, 2014, Schlager, 2003). Due to the absence of this reef buildup, deep water waves are able to propagate across much of the shelf. Thus, this type of carbonate margin is more dramatically impacted by storm and high-

energy processes (Adams and Kenter, 2014; Hine and Mullins, 1983). The break between shelf and slope in a non-rimmed margin is a relatively broad area compared to the abrupt shelf edge of rimmed carbonate margins (Hine and Mullins, 1983).

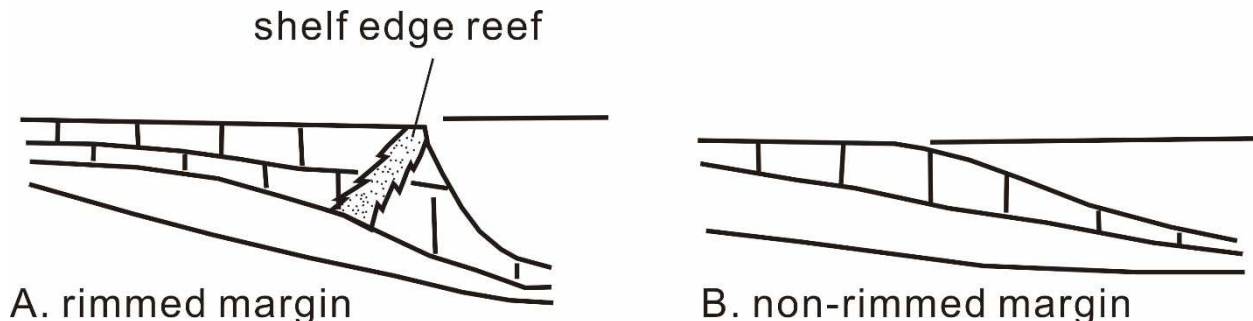


Figure 1.5 Sketches of rimmed margins and non-rimmed margins. A) Showing the reef growth on the rimmed margin. Rimmed margins are characterized by flat tops, linear trends of the shelf edge and a sharp shelf break. This type of carbonate margin has a relatively steeper gradient slope foreset compared to non-rimmed margins. B) Non-rimmed carbonate margins generally lack a protecting reef at the shelf edge to act as an energy barrier. This type of carbonate margin is easily reworked by storm and high-energy processes. The break between shelf and slope is a relatively broad area compared to the abrupt shelf edge of rimmed carbonate margins. Modified from Read, 1985.

1.3.5 Strata Terminations: Onlap, Downlap and Truncation

The stratal terminations within depositional sequences and their composing systems tracts are used to describe the architectures of the sequences and discriminate the location of the depositional setting of a systems tract. Both onlap and downlap are terminations occurring above a key surface (Mitchum Jr, 1977). Onlap (Figure 1.6A) is a stratal relationship in which the initially horizontal strata terminate against an initially inclined surface, or the initially inclined strata terminate progressively updip against a surface of greater initial inclination. Downlap (Figure 1.6B) is a stratal relationship causing seismic reflections of inclined strata to terminate downdip against a surface

(Mitchum Jr, 1977). Truncation (Figure 1.6C) is the termination below a surface. It represents a stratal relationship where the strata is eroded by post-depositional processes (Mitchum Jr, 1977).

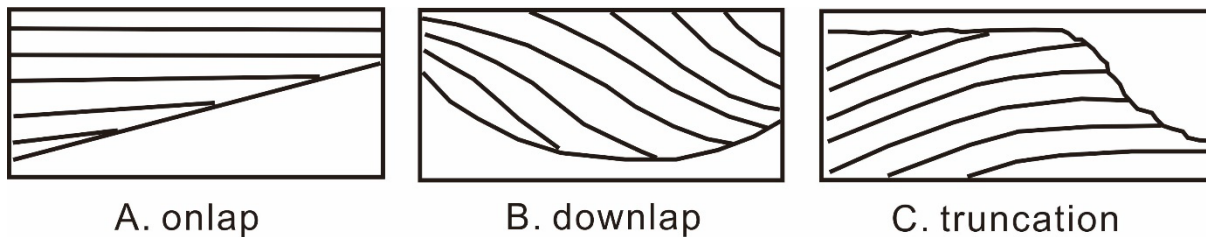


Figure 1.6 Sketches of strata terminations. A) Onlap is a relationship in which initially horizontal strata terminate against an initially inclined surface, or the initially inclined strata terminate progressively updip against a surface of greater initial inclination; B) Downlap is a relationship that seismic reflections of inclined strata terminate downdip against an surface. C) Truncation is the termination below a surface, it represents the relationship that the strata is eroded by the post-depositional erosional or structural effects. Modified from Mitchum Jr, 1977.

1.4 Dataset

This research uses data of industry-acquired high quality 3D seismic volume and a single well, the Kronos-1, and associated data to interpret and describe the geomorphology of the study area. The 3D seismic data are provided by ConocoPhillips (Browse Basin) Pty Ltd (2011). Exploration well data, including well log, check-shots surveys, lithology reports and well-completions report are provided by ConocoPhillips (2011) and Geoscience Australia (AGSO Browse Basin Project Team, 1997). Data details are discussed below.

The Poseidon 3D seismic data covers an area of approximately 5000 km², and penetrates down to ~7000 ms. Frequency range for this 3D seismic cube is 5-100 Hz, with the dominant frequency ranging from 20 Hz to 60 Hz, yielding an average dominant frequency range of ~40 Hz. The polarity of this seismic data follows the European

normal polarity standard. The reflector appears from low to high impedance between seawater and seabed, and the reflector between seawater and seabed has a positive amplitude. In the Poseidon 3D dataset, reflections in red have a positive amplitude and represent the peak reflection in seismic. In contrast, reflections in blue represent the negative amplitude and are the seismic trough. It is well known that seismic resolution equals 1/4 the wavelength. Check-shots in the Kronos-1 well (Appendix A), collected over the study interval indicate a lowest acoustic velocity of about 3000 m/s and a highest acoustic velocity is about 5000 m/s. The average acoustic velocity of the study interval is about 4000m/s, yielding vertical resolutions of 18.75 m and 31.25 m, respectively. A blank spot (10 km x 6 km) is present in the dataset. This no-data area is caused by the presence of a modern carbonate reef, and seismic was not accessed in this region.

The high quality Poseidon 3D seismic data is ideal to address questions concerning continental margin development. It allows detailed mapping of surfaces over a large portion of the shelf to slope area, and clearly reveals the character of shelf and slope morphologies. The well data, well-completion reports and a previous report titled the Browse Basin High Resolution Study (AGSO Browse Basin Project Team, 1997) provide age control for this study. Age control is based on the previous work of ConocoPhillips (2011), whose work provided the measured depth of several formations in the study interval, as well as the relationship between the depth and two-way vertical time. Thus, the stratigraphic formation and the age can be defined on the seismic profile

1.5 Methodology

One well, Kronos-1 is used in this study for the seismic time-to-depth conversion. Location of Kronos-1 well is indicated in Figure 1.7. Check-shots surveys are provided by ConocoPhillips in their well-completion reports (ConocoPhillips, 2011). The relationship between measured depth, true vertical depth from the Seismic Reference Datum (SRD), two-way vertical time and interval velocity is presented in Appendix A. Seismic Reference Datum (SRD) for the vertical time-depth information in this report is Mean Sea Level (MSL).

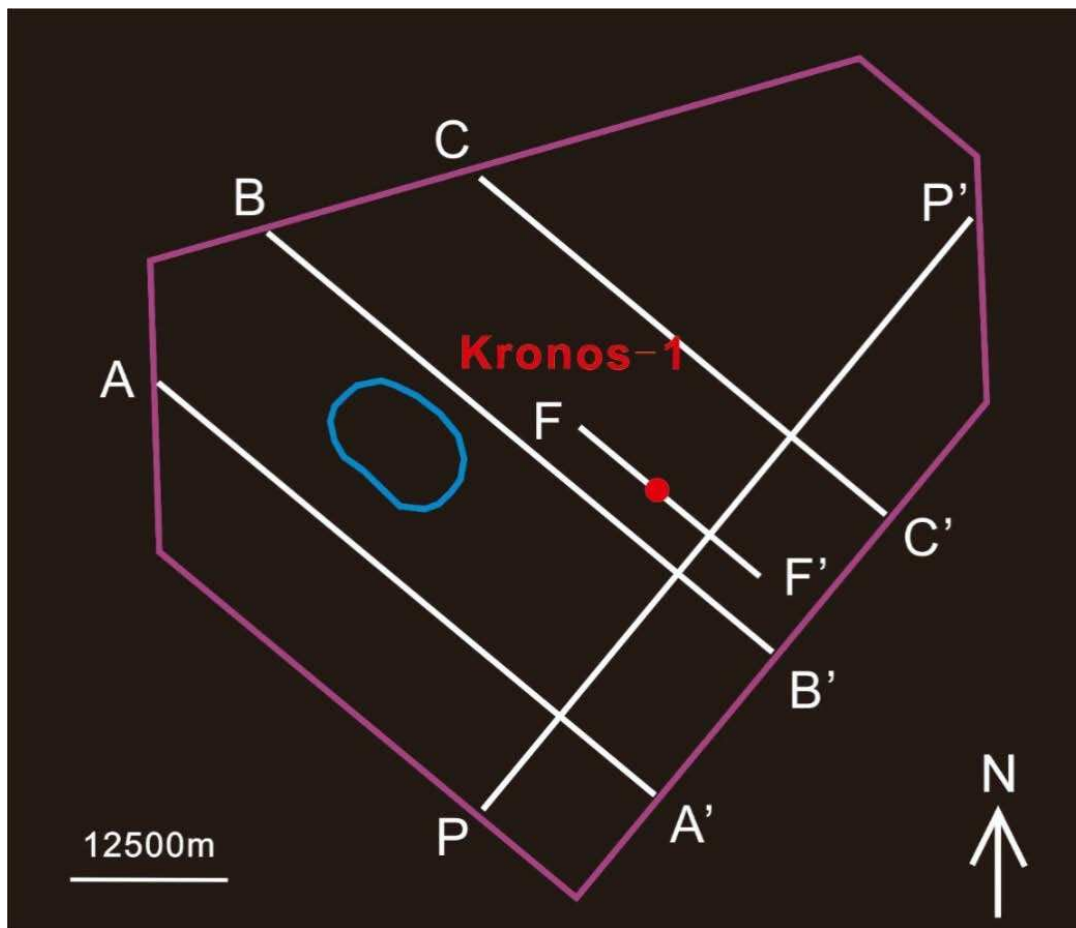


Figure 1.7 Map showing location of the Kronos-1 well and seismic profiles discussed in the text. The purple line outlines the extent of the 3D. The blue circle shows the area of no data.

Based on information from the check-shots surveys (Appendix A), a velocity curve was generated for the Kronos-1 well and used assist with converting geometries measures on the time data to depth values. The Kronos-1 gamma ray log and a corresponding velocity-time curve for the study interval are shown in Figure 1.8. Interval lithology as well as the relationship between time and true vertical depth from SRD are also shown in Figure 1.8. The gamma ray curve shows dramatic changes within the Kecamp, Tbase and Tpal bounded intervals and keeps at a relatively high value within the Tpal-Tolig interval. A relatively low gamma interval is identified in the Tolig to Temio interval, and there is a change to a higher gamma value in the Temio to Tmmio interval. Within the Kecamp to Tmmio study interval, the lowest acoustic velocity is ~3000 m/s and the highest acoustic velocity is ~5000 m/s. The average acoustic velocity of the interval is ~4000 m/s. The interval is lithologically dominated by siliciclastic deposits in the lower strata, beneath the Tolig surface. Strata in the interval overlying the Tolig surface are dominated by carbonate lithologies.

The interpreter used Petrel software to map six key surfaces in seismic. These surfaces were the same as noted in the well-completion reports provided by ConocoPhillips (2011). Reports offer the true vertical depth from SRD and age of each surface. Check-shots surveys were used to identify the relationship between true vertical depth from SRD and time, enabling a good tie at the well location between the well penetration and the seismic. Sweetness attribute was applied into 3D seismic volume to highlight geomorphological features. Sweetness attributes, a combination of the Envelope and Instantaneous Frequency attributes were applied in the seismic data to highlight morphologic features (Riedel et al., 2008).

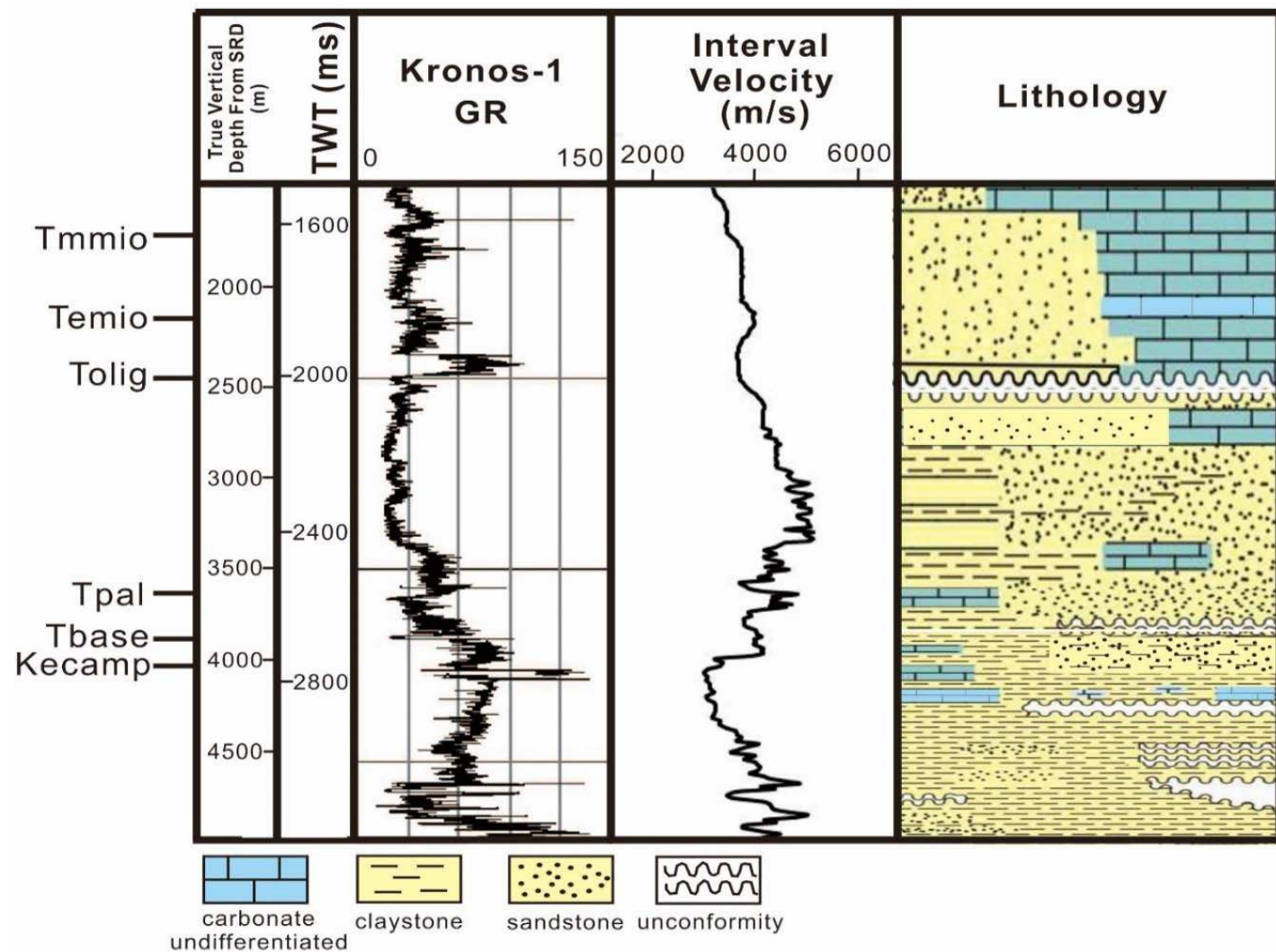


Figure 1.8 Interval velocity tie to the well log and lithology at the Kronos-1 well. Key surfaces (see text for nomenclature) are noted in the log as listed in the well-completion report (ConocoPhillips, 2011). Location of Kronos-1 well is shown in Figure 1.7.

CHAPTER 2

STRATIGRAPHIC EVOLUTION OF THE BROWSE BASIN

2.1 Introduction

The continental margin of the Browse Basin has undergone a long history of evolution. Six tectonostratigraphic phases have been defined in the basin by Struckmeyer et al. (1998), which include two cycles of extension, thermal subsidence and inversion (Symonds et al., 1994). The major interval studied in this research is included in the second thermal subsidence phase, which experienced only minor fault reactivation. Six sequence boundaries, identified in previous publications (AGSO Browse Basin Project Team, 1997) have been recognized from Campanian to Middle Miocene. Sequence boundaries are identified as significant erosional unconformities and their correlative conformities (Van Wagoner et al., 1988). In this study, sequence boundaries are primarily defined by the terminations of the overlying strata and underlying strata, incorporating with the well log features. Sequence boundaries are usually related with a dramatic change in well log response (Vail and Wornardt Jr, 1991). Details of the definition for each horizon will be addressed in the following part of this thesis. The six surfaces shown on seismic profiles (Figure 2.1, 2.2), herein named, from oldest to youngest, the Kecamp, Tbase, Tpal, Tolig, Temio and Tmmio, are interpreted and correlated throughout the study area using reflection seismic data. Location of Figure 2.1 (A-A') and Figure 2.2 (F-F') are indicated in Figure 1.7.

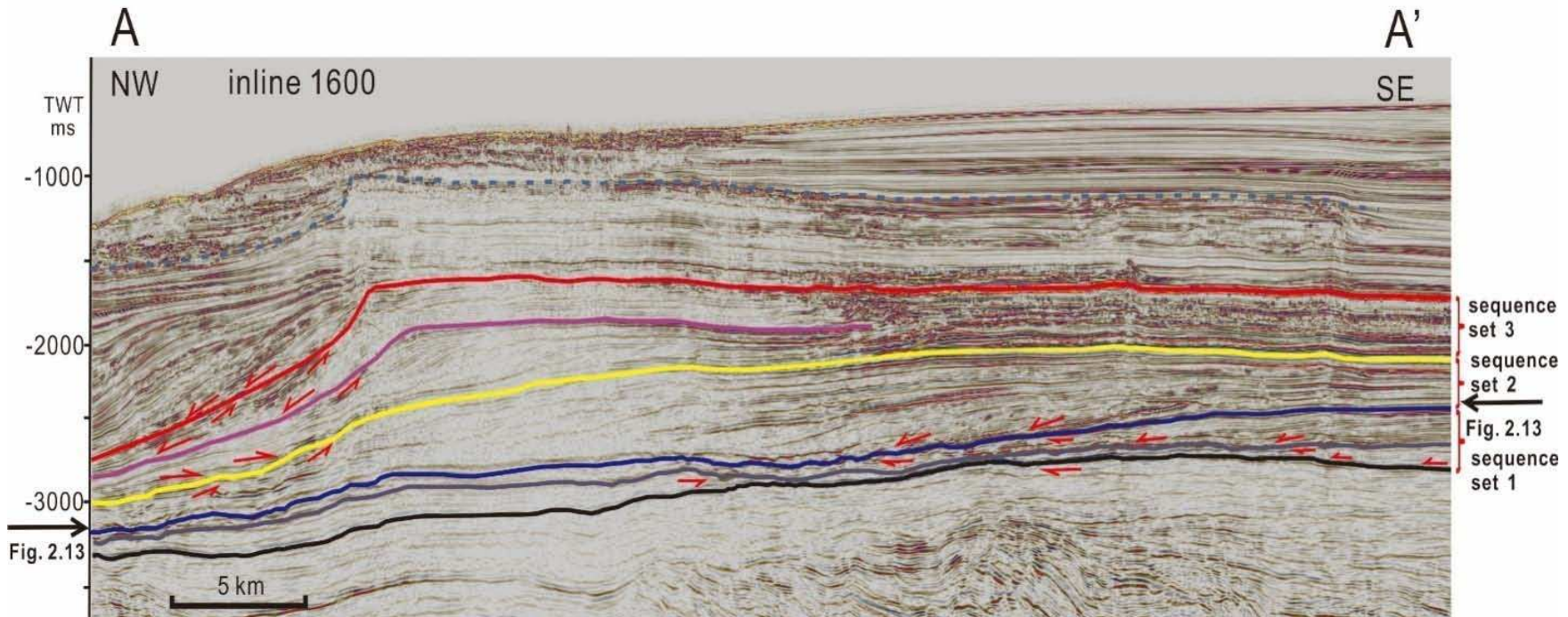


Figure 2.1 Interpreted seismic line showing the six interpreted sequence boundaries within the study area; the Kecamp, Tbase, Tpal, Tolig, Temio and Tmmio, from the deepest to the shallowest. Three sequence sets are defined as the boundaries between them mark major process changes in the basin. Representative strata terminations (red arrows) along each mapped surface are shown on the profile. Location of seismic line is shown on Figure 1.7 (A-A'). Location of Figure 2.13 is indicated by black arrow.

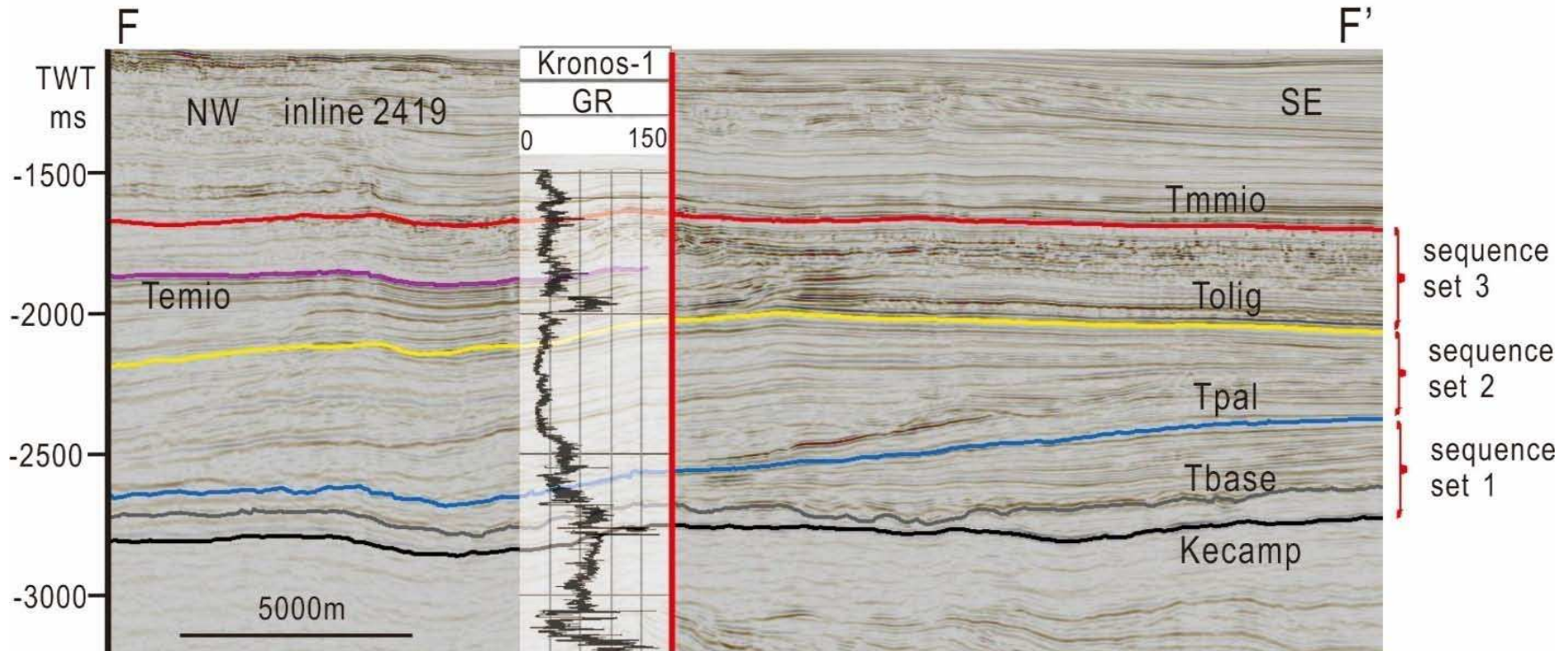


Figure 2.2 Seismic inline 2419 showing the correlation of inline 2419 and Kronos-1 well. Kronos-1 well is marked by red line on this figure, Location of Kronos-1 well and the seismic profile (F-F') are shown in Figure 1.7. Six key surfaces are shown on the seismic profile.

The interpretation methods used in this study include horizon mapping, seismic facies description and seismic attribute extraction and mapping. The six study area extensive surfaces provide a framework within which to examine the basin margin architecture and stratigraphic framework. Six key stratigraphic horizon maps, three isochron of the stratigraphic units were used to examine the geologic character of the Late Cretaceous to Neogene stratigraphy.

2.2 Key Surface Interpretation

Six seismic horizons have been identified and correlated throughout the 3D seismic grid (Figure 2.1, 2.2) and are described below. Kecamp is an unconformity near the base of Campanian horizon (Figure 1.3) and is the deepest mapped seismic horizon in this study. The remaining five surfaces are Paleogene and Neogene in age, ranging from base Paleogene (Tbase) to Top Paleocene (Tpal) to Top Oligocene (Tolig) to Top Early Miocene (Temio) to Top Middle Miocene (Tmmio). Kecamp, Tolig, Temio and Tmmio are on peak reflection, Tbase and Tpal are on trough reflection (Figure 2.3). The Paleogene and Neogene section in Poseidon 3D area composes a nearly 3 km-thick sediment package. These Paleogene and Neogene margins are composed of both carbonate and clastic phases of sedimentation but are dominated by carbonate and carbonate reefs during the Miocene. The seismic horizons are discussed in detail below.

Kecamp (Early Campanian Unconformity) is an unconformity surface on peak reflection (Figure 2.3), which separates the underlying Fenelon Formation and the overlying Puffin Formation (Figure 1.3). The high-amplitude, high-continuity nature of the reflection that represents this unconformity is easily recognized and differentiated from the reflections above and below it, and can be traced over the entire 3D seismic

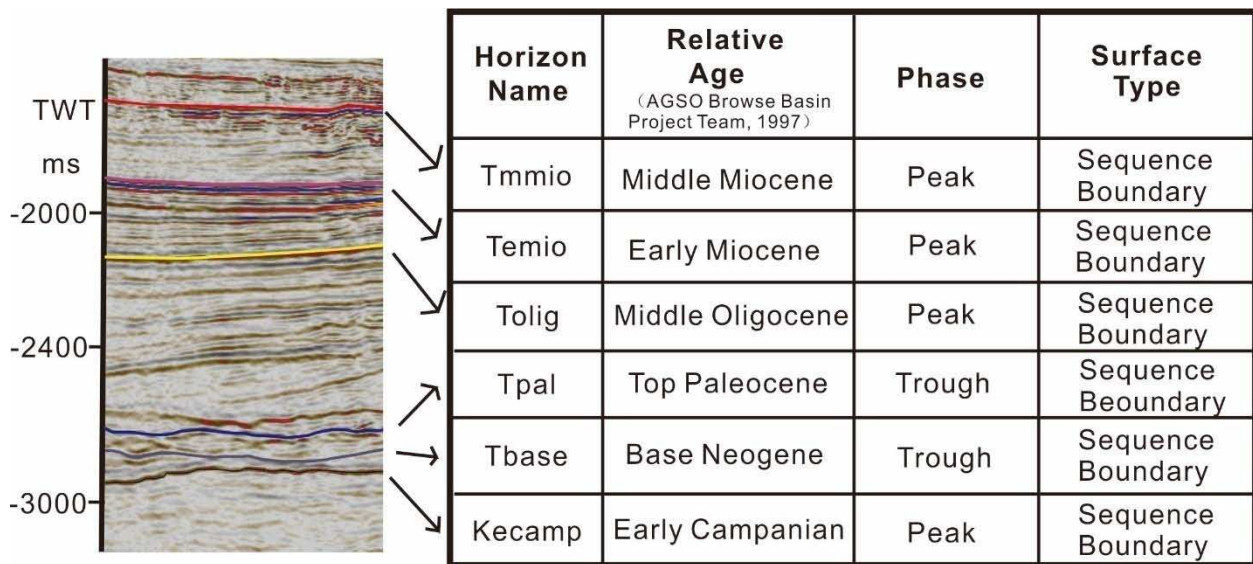


Figure 2.3 Chart showing the correlation from the regional horizons mapped as part of this study and their seismic character (shown on the left).

area (Figure 2.1, 2.2). The lithology of the Puffin Formation consists of calcareous claystone and sandstone (ConocoPhillips, 2011). The Kecamp unconformity truncates the medium-amplitude, medium-continuity reflections of the underlying Fenelon and Gibson Formations. The overlying formation onlaps against the Kecamp unconformity (Figure 2.1). Well log data from the Kronos-1 well show a distinct fluctuation along this surface (Figure 1.8, 2.2). Kecamp is interpreted to be a sequence boundary. The time-structure contour map for Kecamp (Figure 2.4) shows that the structural high of this time is in the eastern portion of the data area. The high dips gradually down to the northwest with relief ranging from -2600 ms to -2800 ms. This surface shows relatively low relief compared to the overlying Temio and Tmmio horizons, discussed later. A significant canyon incision occurs along the slope during this time, the width of the slope canyon is approximately 10km and the average thickness is 250 ms (Figure 2.4, 2.5).

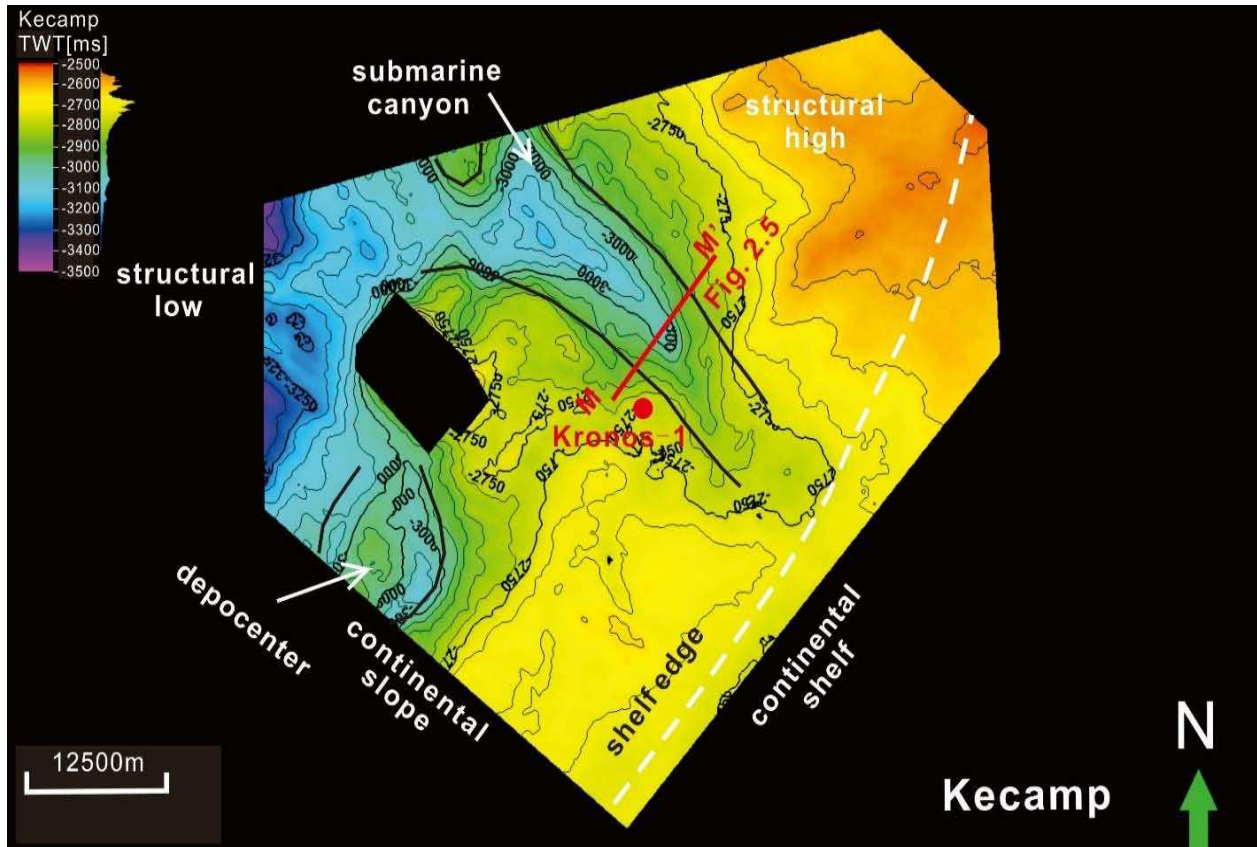


Figure 2.4 Time structure contour map for Kecamp, showing the structural high of this horizon in the southeast portion of the data area, and relief dives to the northwest. Relief on the upper continental slope is low ranging from 2600 m at the eastern shelf edge to 2800 ms before deepening dramatically to the west to nearly 3300 ms. Location of Figure 2.5 is shown on this figure (M-M').

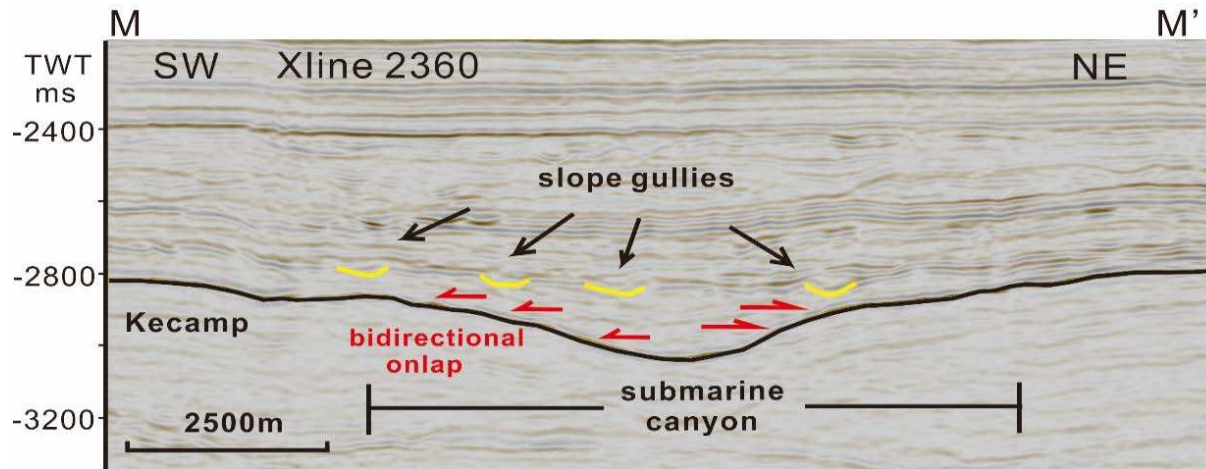


Figure 2.5 Seismic Crossline 2360 showing submarine canyon incision along the horizon Kecamp. The width of the canyon can extend to 10km. Location of seismic line is shown on Figure 2.4. The younger strata above horizon Kecamp show bidirectional onlapping against both sides of the canyon, and multiple late stage channels fill the upper part of the canyon. The average width of these channels is 600m, and the average depth of them is approximately 40ms.

Tbase (near-base Paleogene unconformity) defines the top of the Puffin Formation and the base of Bassett Formation (Figure 1.3). Tbase is an erosional unconformity, which composes a trough reflection in seismic (Figure 2.3). This unconformity is easily recognizable as a high-amplitude and high-continuity seismic reflector (Figure 2.1, 2.2). This unconformity separates underlying moderate-amplitude reflections from overlying medium continuity, medium-amplitude reflections. The underlying reflections are truncated beneath Tbase, showing the erosional character of this horizon. The overlying reflections downlap on Tbase (Figure 2.1). The log data show that a distinct change of gamma ray is present across this surface (Figure 1.8, 2.2). This surface is interpreted as a sequence boundary. The structure map for this horizon (Figure 2.6) has a similar trend as Kecamp, reflecting a structural high in the southeast and a structural low in the northwest. This structure map shows relatively low relief on this horizon from shelf to

slope.

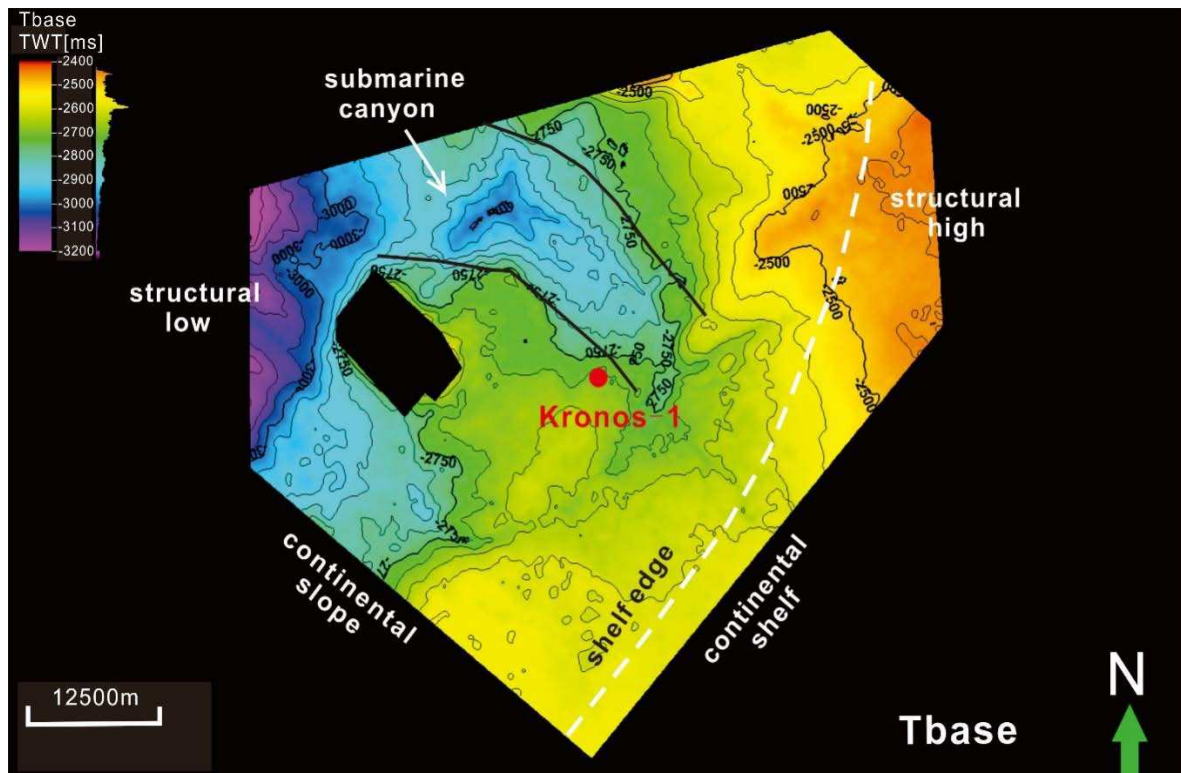


Figure 2.6 Time structure map for horizon Tbase. Tbase has a similar trend to Kecamp, it shows relatively low relief from shelf to slope compared to Temio and Tmmio. The structural high in the east-northeast.

Tpal (Paleocene regional unconformity) is identified by a strong seismic trough (Figure 2.3), which can be recognized across the entire 3D survey. The Tpal horizon is 200 ms above the Tbase unconformity in southeast portions of the study area but is less than 50 ms above the Tbase unconformity in northwestern portions. The Tpal unconformity defines the top of the Bassett Formation and the base of the Grebe Formation (Figure 1.3). This surface is truncated by medium- to high-amplitude, high-continuity reflections, and overlain by occasional downlap of the younger stratal package is observed (Figure 2.1). A dramatic change of gamma ray response occurs in

the Kronos-1 logs across this surface (Figure 1.8, Figure 2.2). Tpal is defined as a sequence boundary. Well data show the lithology above this unconformity surface consists of calcilutite, calcareous claystone and sandstone (ConocoPhillips, 2011). The Tpal time structure contour map (Figure 2.7) continues to show expression of the underlying Kecamp Canyon.

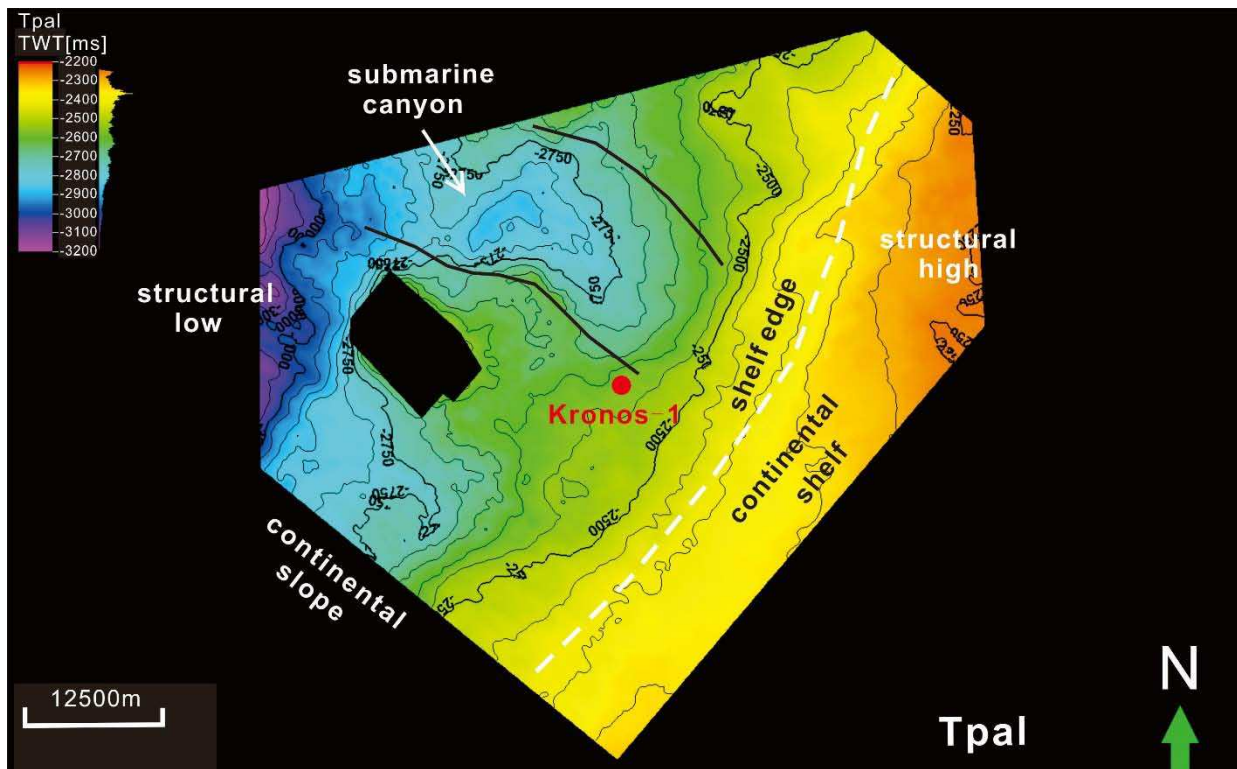


Figure 2.7 Time structure contour map for Tpal, showing a gently steep shelf and upper slope, representing a low angle continental margin.

The Tolig unconformity (Oligocene regional unconformity) is on a peak reflection in seismic (Figure 2.3), and represents a higher-amplitude and higher-continuity reflector than Tpal that is present over the entire 3D seismic area (Figure 2.1). Tolig truncates the underlying formation and is onlapped by the overlying units of the Cartier Formation (Figure .2.1). This Oligocene unconformity marks a sharp transition from clastic-dominated to carbonate-dominated deposition. Seismic character of the underlying

strata and overlying strata show significant differences. Strata beneath this unconformity show packages of low seismic amplitude and low seismic continuity, low angle clinoforming reflectors. The overlying package is recognized by massive, medium- to high-amplitude, medium- to high-continuity, sigmoid to oblique progradational seismic reflections in central and northwest regions of the study area, and very high-amplitude, high-continuity reflectors at shelf-edge location (Figure 2.1). A dramatic change of gamma ray is shown on well log data along this surface (Figure 1.8, 2.2). Strata terminations as well as the sharp differences in the style of the seismic character are utilized in the recognition of the Tolig as the sequence boundary. The Tolig structure contour map (Figure 2.8) ranges from -1950 to -3100 ms and reflects a slight steepening of the slope but it does not show near the steepness of the overlying Temio or Tmmio horizons. In addition, the Tolig horizon does not show a sharp change in dip at the shelf to slope transition. This surface shows a significant healing of the canyon seen in the previous three surfaces, and a significant migration of the shelf edge to a more westward location.

Temio (Early Miocene unconformity) is identified by a medium- to high-amplitude peak reflection in seismic (Figure 2.3). This horizon is present only within the northwestern portion of the Poseidon 3D seismic area (Figure 2.1). The underlying unit is truncated by the Temio unconformity, and the Temio surface is downlapped by the overlying strata (Figure 2.1). Well logs show a change in gamma ray response across this surface (Figure 1.8). These differences in gamma character, and its regional extent support interpretation of this unconformity as a sequence boundary. The seismic

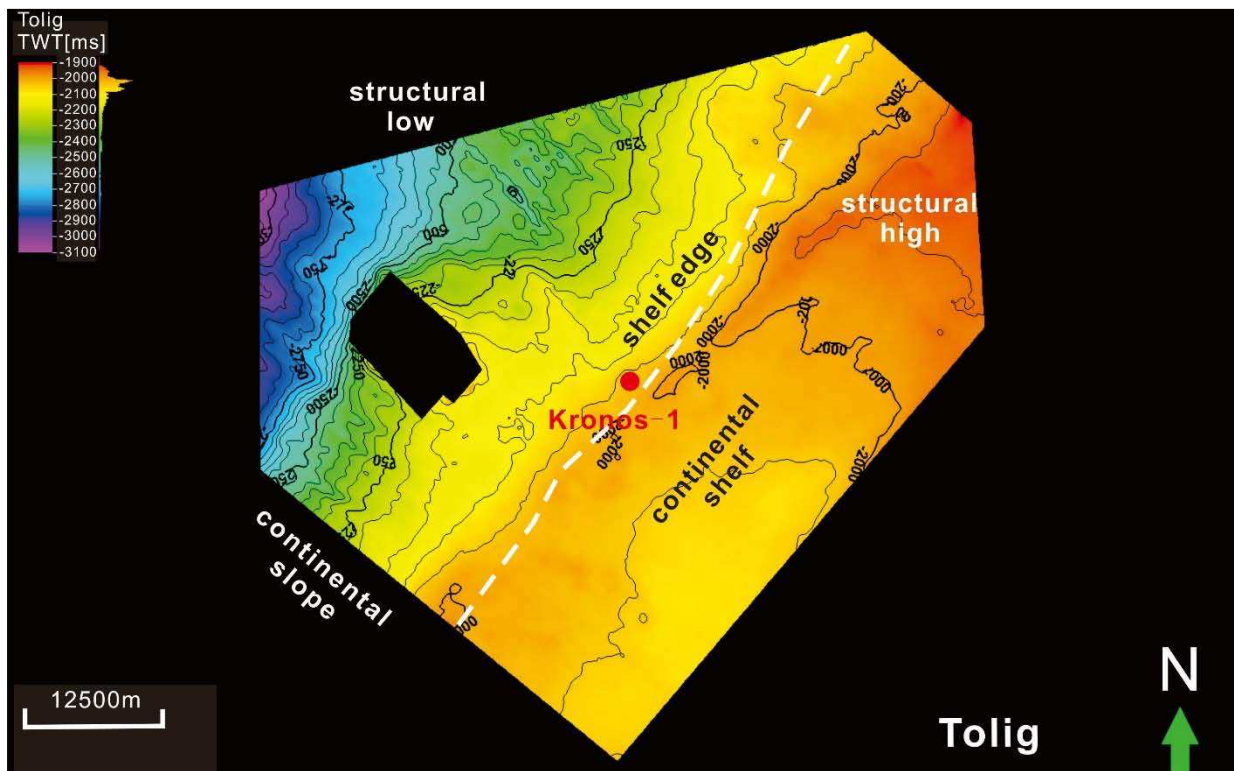


Figure 2.8 Time structure map for horizon Tolig, reflecting a moderately steep slope compared to older margins, but continuing to display a gradual transition between shelf and slope.

architecture of the overlying unit is complex sigmoid-oblique reflectors, showing medium- to high-amplitude. Chaotic, high-amplitude reflections observed in this interval in the southeast portion of the seismic area, reflect the dominantly carbonate stratal nature. The Temio structure map ranges from -1800 ms in the southeast to -2600 ms in the northwest corner of the study area, exhibiting a dip to the northwest (Figure 2.1, 2.9). Compared to the older Tolig unconformity, the Temio unconformity shows a much steeper dip, as well as a distinct break between the paleo-continental shelf and the paleo-continental slope.

Tmmio (Middle Miocene regional unconformity) is marked by an extremely high amplitude peak reflection in seismic (Figure 2.3). Tmmio truncates the underlying strata and is downlapped by high-amplitude, medium-continuity reflectors of the next youngest

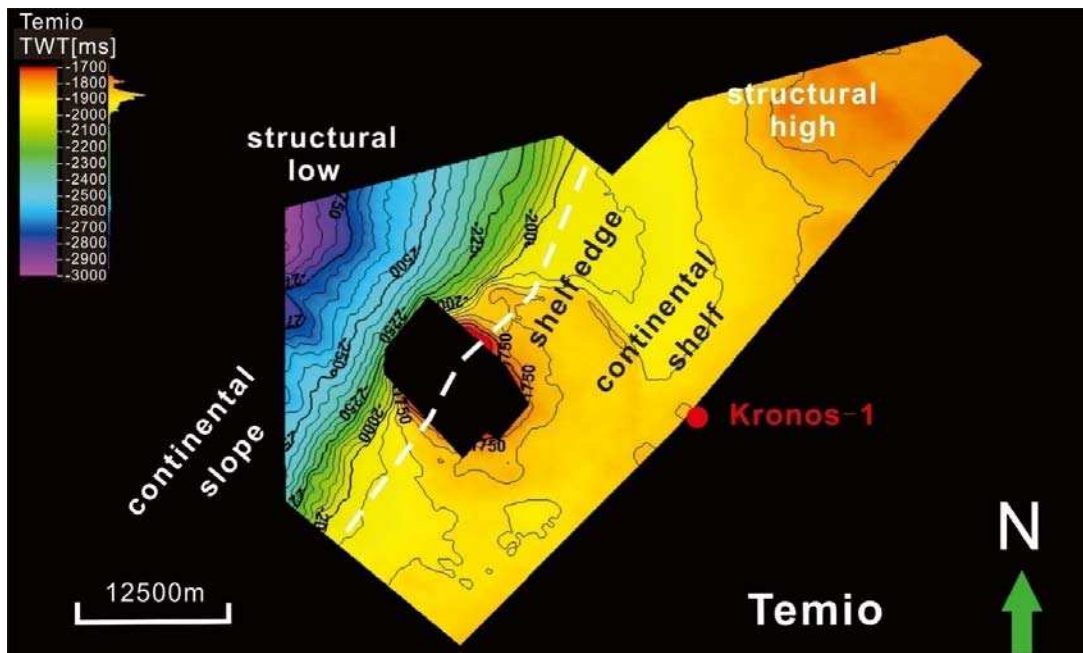


Figure 2.9 Time structure map for Temio, showing a sharp steepening of dip from the shelf to the continental slope.

stratal package (Figure 2.1). Well logs show a distinct change of gamma ray, across this horizon (Figure 1.8, Figure 2.2). This surface is interpreted as a sequence boundary. The seismic architecture of strata overlying the Tmmio is observed as oblique progradational reflections, downlapping to the west (basinward). The underlying unit is composed of high-amplitude and medium- to high-continuity reflections and is truncated by the Tmmio unconformity. Seismic reflections in the southeast portion of the dataset show a chaotic character, and are interpreted to represent carbonate strata. The Tmmio time structure map shows a bunching of contours indicating a steepening of slopes (Figure 2.10). Location of the break between shelf and slope moved basinward from Temio to Tmmio time. This migration of the shelf break reflects the progradation of the system northwestward during Early Miocene and Middle Miocene.

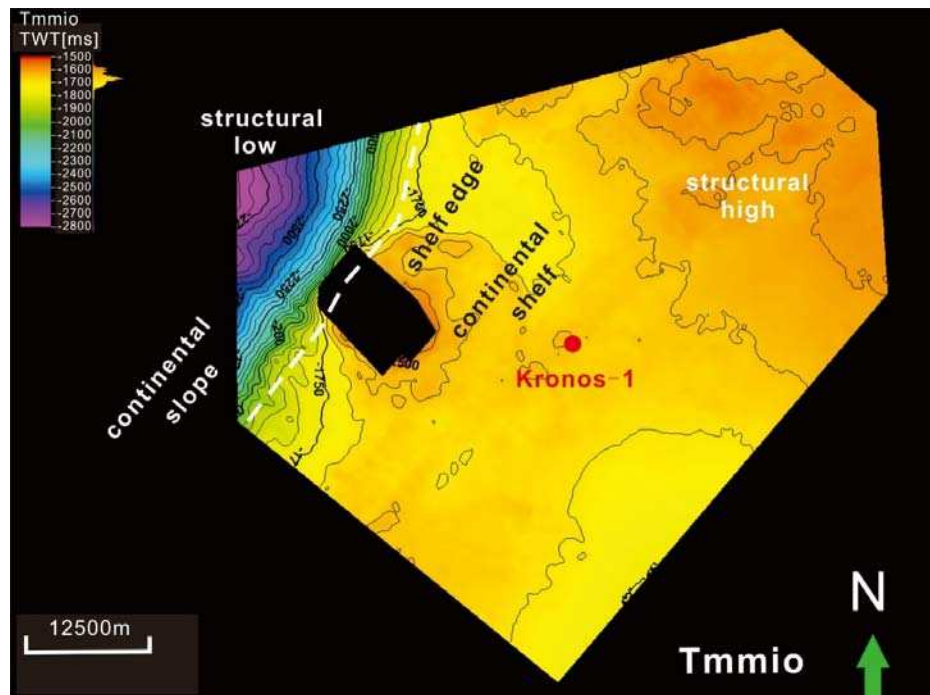


Figure 2.10 Time structure map for Tmmio. The shelf break, marked at the dramatic change in structural dips, continues to migrate west-northwest as the margin progrades.

2.3 Sequence Set Interpretation

This study focuses on the evolution of the Browse Basin continental margin from Late Cretaceous to Middle Miocene time. Based on the interpretation of the key seismic horizons described above, three sequence sets which consist of several high-frequency sequences have been defined and are discussed below (Mitchum Jr and Van Wagoner, 1991; Neal and Abreu, 2009). Sequence set in this study is defined as a combination of two or more than two sequences. Within a single sequence set, seismic reflections, lithologies and paleoenvironment are consistent. These sequence sets are Campanian to Paleocene, Eocene to Early Oligocene and Late Oligocene to Middle Miocene. Summary of the characteristics of each sequence set is shown in table 2.1.

Table 2.1 Summary of the main geological characteristics associated with each sequence sets.

Sequence Set	Boundaries	Seismic Character	Reflection Terminations	Age	Lithology	Paleo environment
Sequence Set 3 (SS3)	Top: Tmmio Base: Tolig	Chaotic amplitude in the southeast. The central and northwest portion is characterized by medium-amplitude, medium-continuity reflections with hummocky to subparallel patterns.	Temio truncates the underlying unit. Tolig is associated with downlaps in the overlying deposits	Late Oligocene-Early Miocene	Calcareite, calcilutite and chert	Reef growth system
Sequence Set 2 (SS2)	Top: Tolig Base: Tpal	High-amplitude and high-continuity in the southeast, change to medium-amplitude and medium-continuity in northwest. Hummocky patterns shown in central region, reflections with parallel patterns are found at the upper part.	The underlying offlaps against the top of sequence set 2. Occasional downlap terminations against Tpal.	Eocene-Early Oligocene	Fluvial and delta plain sandstone and siltstone, interbedded coals mostly occur within the lower part of this sequence set.	Fluvial to deltaic
Sequence Set 1 (SS1)	Top: Tpal Base: Kecamp.	Combination of medium and high amplitude, with medium continuity reflections; hummocky patterns at lower part, change to parallel-subparallel at the uppermost part of the easternmost region of the sequence set	Kecamp is conformably underlain by reflectors, overlying onlaps against the surface.	Campanian-Paleocene	Fine-grained sedimentation, shales and turbidite sands interbedded with calcareous claystone	Shelf incised canyon

2.3.1 Sequence Set 1: Campanian to Paleocene

Sequence set 1 includes the Kecamp to Tbase sequence and the Tbase to Tpal sequence. The base of this sequence set is defined by the Kecamp horizon, a major unconformity surface which is Early Campanian in age (Figure 1.3), is coincident with a sea level fall. A time structure map of this surface is provided in Figure 2.4. The upper boundary of sequence set 1 is defined by the unconformity surface Tpal (Figure 2.7). This surface has a relatively lower relief (~300 ms) compared to surface Tmmio and surface Temio, and is traceable over the entire 3D seismic area across the Browse Basin. A number of erosional surfaces have been recognized internal to this sequence set, however, only the significant ones have been interpreted in this research. According to the previous study (AGSO Browse Basin Project Team, 1997), lithology of sequence set 1 consists of fine-grained sediments, including shales, and muddy, sandy turbidite deposits interbedded with calcareous claystone (Table 2.1). Kronos-1 well data show a change from high gamma ray to relatively low gamma ray within the study interval, reflect the lithology of this interval composed mostly of mud, but become sandier in the upper portions of this sequence (Figure 1.8. 2.2). The seismic character of this sequence set is that of medium-continuity, medium- to high-amplitude reflections. Seismic amplitudes show hummocky patterns in the basal portions of sequence set 1. Seismic facies character changes to parallel-subparallel in the uppermost part of the easternmost region of the sequence set and likely indicate the fluvial facies within the interval.

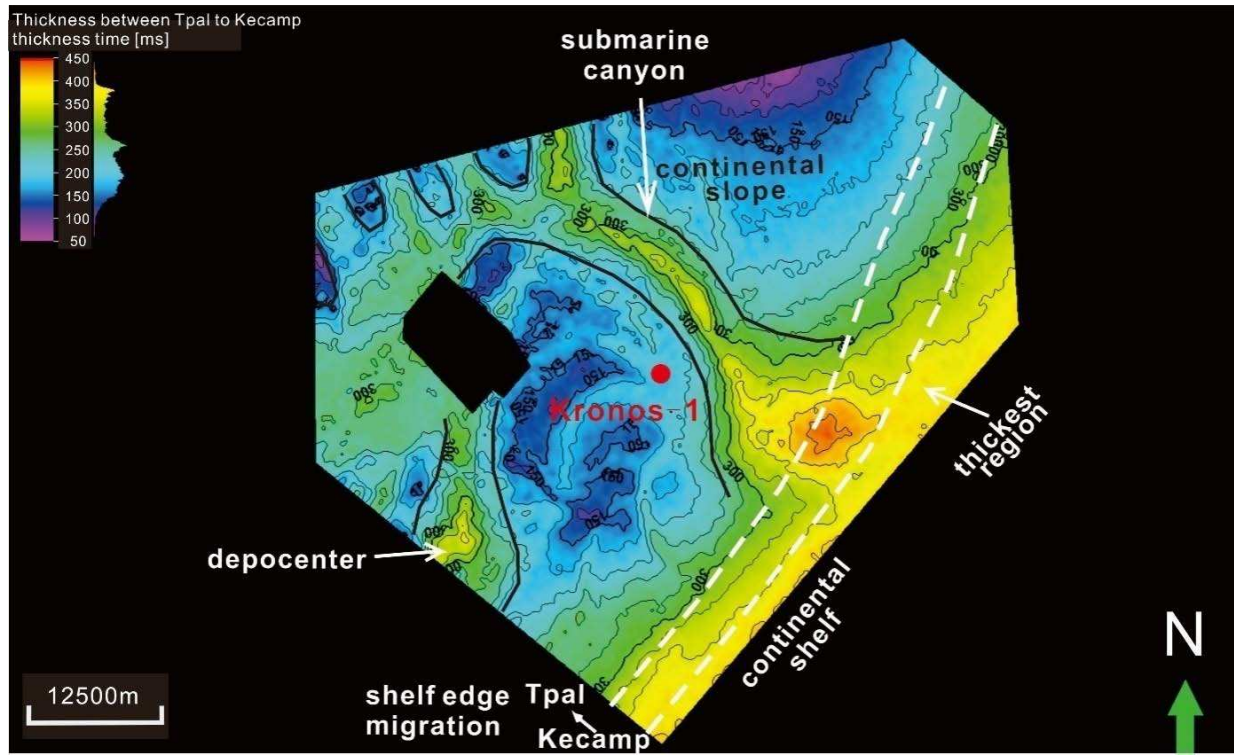


Figure 2.11 Isochron map for sequence set 1, bounded by Tpal and Kecamp. This map shows that the southeast area of the seismic data contains the thickest strata between horizon Kecamp and horizon Tpal. The unit does show a gradual thinning to the northwest from approximately 450 ms to 50 ms. A 60 km^2 ($7.5 \text{ km} \times 8 \text{ km}$), 250 ms thick unit is present at the central area of the southernmost portion of the dataset, and a northwestward oriented incision is clearly present in the data.

The isochron map for sequence set 1 (Figure 2.11) shows that the southeast area of the seismic data contains the thickest strata between horizon Kecamp and horizon Tpal. The thickness of sequence set 1 across most of the study area ranges from 100 ms to 300 ms. The unit does show a gradual thinning to the northwest from approximately 450 ms to 50 ms. A 60 km^2 ($7.5 \text{ km} \times 8 \text{ km}$), 250 ms thick unit is present at the central area of the southernmost portion of the dataset, and a northwestward oriented incision is clearly present in the data. The widest part of this incision is over 10 km, however the average width at the deepest point of incision is $\sim 5 \text{ km}$. Seismic reflections of this incision show bidirectional onlap against both steep sides of the incision (Figure 2.5). This submarine incision has a larger dimension than channel or gully that are generally hundreds of meters wide. This incision is interpreted to be a canyon. Multiple channel architectures can be found within the canyon, the average width of these channels is 600 m, and their average depth is $\sim 40 \text{ ms}$ (Figure 2.5). This canyon splits into multiple smaller branches downdip which transport sediments to the northern and northwestern portion of the shelf margin area. It is likely that these sediments feed several deep marine fans in more distal areas of the basin. Another depocenter is likely present in the southwestern region of the dataset. This sequence set is dominated by deposition within a shelf incised canyon which is filled with multiple phases of channelized fill.

2.3.2 Sequence Set 2: Eocene to Early Oligocene

Sequence Set 2 is bounded by horizons Tpal and Tolig. This sequence set includes Tpal to Teoc and Teoc to Tolig sequence. Teoc is a sequence boundary recognized by previous work from ConocoPhillips (2011) but it is not easily traced in this dataset. This

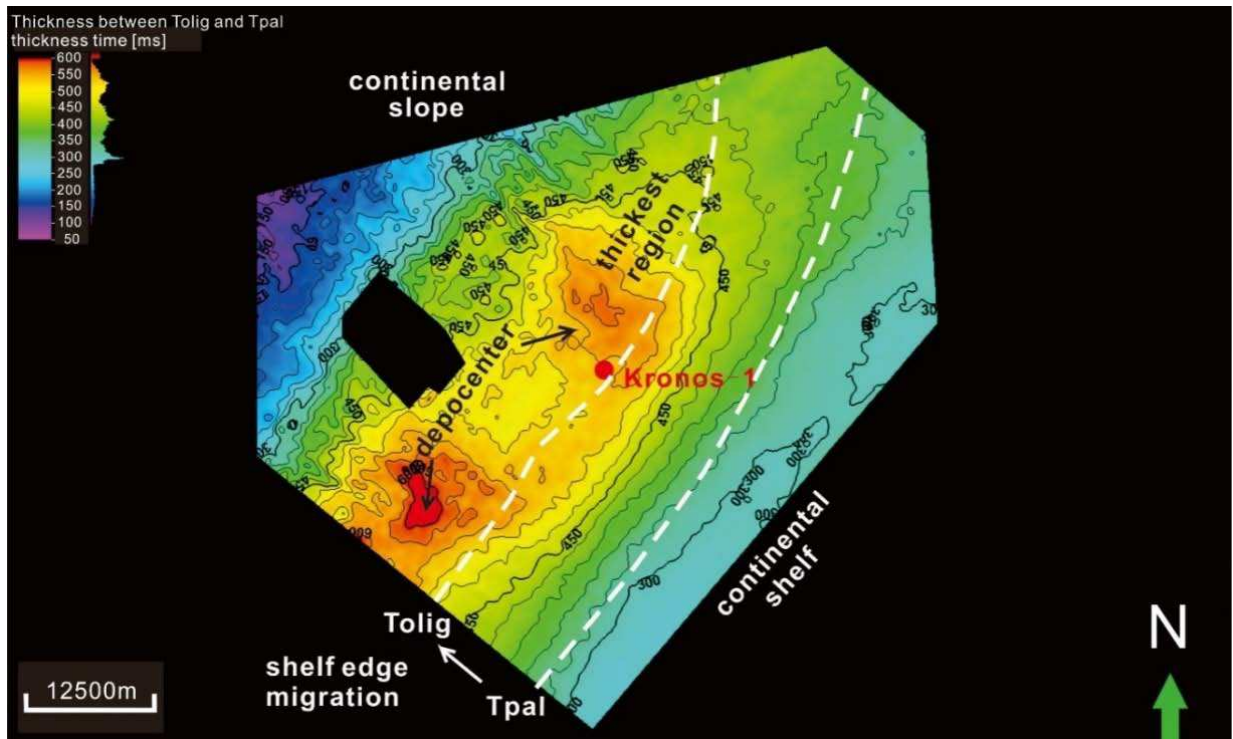


Figure 2.12 The isochron map for sequence set 2 indicates that throughout this interval, the thickest area is over the central part of the seismic data. The unit thickens from southeast to center from 300 ms to 600 ms and then thins to the northwest to approximately 100 ms , the northeast portion has a relatively thinner thickness as 400 ms compared to the center.

Sequence set represents the siliciclastic-dominated stage of deposition throughout the study area. The lower stratigraphic boundary of sequence set 2 is the Tpal unconformity (Figure 2.7). The Tolig unconformity (Figure 2.8) is the upper boundary of this sequence set. This unconformity separates sequence set 2 and sequence set 3 (Figure 2.1, 2.2) and marks a distinct shift from siliciclastic-dominated to carbonate-dominated deposition. Central and southeast portions of the study area at this time, show clinoforms with relatively steep dips thinning sharply toward the northwest (Figure 2.1, Figure 2.8). Study done by AGSO Browse Basin Project Team (1997) show that lithology associated with sequence set 2 comprises sandstone, siltstone and calcareous claystone, and interbedded coals information from the Kronos-1 well show a shifting from relatively high gamma ray to low gamma ray which remains low to the top of the sequence set. These low values are reflective of sandier lithology in the upper part of sequence set 2 (Figure 1.8). Seismic reflections within this sequence set show high-amplitude and high-continuity in the southeastern portion of the study area, gradually becoming medium-amplitude and medium-continuity in central and northwest portions of the study area. The seismic amplitudes of this interval show mostly hummocky patterns, especially in the northwest region. In the southeast region of this interval, reflection character is that of parallel-subparallel patterns. Central region of the seismic data is characterized by sigmoidal progradational reflections in dip view, indicate the deltaic system within this interval (Figure 2.1; Table 2.1).

The isochron map for sequence set 2 (Figure 2.12) indicates that this interval is thickest in the central part of the study area. The sequence set thickens from ~300 ms in the southeast toward this central region where sequence set 2 is over ~600ms thick.

Sequence set 2 thins to the northwest to approximately ~100 ms. The shelf edge migrates northwestward within this interval. The time period of Paleocene, Eocene and Oligocene is characterized by a thick, shelf margin prograding wedge (Figure 2.1). This sequence set is formed by siliciclastic shelf development. Sequence set 2 contains numerous channels (Figure 2.13). These low sinuous channelized incisions ($S=1.02-1.21$) are prolific at the base of sequence set 2 and they frequently cut down into the Cretaceous Puffin Formation, suggesting that they are slope gullies. Hundreds of small incisions incised on the foreset slopes, likely moved sediments from clinoforming topsets to toesets and into base of slope locations. Sequence set 2 is interpreted as a dominantly siliciclastic fluvial-deltaic deposit.

2.3.3 Sequence Set 3: Late Oligocene to Early Miocene

Sequence set 3 comprises the upper Oligocene sequence and Early Miocene to Middle Miocene sequence. The base of sequence set 3 is the Tolig unconformity. This surface marks the transition from dominantly siliciclastic deposition to dominantly carbonate deposition. The upper boundary is defined by the Tmmio unconformity (Figure 2.1). Work done by AGSO Browse Basin Project Team (1997) show the lithology of sequence set 3 to be primarily bioclastic carbonate and calcareous shales. Gamma ray from Kronos-1 well show a dramatic change near the base of sequence set 3, indicating a possible paleoenvironment change during Oligocene time (Figure 1.8). Seismic reflections within this unit is characterized by high-amplitude, high-continuity reflections in the southeast portion of the stud area, show hummocky to subparallel patterns, while the central and northwest portion of the study area is characterized by low-amplitude, low- to medium-continuity blank reflections, indicate the carbonate

system within this interval. Extremely large, complex sigmoid-oblique progradational reflections are also observed within this sequence set (Figure 2.1; Table 2.1). The continental margin of the study area transitions during this time from a siliciclastic-dominated margin to a mixed clastic-carbonate system. This seismic sequence set shows a thick wedge-shaped form with a sharp shelf break and a concave profile (Figure 2.1). The sequence set 3 isochron map (Figure 2.14) shows that interval thickens northwestward from approximately ~400 ms to ~800 ms, then thins to ~200 ms from the central region to the westernmost area. The shelf edge migrates northwestward within this sequence set. Sequence set 3 is dominated by progradation and is interpreted as a reef growth prograding system.

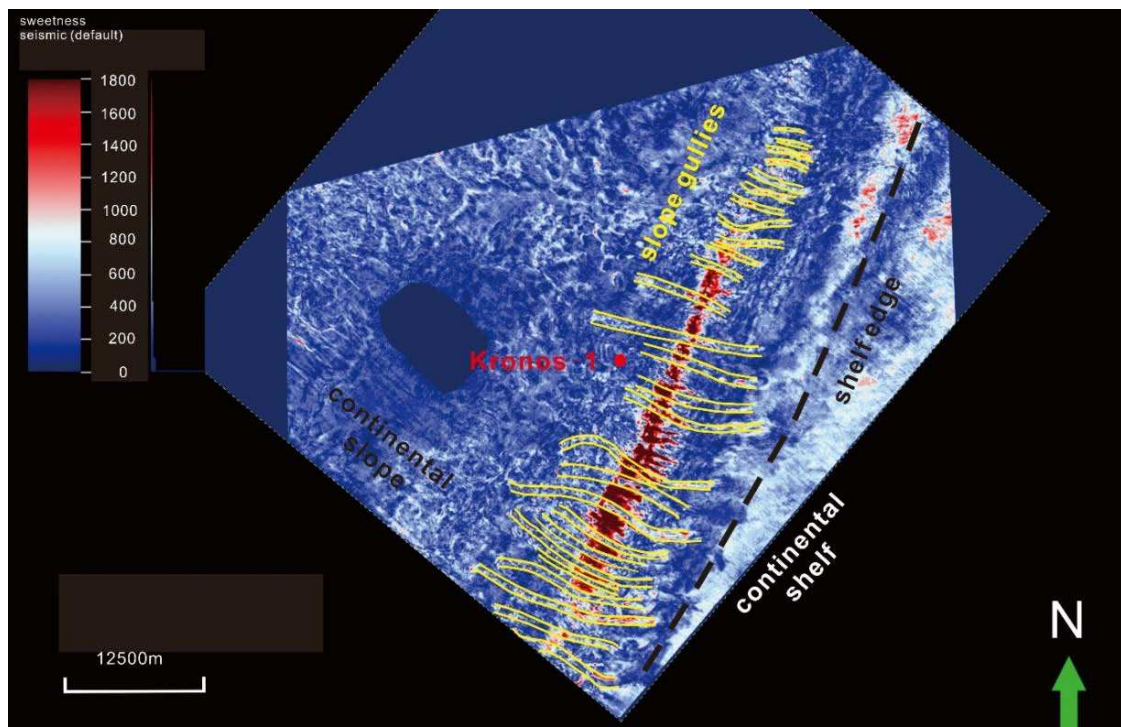


Figure 2.13 Sweetness attribute map showing gullies along the Tpal surface. These channel incisions are prolific at the base of sequence set 2 and they frequently cut down into the Cretaceous Puffin Formation

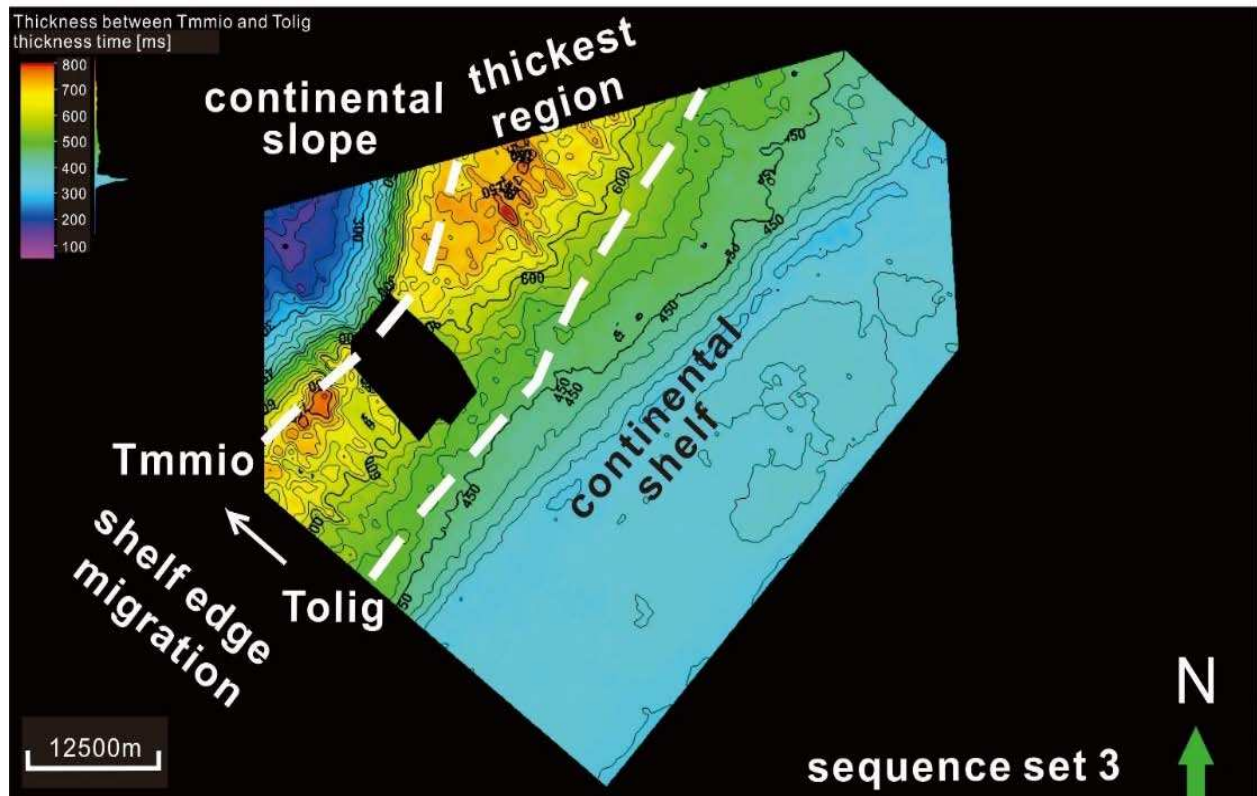


Figure 2.14 The sequence set 3 isochron map shows that interval thickens northwestward from approximately ~400 ms to ~800 ms, then thins to ~200 ms from the central region to the westernmost area. The shelf edge migrates northwestward within this sequence set.

CHAPTER 3

CONTRASTING CLASTIC TO CARBONATE CLINOFORMING MARGINS OF THE BROWSE BASIN

3.1 Introduction and Methodology

Interpreting continental margin architecture and the depositional morphological style of slopes from 3D seismic data is a basic, but challenging task for researchers (Fulthorpe and Austin, 1998; Posamentier and Kolla, 2003). Both carbonate-strata dominated and siliciclastic-strata dominated continental margins can develop clinoform-shaped architectures. This chapter will examine the nature and morphologic character of the Browse Basin of the Northwest Shelf of Australia (NWSA) at it transitions from a clastic-dominated to a carbonate-dominated margin.

Three shelf-to-slope-to-basin seismic profiles were chosen from the 3D seismic data; one located in the far west (A-A'), one located in the far east (C-C') and one located central to these other two (B-B') (Figure 1.7). From these seismic profiles, the shelf break points were marked for each clinoform in the profile, denoting the break between the clinoform topset and foreset at each time the margin was building. These data were used to examine the spatial and temporal variability through continental margin evolution. Shelf break points were connected to visually map the shelf trajectories through time to determine the nature of the shelf margin, as rising, falling or flat (Steel et al., 2003; Carvajal and Steel, 2006).

Researchers working on a variety of margin types worldwide, recognize three types of continental slope profile shapes; planar, concave and sigmoidal, each of which is

believed to correspond to several types of depositional environment (Adams et al., 1998; Adams and Schlager, 2000; Schlager and Adams, 2001). These shapes will be examined in time data along the Browse basin to gain insight into the nature of the margin over Cretaceous to Neogene time.

3.2 Classification of Siliciclastic Margin

A variety of classifications exist for siliciclastic continental margins. According to Carvajal et al. (2009), two types of siliciclastic shelf-margins have been recognized based on clinoform height and water depth (Figure 3.1). Low-to-moderately deep-water margins have clinoforms less than 1000 m high, and very deep-water margins produce clinoforms more than 1000 m high. Carvajal et al. (2009) studied 12 shelf margins all around the world including quantifying the progradational rate and aggradational rate of the clinoforms forming these margins. The authors noted that a margin along its extent can exhibit progradation and aggradation simultaneously, but for one spot, it is dominated either by progradation or aggradation. On very deep-water margins (Gulf of Mexico, North West Borneo and Orinoco regions of the northeastern South American margin), aggradation rates (100's to 1000's of meters/my) reach high values, the progradation rates are relatively low (7 to 30.5 km/my) (Carvajal et al. 2009). In contrast, the low-to-moderate deep-water margins (Lewis-Fox Hills, Spitsbergen and North Slope) show very high progradation rates (1 km/My to 61 km/My) but low aggradation rates (less than 270 m/My) (Carvajal et al. 2009). The reduced space at the front of any margin provides for rapid fill of accommodation and thus higher progradation rates.

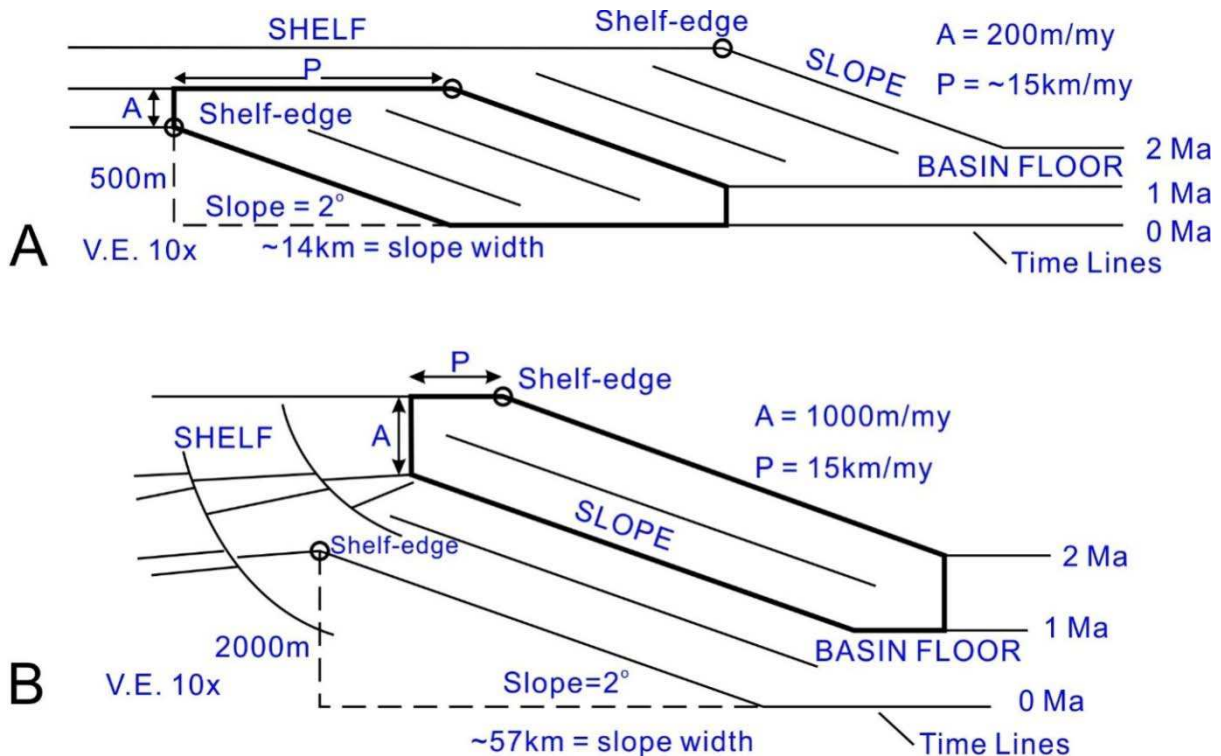


Figure 3.1 Two types of siliciclastic shelf margins, modified after Carvajal et al., 2009. A) showing clinoform growth in moderately deep water basins (<1000 m water depth), and B) showing clinoform growth in very deep water basins (>1000 m water depth).

Prograding distance can be measured in meters along seismic profiles. However the measure of the amount of aggradation in similar meters requires time-to-depth information for conversion. The calculation of the depth/thickness in meter is converted from time and the subsequent meters of thickness measure can be used to calculate progradation/aggradation ratio (ie., P/A). The check-shots data from the Kronos-1 well provides these data for the study area (Appendix A). Since only one well is available, the time-depth relationship at Kronos-1 well is applied to the entire study area. The use of these data for such conversions decreases in certainty as we move away from the Kronos-1 well but such is a common approach in other studies of the Browse margin (Rinke-Hardekopf, et. al., 2018).

The check-shots data includes the relationship between measured depth, true vertical depth from SRD, two-way vertical time and average interval velocity. ConocoPhillips (2011) provides the interval velocity for every 15.1 or 15.2 m, nearly 200 interval velocity measurements are provided in Appendix A over the study interval from Kecamp to Tmmio. Measured depths of key surfaces are also offered by ConocoPhillips (2011) in their well reports, and the corresponding true vertical depths and two-way vertical time of the key surfaces taken from these reports.

Three sequence sets (Kecamp-Tpal, Tpal-Tolig, Tolig-Tmmio) are bounded by six key surfaces. This study uses the average velocity of each sequence sets to calculate the time-depth conversion of shelf edge aggradational rate. The average interval velocity of the three sequence sets are shown in Table 3.1. The calculation of the average interval velocity of Kecamp-Tpal, Tpal-Tolig, Tolig-Tmmio units is based on the 200 average interval velocities(Appendix A). With the two-way vertical time of surfaces Kecamp, Tpal, Tolig and Tmmio, the corresponding average velocity in 15.1 m interval of these four surfaces can be found from Appendix A, and we utilize the numerous average interval velocities (in 15.1 m interval) within a single sequence set. Finally, the sequence set average interval velocity is calculated using the total of all the interval velocity bins within that sequence set and dividing by the total number of velocity bins within the sequence set. Results show that the average interval velocity of the Kecamp-Tpal sequence set is 4111.7 m/s, of the Tpal-Tolig sequence set is 4497.4 m/s and of the Tolig-Tmmio sequence set is 3769.3 m/s. The aggrading distance in meter equals to 1/2 two-way vertical time (s) multiplied by the average interval velocity (m/s).

Table 3.1 Measured depth, true vertical depth from SRD, two-way vertical time and average interval velocity for sequence sets 1, 2 and 3.

	Measured Depth	True Vertical Depth From SRD (m)	Two-way Vertical Time (s)	Average Interval Velocity (m/s)
Tmmio	1737	1715.0	1.6344	
SS3				3769.3
Tolig	2443	2420.8	2.0067	
SS2				4497.4
Tpal	3674	3652.7	2.5580	
SS1				4111.7
Kecamp	4064	4041.5	2.7499	

The model built by Carvajal et al., (2009) discussed the relationship between aggradation rate, progradation rate and water depth in siliciclastic systems. In this study, the Kecamp-Tolig interval is clastic dominated. The progradation rate and aggradation rate is measured and calculated within the Kecamp-Tolig unit on the western (A-A'), central (B-B')and eastern (C-C') profiles (Figure 1.7). Average interval velocity of Kecamp-Tpal and Tpal-Tolig are applied to time-depth conversion in different sequence sets, respectively. Results show that the study area, has a relatively high aggradation rate (A) of 22.7 m/My and 35.5 m/My in Kecamp-Tpal interval and Tpal-Tolig interval, respectively, and low progradation rate (P) of 0.13 km/My and 0.43 km/My within Kecamp-Tpal unit and Tpal-Tolig unit, respectively (Table 3.2). Since this time period shows the margin to have a water depth of more than 1000 m across the shelf break, such P and A behavior is in keeping with the observations of Carvajal.

The shelf-edge trajectory changes in the study area reflect the influence of sea level change on margin development. The spatial variability of the trajectory patterns between the western, central and eastern regions of the study area are driven by

Table 3.2 Aggradation rate (A) and progradation rate (P) of siliciclastic dominated margin in study area. P. refers to progradation, while A. refers to aggradation.

Interval	Vavg (m/s)	Seismic Profile	A (ms)	A (m)	P (km/My)	Time (My)	Arate (m/My)	Prate (km/My)	Average A rate	Average Prate
Tpal-Tolig	4497.4	western profile	420	945	12.3	27.9	33.9	0.4	35.5	0.43
		central profile	450	1012	13.9	27.9	36.3	0.5		
		eastern profile	450	1012	10.0	27.9	36.3	0.4		
Kecamp-Tpal	4111.7	western profile	272	600	3.9	28.6	21.0	0.1	22.7	0.13
		central profile	220	485	3.3	28.6	17.0	0.1		
		eastern profile	390	860	4.3	28.6	30.1	0.2		

differences in sediment supply to portions of the margin. The shelf-edge trajectories, as mapped from seismic cross-sections, can be used as an indicator of relative shoreline movements, or a change in “base-level” through time. Any fall in relative sea-level causes a falling shelf-edge trajectory, whereas a rise in relative sea-level can cause a rising shelf-edge trajectory (Johannessen and Steel, 2005). Although the seismic dataset were not depth converted or decompacted, the comparison of the trajectory style in Poseidon 3D dataset, with a limited area can still be used to get a general sense of the relative sea level change.

Within the Tpal-Tolig interval, both the western (Figure 3.2B) and central profiles (Figure 3.3B) show a nearly flat trajectory following with a slightly rising behavior. Location of the profiles are indicated in Figure 1.7. The rising trajectory shows both aggradation and progradation, suggesting a relative sea-level rise during this clastic-dominated phase. From Tolig to Tmmio, a relatively flat trajectory followed by a rising trajectory is observed. This stationary to rising trajectory suggests the margin was

growing dramatically upward by whatever means from Tolig to Tmmio time. Since the continental margin is dominated by carbonate during Tolig-Tmmio, reef growth is the likely cause for the rise in trajectory. Although some clastics were reported in the Kronos-1 well, it seems unlikely that these could overwhelm the carbonate processes, especially since subsidence was increasing along this margin and driving sea level upward. On the eastern seismic profile (Figure 3.4B), we see a rising trajectory observed from Tpal to Tolig, a flat trajectory developed from Toilg to Temio time, and a backstepping trajectory after Temio. In general, the relative sea-level rises in the study margin during Paleogene and Neogene time. However, in the eastern portions of the study margin, in contrast, backstepping trajectory is likely a lack of reef buildup accompanying this rise in sea level and a clear lack of clastics to fill the void.

3.3 Classification of Carbonate Margin

Three basic types of continental slope profiles (planar, concave and sigmoidal) have been recognized on margins around the world, with each defining a mathematical expression of margin shape (Adams and Schlager, 2000) (Figure 3.5). The study of these three expressions can offer a clue to the slope system origination and provide a method to discuss and compare continental slopes which developed from various settings.

The carbonate margins can be classified as three types, rimmed margins, non-rimmed margins and margins that include slope shedding (Kenter et al, 2005), and each of these has a corresponding seismic profile and mathematical expression (Figure 3.5). The most common curvatures on rimmed margins are exponential, with almost 50 percent of carbonate continental slopes exhibiting exponential profiles (Adams and

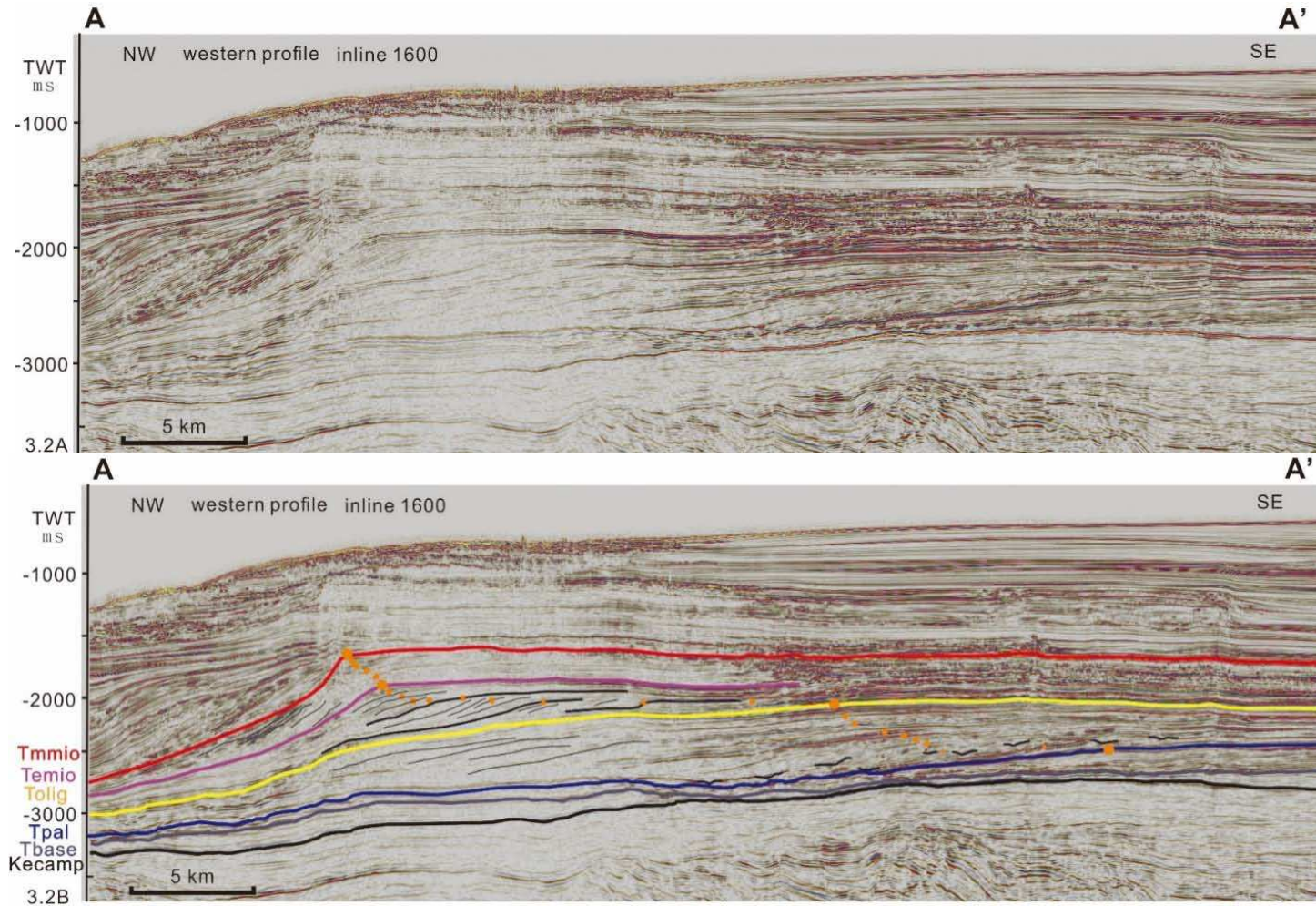


Figure 3.2 Western dip-oriented (southeast-northwest) seismic profile showing the shelf-edge positions (orange dots) relative to times, as well as the profile of siliciclastic slope, sequence boundaries are shown in their defined colors. Location of the profile is shown in Figure 1.7 (A-A').

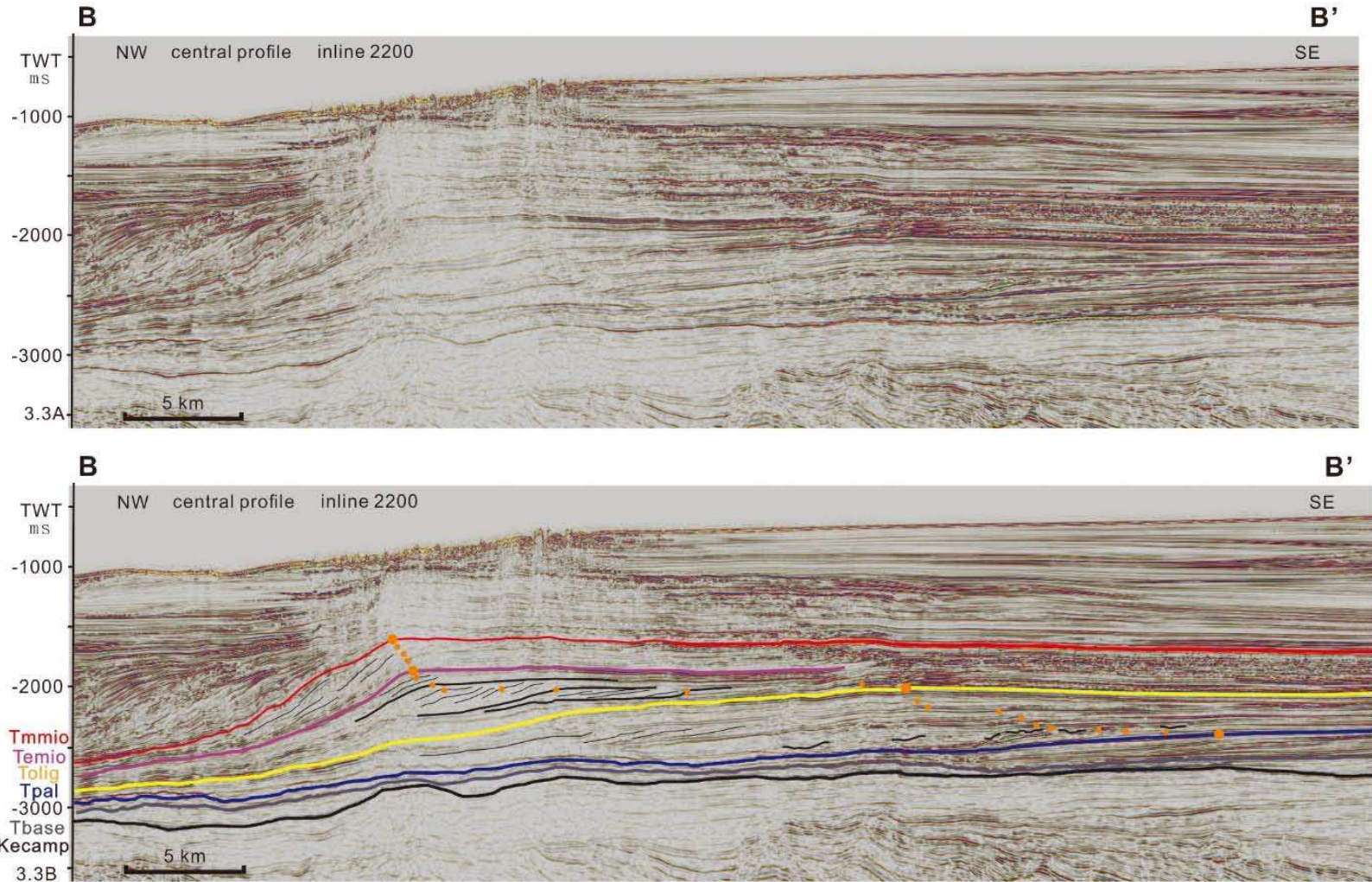


Figure 3.3Central dip-oriented (southeast-northwest) seismic profile showing the shelf-edge positions relative to times, as well as the profile of siliciclastic slope. Location of the profile is shown in Figure 1.7 (B-B')

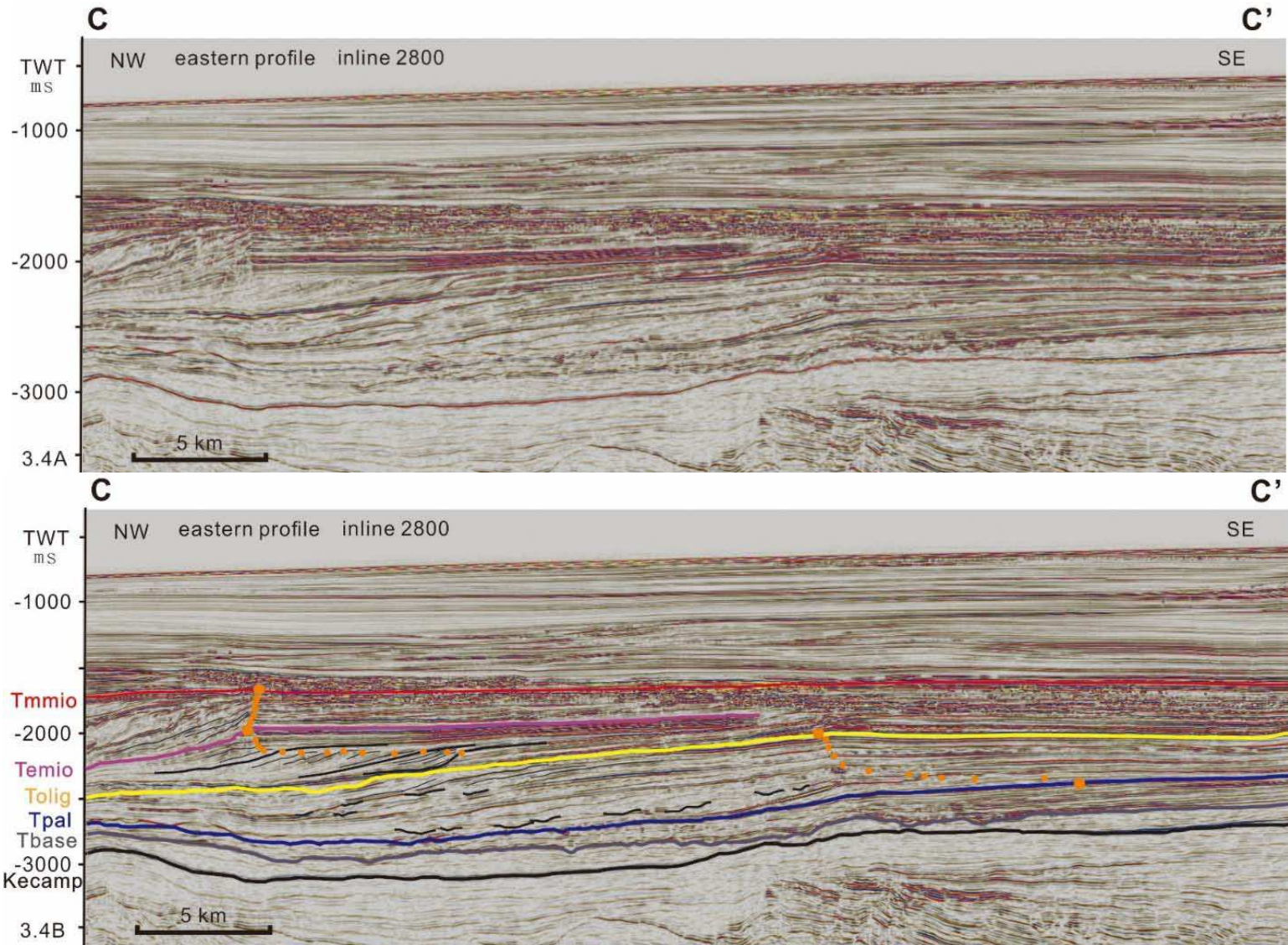


Figure 3.4 Eastern dip-oriented (southeast-northwest) seismic profile showing the shelf-edge positions relative to times, as well as the profile of siliciclastic slope. Location of the profile is shown in Figure 1.7 (C-C').

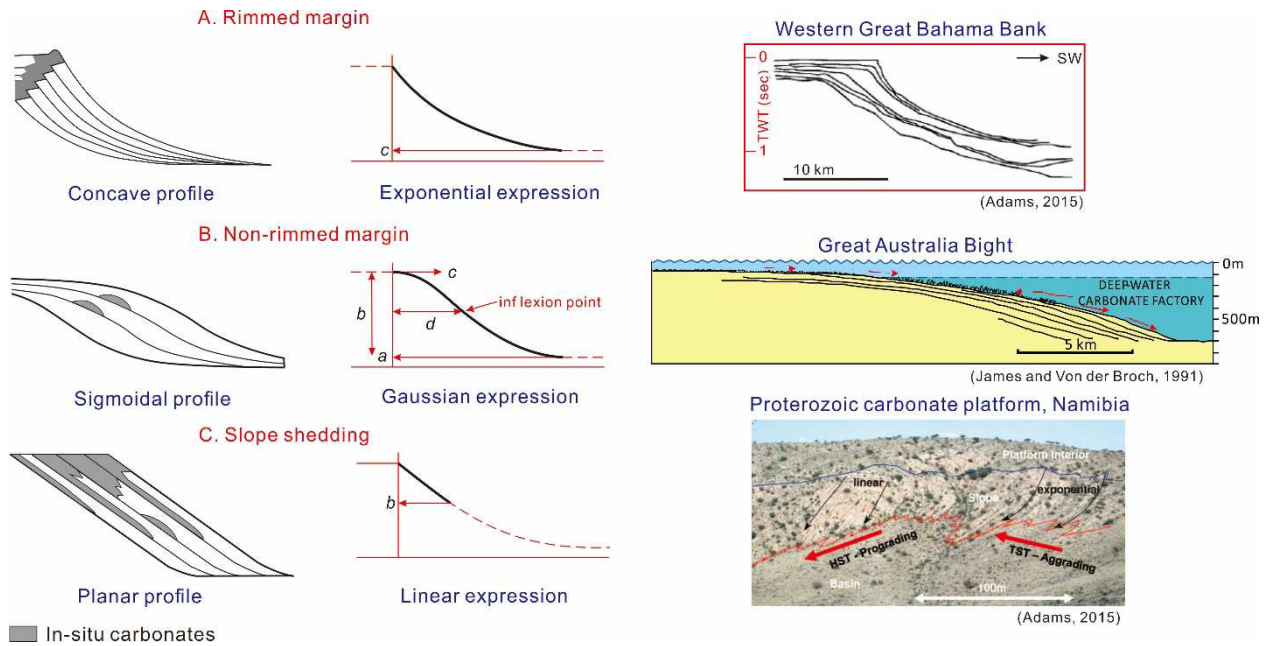


Figure 3.5 Classification of carbonate slopes and the corresponding mathematical expressions. A) Rimmed margins always exhibit slopes with concave profile, the descriptive expression is exponential, an example from Western Great Bahama Bank is observed (Adams and Kenter, 2014). B) Sigmoidal profile and the corresponding Gaussian expression is common of the non-rimmed margins, the example is the Great Australia Bight (James and Christopher, 1991). C) Carbonate margins that include slope shedding always show planar profile, the example of this type of carbonate margin has been found in Proterozoic carbonate platform, Namibia (Adams and Kenter, 2014).

Kenter, 2014). This type of profile is characterized by a sharp shelf break and an exponential-shaped slope curvature (Figure 3.5) (Kenyon and Turcotte, 1985). The causal mechanism for this shaped profile is that the ratio between the rate of vertical fluctuations of sedimentary base level and the rate of horizontal slope progradation is relatively small (Adams and Kenter, 2014). Therefore, carbonate continental shelves are stable vertically, and a rimmed platform builds, forming an exponentially curved slope. In contrast, the Gaussian profile is common on the non-rimmed carbonate margins. The profiles from carbonate continental slopes absent of a protective and stable reef are Gaussian shaped. Lack of a rimmed stable reef, means that the shelf edge is easily

reworked by storm and high-energy wave processes. The third type, the linear profile, develops in a non-rimmed carbonate setting, due to biotically-induced, slope-stabilizing microbial "reefs" (Adams and Kenter, 2014).

Although time-depth conversion or decompaction was not applied to the seismic data in the study area, it is our intent to simply compare these margins internally to the Browse Basin. The comparison of the continental margin curvature through time can show some relationship between the reef growth and margin profile within this certain region. This shape is considered in this analysis however caution must be used in direct comparison to other worldwide margin shapes.

The western profile shows what appears to be steep reef growth from Oligocene to Middle Miocene time (Figure 3.6A). This seismic morphology is supported by the well data and regional publications (Rinke-Hardekopf, et. al., 2018). The development of the reef inhibited erosion, and promoted progradation. The Tertiary to Tammio time carbonate slopes show the exponential curvature reflecting what Adams and Schlager (2000) would define as a rimmed margin basin. The reef forming the rimmed margin on the western profile extends laterally to the central profile (Figure 3.6B), where the continental slope shows a similar curvature as the western profile but with a slightly lower angle. The eastern seismic profile appears to show a flatter profile and appears to be a more non- reef rimmed margin (Figure 3.6C).

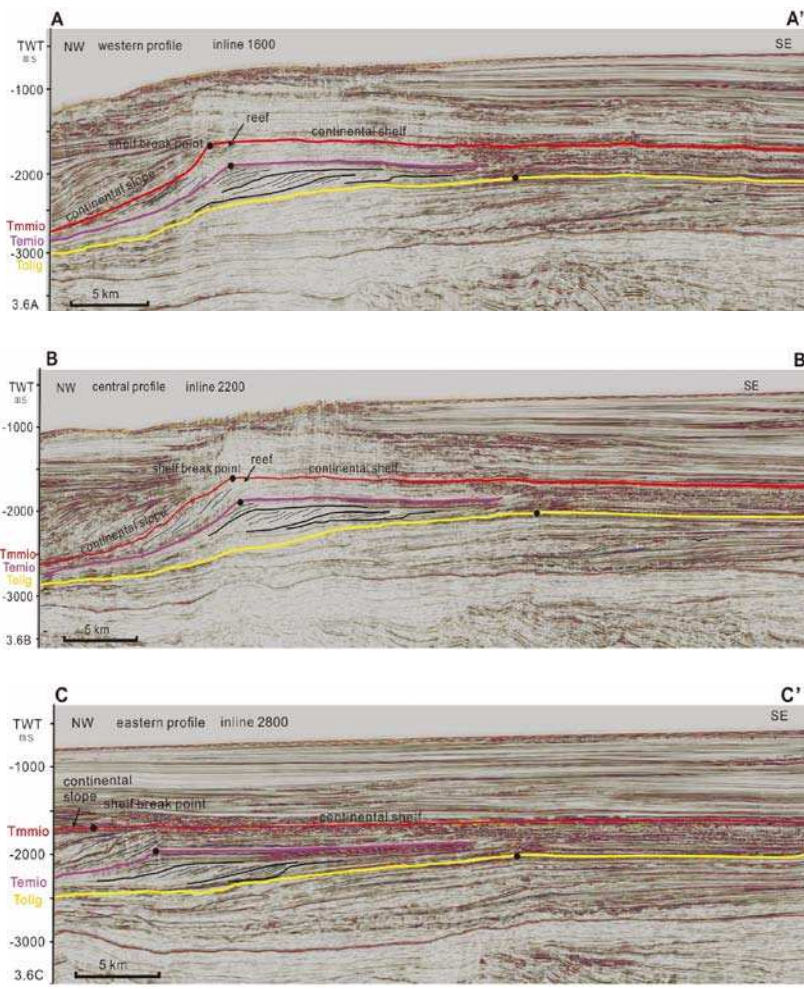


Figure 3.6 Seismic lines extracted from the 3D seismic data set of the Browse Basin study area and used to examine temporal and spatial changes in margin shape. Western profile 3.6A and central profile 3.6B of the study area show an exponential curvature of the carbonate margin, reflecting its development as Rimmed Margin basin. The eastern profile 3.6C has a slight concave or straight curvature, suggests it developed as a Non-rimmed Margin basin. Location of the profiles are shown in Figure 1.7.

CHAPTER 4

MORPHOLOGY OF SLOPE GULLIES

4.1 Morphology of Slope Gullies

Slope gullies are the primary conduits to transport sediments from the shelf edge into the deep basin (Lonergan, 2013). An abundance of slope gullies developed within the Browse Basin continental slope during Eocene and Oligocene. They are not stationary on the slope, but migrate through time. Gully fills show relatively high amplitude, pod-shaped reflections in seismic. In this study, significant slope gully incision is observed within sequence set 2, the interval bounded by the Tpal and Tolig unconformities. During this time, the continental margin was dominated by siliciclastic sedimentation. In contrast, the interval bounded by Tolig and Tmmio is dominated by carbonate sedimentation and slope channels are rarely observed.

Variations exist in Tpal-Tolig time gully morphology both spatially and temporally. Morphometrics of slope gullies were collected from sweetness maps and seismic profiles. The sweetness attribute was applied to the 3D Poseidon seismic cube, and the resulting attribute cube was flattened on horizon Tpal. Four attribute slices; A, B, C and D, with A being the oldest and D being the youngest were extracted from the cube parallel to the Tpal horizon. Sweetness maps A, B, C and D were interpreted for seismic geomorphologic character in the interval Tpal-Tolig (Figure 4.1). The architecture and morphology of the slope gullies record erosion, deposition and migration history of the continental slope.

Slope gully widths are measured in meters, however thicknesses were measured in milliseconds. According to the method of time-depth conversion discussed in chapter 3, the average interval velocity applied in this interval is 4497.4 m/s. The Tpal-Tolig interval averages 550 ms in thickness which calculates to ~ 1200 meters. However, gully measurements were collected across this interval in three sub-intervals; the lower 183 ms, the middle 183 ms and the upper 183 ms. To convert their thickness from time to depth, a more detailed parsing of interval velocity was done (see Table 4.1). Resulting interval velocities for the lower, middle and upper intervals as 4527.3 m/s, 4781.6 m/s and 4169.8 m/s, respectively. Therefore, slope gully thickness in milliseconds is converted to meters using the formula of 1/2 two-way vertical travel time (ms) times the average interval velocity (m/s).

Table 4.1 Table showing measured depth, true vertical depth, two-way vertical time and average interval velocity of surface Tpal, Tolig and boundaries which separate the lower part, middle part and upper part of Tpal-Tolig unit.

	Measured Depth (m)	True Vertical Depth From SRD (m)	Two-way Vertical Time (s)	Average Interval Velocity (m/s)
Tolig	2443	2420.8	2.0067	
				4169.8
middle/upper	2828.5	2806.3	2.1920	
				4781.6
lower/middle	3267.0	3244.7	2.3762	
				4527.3
Tpal	3674	3652.7	2.558	

4.2 Observations

Sweetness attribute map A (Figure 4.2) is the lowermost interpreted attribute map for the study of slope gullies. The average interval velocity applied in time-depth conversion of slope gullies on attribute map A is 4527.3 m/s. A total of 27 slope gullies

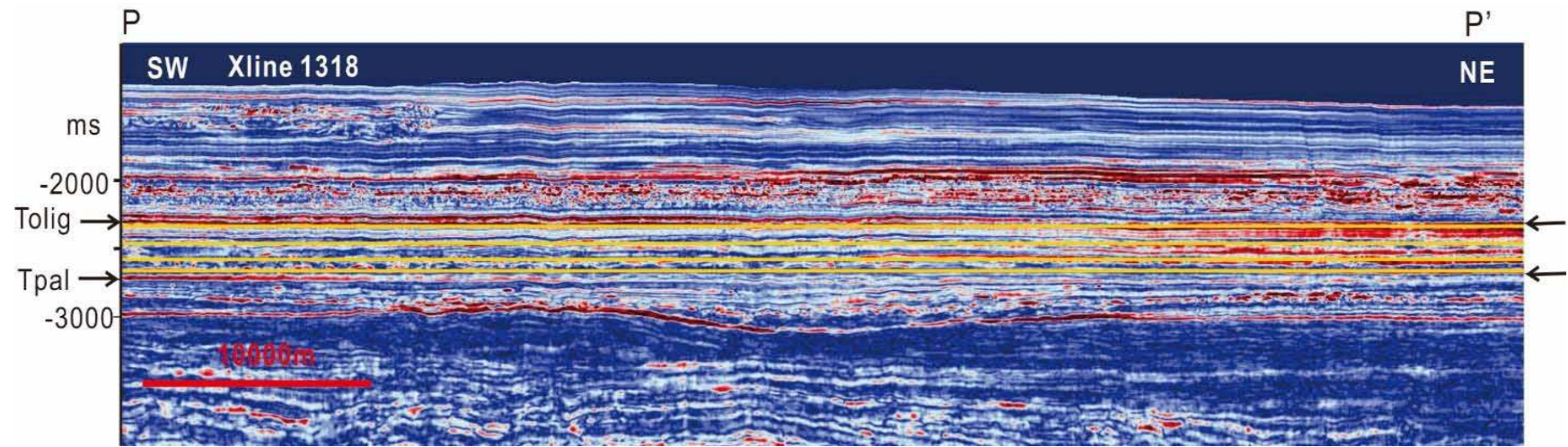


Figure 4.1 Seismic cross-section line 1318 extracted from the sweetness cube showing the location of four attribute slices; A, B, C and D used to identify and measure the shape, size and orientation of slope gully channels in the lower, middle and upper portions of the Tpal-Tolig sequence set 2. Location of unconformity Tpal and Tolig is marked on the profile. Location of this seismic profile is shown in Figure 1.7.

are observed on this surface. From southwest to northeast, each gully is numbered in order from 1 to 27. Gullies on this map are straight to slightly sinuous with sinuosities ranging from 1.02 to 1.21, and are arranged parallel to each other along the slope. The density between gully 1-11 and 17-27 is higher than that of gullies 12-16. Gullies range from 250 to 950 m wide, are 45-140 m (20-60 ms) deep and are 2 to 11 km long. A scatter plot of these gully morphometrics reveal a bi-model distribution (Figure 4.3). Gullies 1-16 are relatively wider, deeper and longer in contrast to gullies 16-27 (Figure 4.3, Table 4.2). Gullies 1-16 are approximately 600-950 m wide, 90-140 m (40-60 ms) deep, all are over 10 km long. Gullies 17-27 are located in the northeast portion of the slope, dimensions ranging from 250-600 m wide, are 40-80 m (20-35 ms) deep and are 2-10 km long. The depth and width are positively correlated with depths increasing as widths increase. The aspect ratio of slope gullies on attribute map A ranging from 5.4-8.8, the average aspect ratio is 7.1. Gully cross-section shown in Figure 4.4 represent the gullies developed on attribute map A, the lower 1/3 of the Tpal-Tolig interval. Both map and seismic profile show that only a few gully complexes are observed from this surface.

Sweetness attribute map B (Figure 4.5) is extracted an average of 90 ms shallower in the data than attribute map A. Slope gullies were not well developed on this surface, but six low sinuosity gullies ($S=1.03-1.22$) are mapped (length on gullies 1 and 2 may be overlie short due to data margin limits and thus only width and depth are collected). These gullies show a near constant width at 700-850 m wide, are 110-145 m (45-60 ms) deep and are approximately 10-20 km long (Fig. 4.5, 4.6; Table 4.3). Four gullies are developed in the southern portion of the study area. They are remarkably

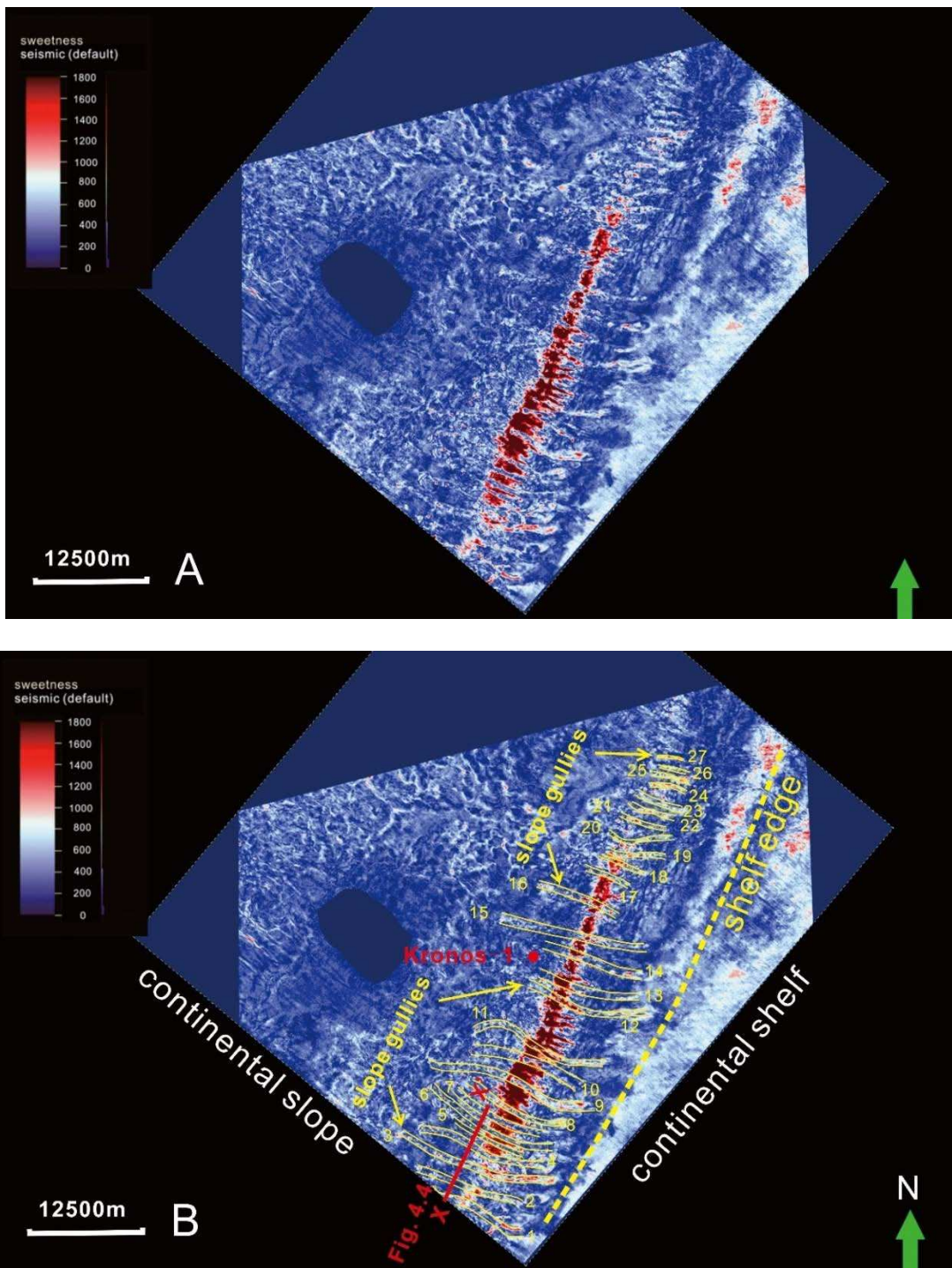


Figure 4.2 Sweetness attribute map A. A) Uninterpreted attribute map A. B) Interpreted attribute map A showing the paleogeomorphology and gully development for the lowermost 1/3 of the Tpal-Tolig interval. A total of 27 slope gullies are observed on this surface. From southwest to northeast portion, each gully is numbered in order from 1 to 27. The red line (X-X') marks the location of the seismic profile in Figure 4.4. In this map, blues represent low sweetness and reds represent high sweetness.

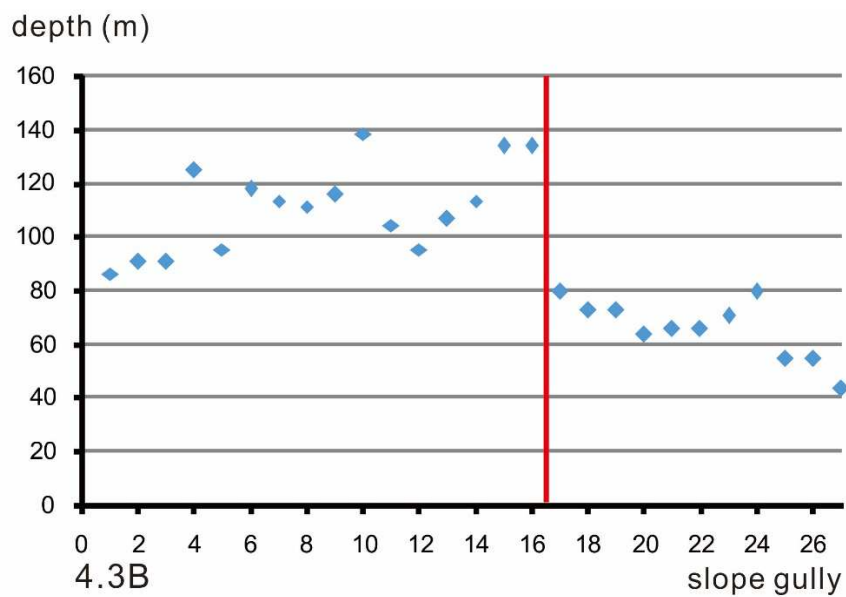
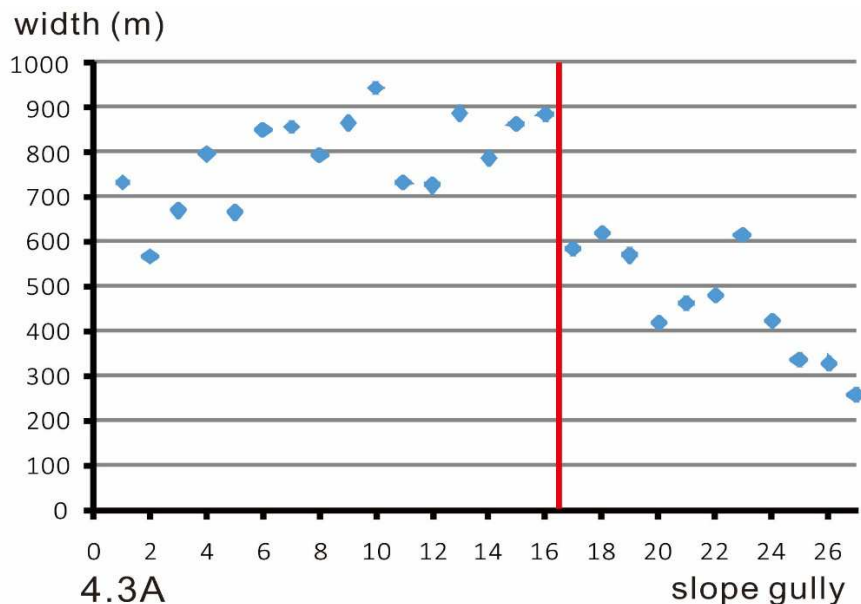


Figure 4.3 Scatter diagram showing the dimensions of the slope gullies on attribute map A. Two groups of gullies are recognized. Gully 1-16 are relatively wider, deeper and longer in contrast to gully 17-27. The depth and width keeps a positive relationship as the depths increase while widths increase.

Table 4.2 Summary of the slope gully dimensions collected from Map A. Average interval velocity applied in this calculation is 4527.3 m/s.

	width(m)	depth(ms)	depth (m)	straight length (m)	actual length(m)	sinuosity	aspect ratio
1	732	38	86	10616	12038	1.13	8.5
2	565	40	91	12619	13698	1.09	6.2
3	670	40	91	18764	21200	1.13	7.4
4	796	55	125	14918	17500	1.17	6.4
5	664	42	95	9312	11010	1.18	7.0
6	850	52	118	14753	16742	1.13	7.2
7	859	50	113	11212	12815	1.14	7.6
8	793	49	111	13058	14808	1.13	7.1
9	865	51	115	21346	25980	1.22	7.5
10	946	61	138	12486	13973	1.12	6.9
11	733	46	104	15369	18700	1.22	7.0
12	726	42	95	12665	14900	1.18	7.6
13	888	47	106	11489	12911	1.12	8.3
14	787	50	113	10819	11500	1.06	7.0
15	863	59	134	16951	18000	1.06	6.5
16	885	59	134	9370	10100	1.08	6.6
17	583	35	79	6194	6380	1.03	7.4
18	620	32	72	6085	6253	1.03	8.6
19	570	32	72	7074	8317	1.18	7.9
20	419	28	63	7932	9600	1.21	6.6
21	462	29	66	6382	7090	1.11	7.0
22	480	29	66	5704	6374	1.12	7.3
23	615	31	70	5982	6210	1.04	8.8
24	424	35	79	4552	4920	1.08	5.4
25	335	24	54	4600	4725	1.03	6.2
26	326	24	54	3175	3280	1.03	6.0
27	256	19	43	2735	2960	1.08	6.0

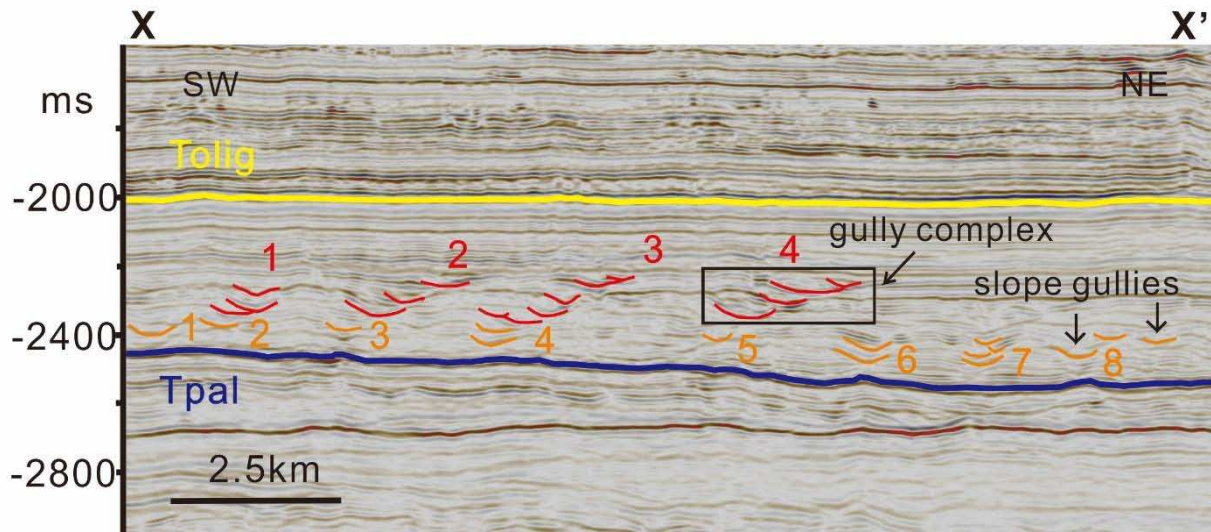


Figure 4.4 Seismic random cross-section line, location is shown in Figure 4.2 and 4.5 (X-X'). Gullies imaged in Map A are shown in orange and gullies imaged in Map B are shown in red. Individual gullies appear to stack vertically (orange) or laterally (red) into gully complexes with thicknesses of up to 450 m (200 ms). Gully migration at Map B time is towards the northeast.

parallel and evenly spaced at 1400-1500 m. Two single gullies formed on the northern slope. The northernmost gully is formed by the merger of two smaller gullies which are both approximatley 500 m wide and 80 m (35 ms) deep (Figure 4.5). The aspect ratio of slope gullies on attribute map B ranging from 5.6-6.3, the average aspect ratio is 6.0. Gully complexes in the attribute map B interval are marked on the seismic profile with a red color (Figure 4.4). The complexes are composed of three to four gully-forms in a single complex. These complexes can be up to 480 m (200 ms) thick, with gullies stacked in vertical patterns and shifting laterally to northeast through time. Slope gullies developed on Map B are located within the middle 1/3 of the Tpal-Tolig unit. The average interval velocity applied in time-depth conversion of slope gully thickness on Map B is 4781.6 m/s.

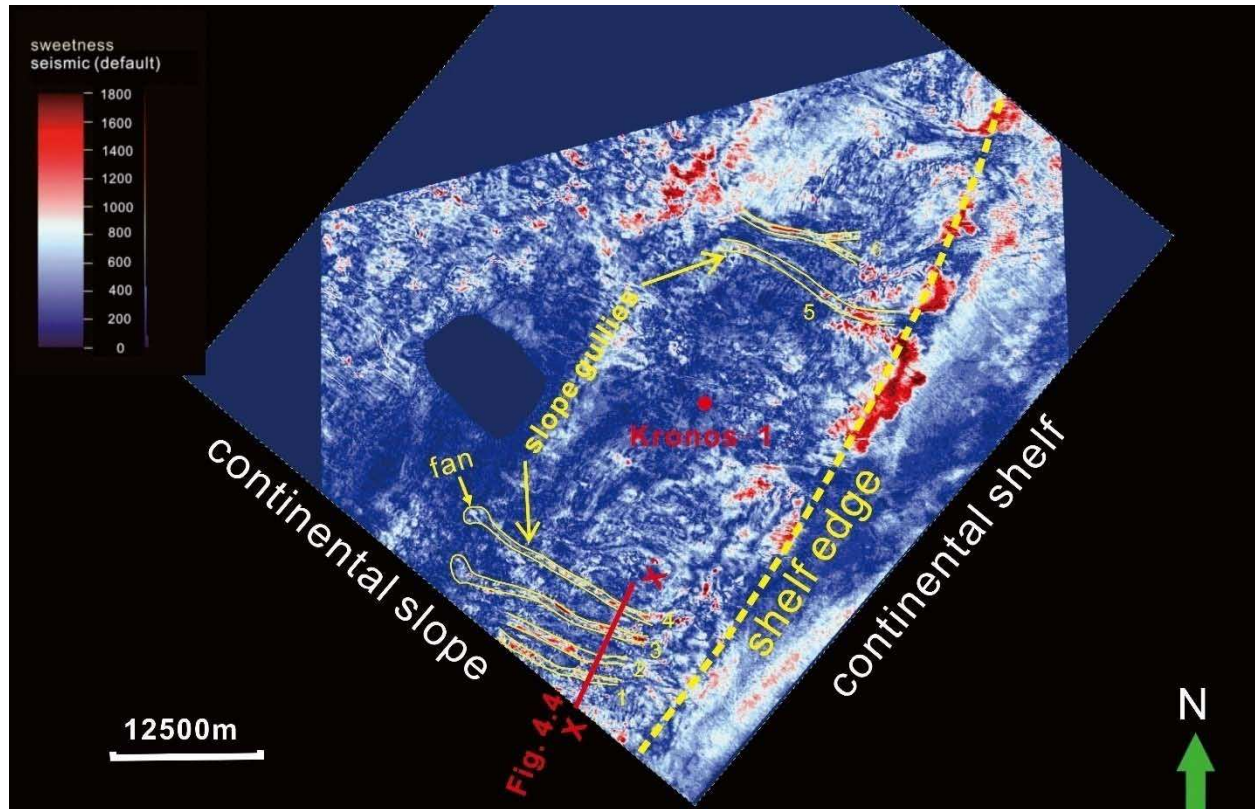


Figure 4.5 Sweetness attribute map B showing the paleogeomorphology and gully development for the middle 1/3 of the Tpal-Tolig interval. A total of six slope gullies are observed on this surface. From southwest to northeast portion, each gully is numbered in order from 1 to 6. The red line (X-X') marks the location of the seismic profile in Figure 4.4. In this map, blues represent low sweetness and reds represent high sweetness.

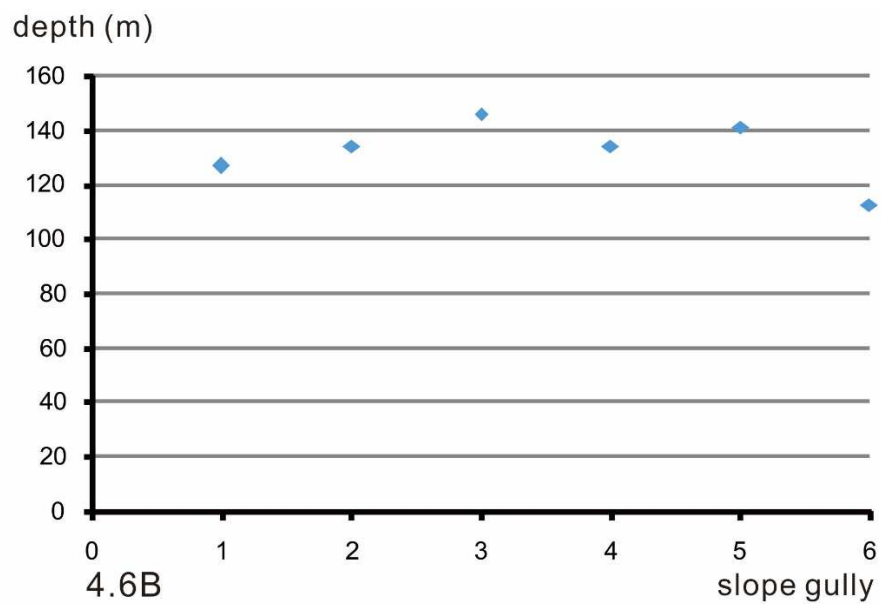
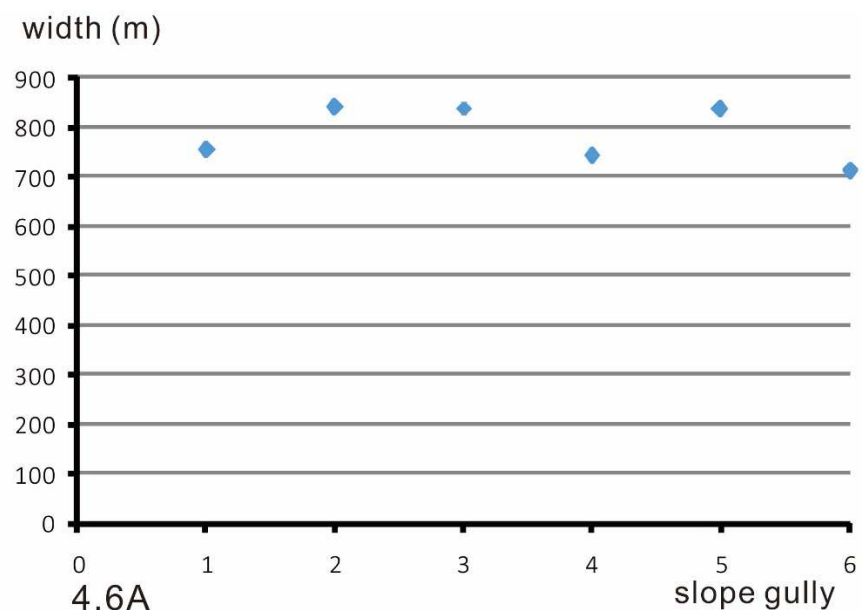


Figure 4.6 Scatter diagram showing that gullies along attribute map B remain constant dimensions at the range of 700-850 m wide, 110-145 m (45-60 ms) deep and approximately 10-20 km long. Widths and depths for these six gullies show much less variation than gullies found in the older portions of this interval.

Table 4.3 Summary of the slope gully dimensions on attribute map B. Average interval velocity used in this calculation is 4781.6 m/s.

	width(m)	depth(ms)	depth (m)	straight length(m)	actual length(m)	sinuosity	aspect ratio
1	755	53	127	11543	12800	1.11	6.0
2	841	56	135	12198	13200	1.08	6.3
3	840	61	146	19525	20500	1.05	5.8
4	744	56	134	21254	22000	1.04	5.6
5	839	59	141	19354	23800	1.23	5.9
6	713	47	112	11551	13531	1.17	6.3

Sweetness attribute map C is extracted approximately 80 ms from the Map B horizon. Two groups of slope gullies are developed along this horizon (Figure 4.7), a southern group and a northern group. Each group contains gullies that are very low sinuosity ($S=1.03-1.2$) and distributed parallel to each other. The gullies show widths that range from 650 to 800 m, depths that range from 95-125 m (45 ms-60 ms) and lengths that range from 14 km to 17 km. Gullies on the northern slope are evenly spaced at between 600 to 900 m, show widths from 450 to 650 m, depths from 70-115 m (35 to 55 ms) and lengths from 3 to 8 m (Table 4.4). Southern gullies (C1 to C5) are wider and slightly deeper than northern gullies (C6 to C15) (Figure 4.8). The aspect ratio of slope gullies on attribute map C range from 5.2-7.3, the average aspect ratio is 6.3. Gully complexes are common along surface C and exhibit dominantly vertical stacking patterns. Gully complexes reach up to 520 m (250 ms) in thickness, and a lateral shifting of gully-forms is from southwest to northeast through time (Figure 4.9). Slope gullies developed on attribute map C are located within the upper 1/3 of the Tpal-Tolig unit. The average interval velocity applied in time-depth conversion of slope gully thickness on attribute map C is 4169.8 m/s.

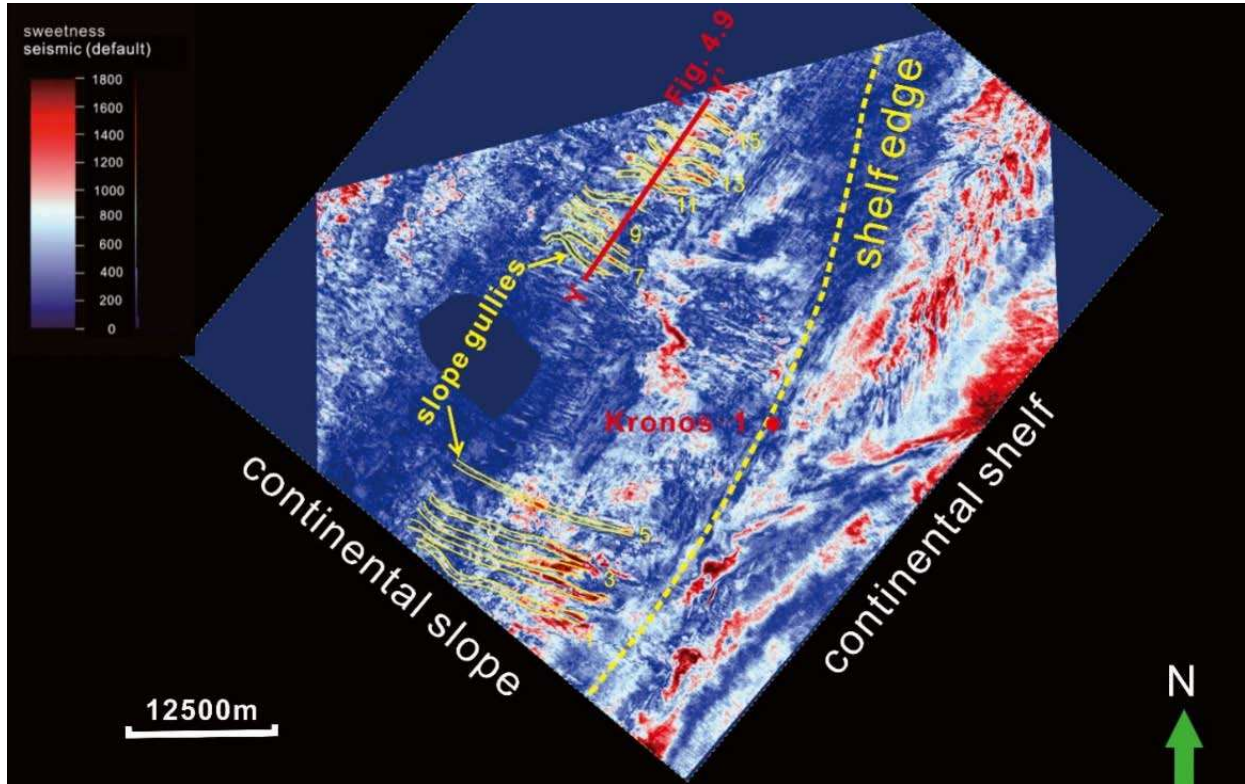


Figure 4.7 Sweetness attribute map C showing the paleogeomorphology and gully development for the uppermost 1/3 of the Tpal-Tolig interval. A total of 15 slope gullies are observed on this surface. From southwest to northeast portion, each gully is numbered in order from 1 to 15. The red line (Y-Y') marks the location of the seismic profile in Figure 9. Blues represent low sweetness and reds represent high sweetness.

Table 4.4 Summary of the slope gully dimensions on attribute map C. Average interval velocity used in this calculation is 4169.8 m/s.

	width(m)	depth(ms)	depth (m)	Straightlength(m)	actual length(m)	sinuosity	aspect ratio
1	664	46	956	15841	18589	1.17	6.9
2	803	53	110	16672	17523	1.05	7.3
3	765	60	125	14208	15385	1.08	6.1
4	793	55	1148	14321	16283	1.14	6.9
5	827	57	119	16377	17939	1.10	7.0
6	539	45	94	7083	8266	1.17	5.7
7	650	54	113	6565	6889	1.05	5.8
8	580	47	98	7250	7587	1.05	5.9
9	580	41	86	4281	4737	1.11	6.8
10	592	43	90	5221	5960	1.14	6.6
11	546	48	100	6621	7983	1.21	5.5
12	485	35	73	8393	9838	1.17	6.6
13	524	40	83	7648	9024	1.18	6.3
14	520	48	100	7180	8106	1.13	5.2
15	460	42	88	3192	3298	1.03	5.3

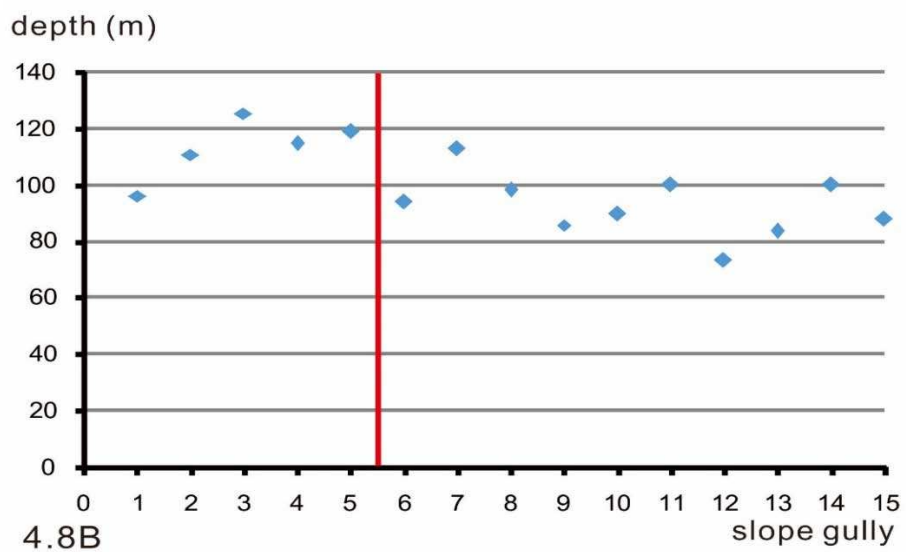
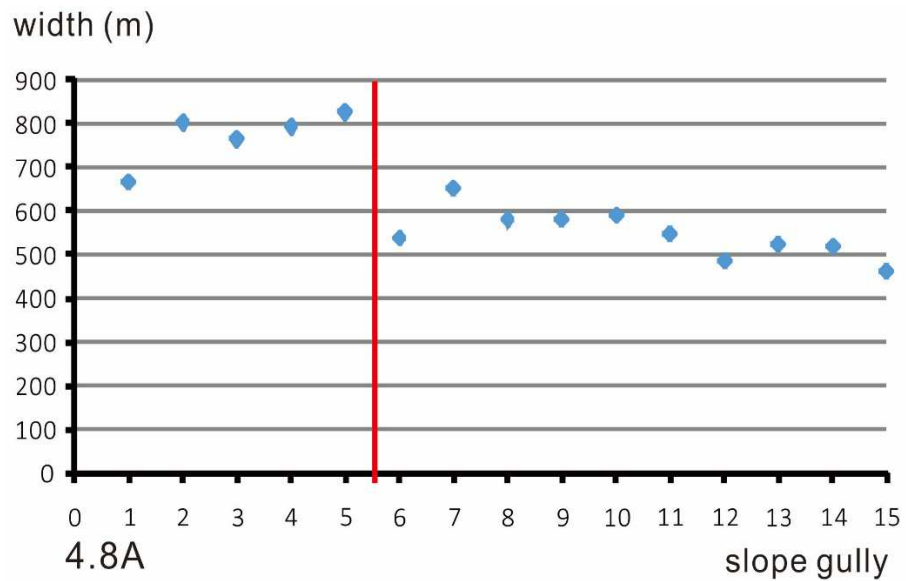


Figure 4.8 Scatter diagram showing dimensions of the gullies along attribute map C. Widths, depths and lengths are approximately 450-650 m, 70-115 m (35-55 ms), 3-8 km, respectively (Table 4.3). Southern gullies (gullies 1-5) are wider than northern gullies (gullies 6-15). Depth vary little, but a trend toward decrease in depth can be observed from gully 1 to gully 15.

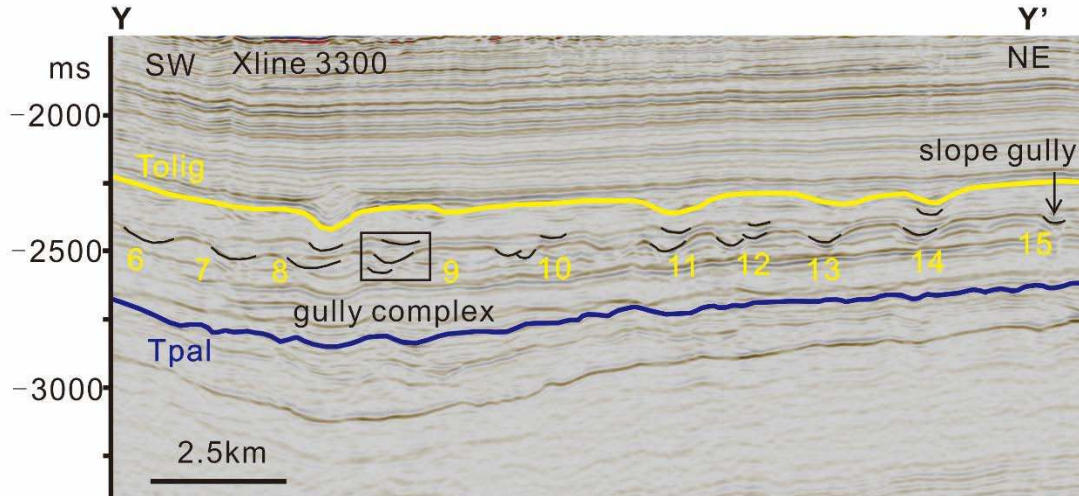


Figure 4.9 Seismic cross-section random line. Location is shown in figure 4.7 (Y-Y'). Gullies imaged in Map C are shown in black line traces. Individual gullies appear to stack vertically in to gully complexes with thicknesses of up to 420 m (200) ms. There is a slight migration toward the northeast.

Sweetness attribute map D is extracted from the sweetness cube approximately 120 ms above the map C horizon (Figure 4.10) and documents the uppermost portions of interval Tpal-Tolig. Twelve parallel, evenly spaced (Spacing = 700-1000 m) slope gullies are observed on this attribute map. Sinuosities range from 1.05 to 1.2. Gullies, numbered from 1 to 12 range in width from 550-1000 m, in depth from 90-200 m (40 to 95 ms) and show lengths ranging from 8 to 14 km. Gullies 6 and 7 have larger widths and depths than the other ten gullies on this horizon (Figure 4.11, Table 4.5). The dimensions of gully 6 and gully 7 can reach up to 1000 m wide and over 200 m (90 ms) deep. Gullies 1-5 are slightly deeper and wider than gullies 8-12. The aspect ratio of slope gullies on attribute map C ranges from 5.1-7.0, with an average aspect ratio is 6.1. Gullies vertically stack in to gully complexes up to 300 m (150 ms) thick, each composed of 2 to 3 individual gullies (Figure 4.12). Gullies show very subtle migrate lateral migration southwest to northeast. Slope gullies developed on attribute map D are

located within the upper part of the Tpal-Tolig unit. The average interval velocity applied in time-depth conversion of slope gully thickness on attribute map C is 4169.8 m/s.

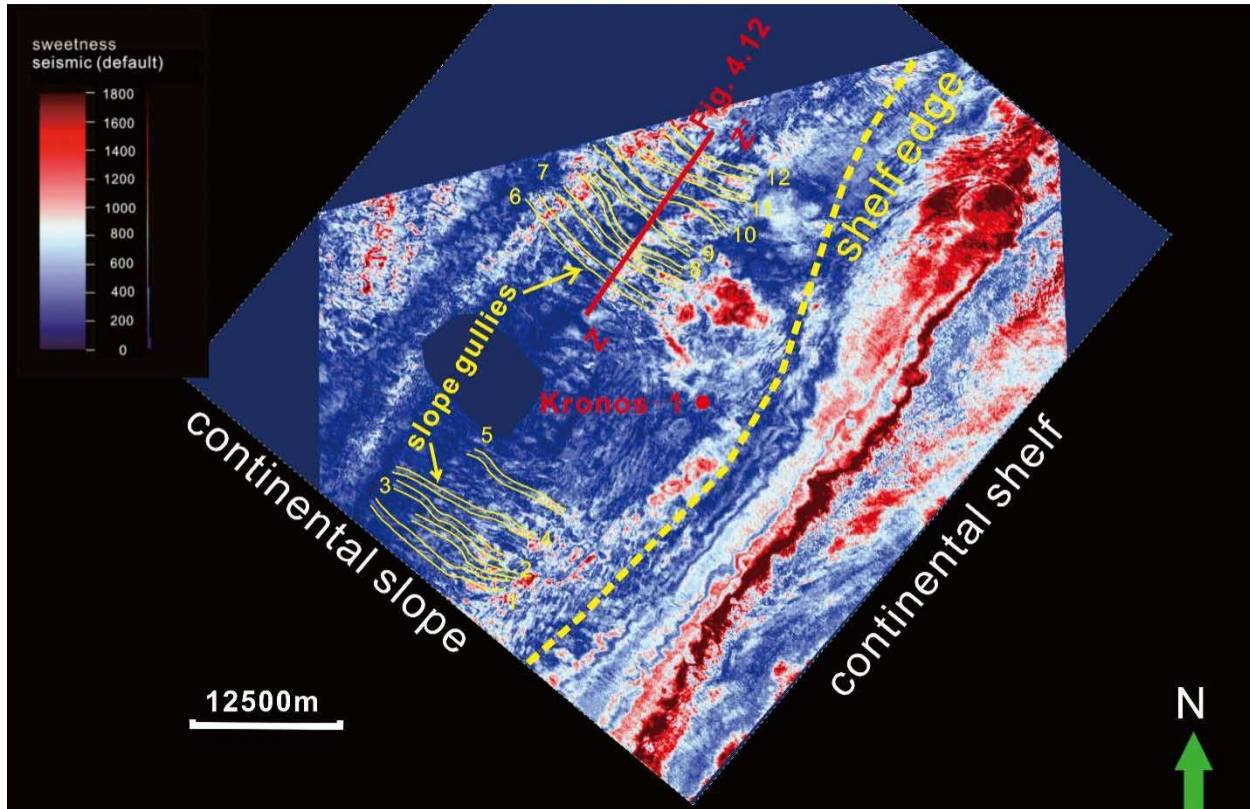


Figure 4.10 Sweetness attribute map D showing the paleogeomorphology and gully development for the topmost horizon of the Tpal-Tolig interval. A total of 12 slope gullies are observed on this surface. From southwest to northeast portion, each gully is numbered in order from 1 to 12. The red line (Z-Z') marks the location of the seismic profile in figure 4.12. Blues represent low sweetness and reds represent high sweetness.

4.3 Interpretation

Four sweetness attribute maps document the seismic geomorphology of the Tpal to Tolig interval along the continental margin of the Browse Basin. Slope gullies here are used as a proxy for sediment movements from shelf edge to slope to deep basin. Sweetness attribute maps document slope gully architecture belts prograding northwestward in the dip direction, indicating margin progradation from southeast to

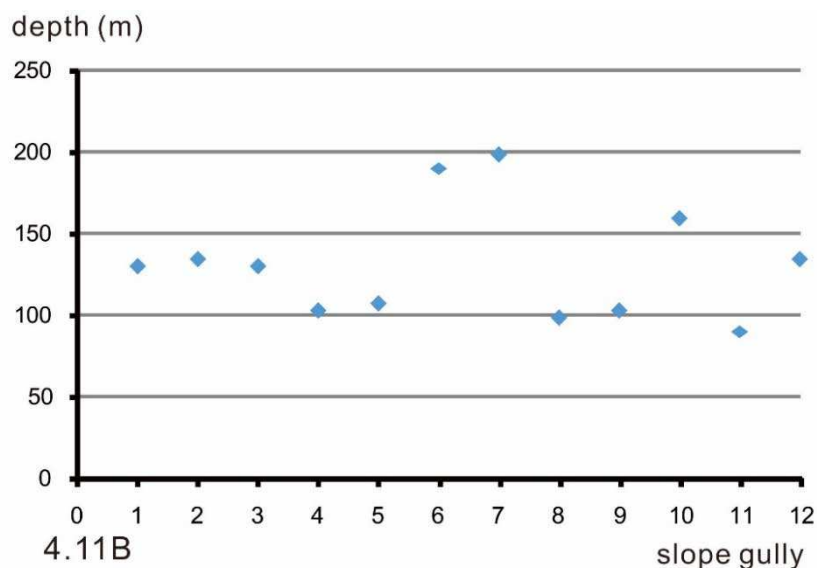
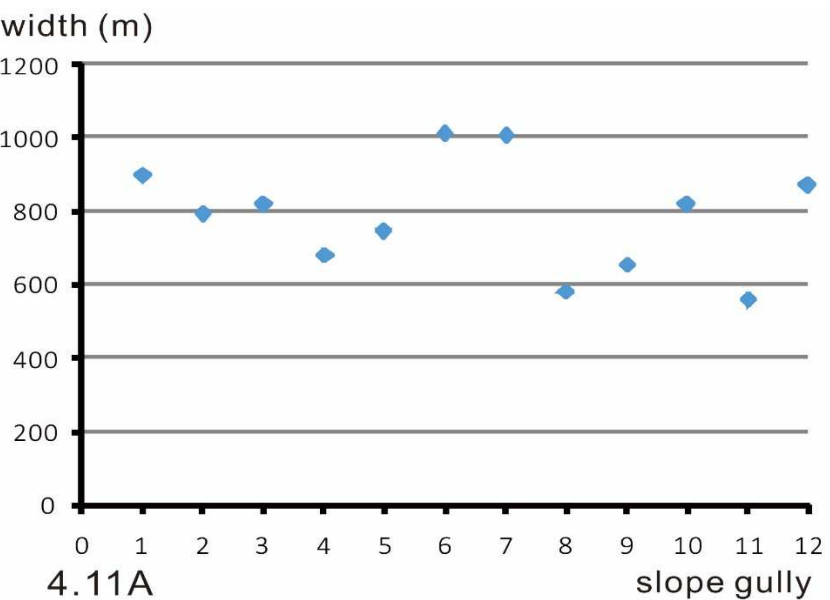


Figure 4.11 Scatter diagram showing the dimensions of the gullies along attribute map D. They are 550-1000 m wide, 90-200 m (40-95 ms) deep and 8-14 km long. Gully 6 and 7 have larger width and depth than the other ten gullies. The dimensions of gully 6 and 7 can reach up to 1000 m wide and over 200 m (90 ms) deep. Gully 1-5 and 8-12 show similar dimensions from scatter diagram.

Table 4.5 Summary of the slope gully dimensions on attribute map D. Average interval velocity applied in this calculation is 4169.8 m/s.

	width(m)	depth(ms)	depth (m)	straight length(m)	actual length(m)	sinuosity	aspect ratio
1	899	62	129	13809	15221	1.10	7.0
2	795	64	133	10526	12013	1.14	6.0
3	818	62	129	11485	12519	1.09	6.3
4	679	49	102	13554	14481	1.07	6.6
5	746	51	106	10080	11219	1.11	7.0
6	1014	91	190	14103	14918	1.06	5.3
7	1008	95	198	13442	14228	1.06	5.1
8	582	47	98	12397	15084	1.22	5.9
9	656	49	102	11042	11922	1.08	6.4
10	820	76	159	13063	15504	1.19	5.2
11	560	43	90	10012	10693	1.07	6.2
12	872	64	133	8414	9264	1.10	6.5

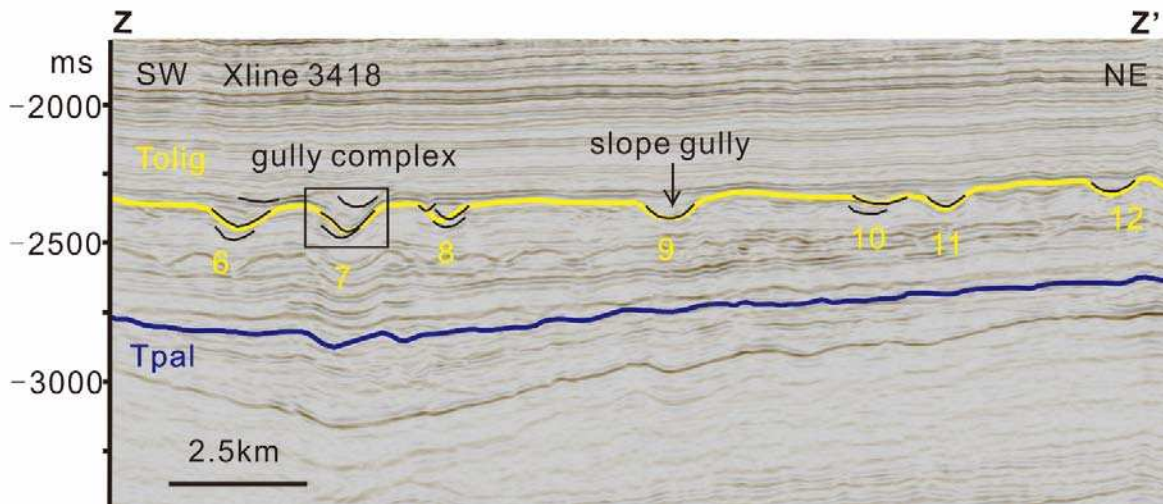


Figure 4.12 Seismic cross-section line 3418. Location is shown in figure 4.10. Gullies imaged in Map D are shown in black line traces. Individual gullies appear to stack vertically in to gully complexes with thicknesses of up to 315 m (150 ms). There is a slight migration toward the northeast.

the northeast. Gullies in the southwest and central portion are consistently deeper, wider and longer than the gullies on the northeast region of the slope. The changes in gully dimensions are probably caused by sediment supply changes through time. More

sediments are transported and deposited in the central to southwest region, an interpretation supported by thickness observations from the Tpal-Tolig isochron map (Figure 2.12), showing increased thicknesses in this area and package thinning to the northeast. Gully migration is consistent from southwest to northeast and likely reflects the increasing roll of marine currents in inducing northeastward migration of shoreline sediment sources in the Paleogene and Neogene.

CHAPTER 5

DISCUSSIONS AND CONCLUSIONS

5.1 Model for theDepositional System

Early Campanian to Oligocene time, the study area within the Browse Basin experienced a change from shelf-incised canyons to deltaic system. This change is reflected in attribute maps and thickness maps of the study area. The Kecamp-Tpal isochron map reveals a 5 km wide shelf edge and slope incision that contains a ~500 m (250 ms) thick fill (Figure 2.11). This canyon initiated at the shelf edge and acted as a conduit to transport sediments downslope to the northwest. A second incision and fill is shown by the isochron thick found to the south (Figure 2.11). A possible source for this thick sedimentary pile is in the southern uplands located south of the 3D seismic cube location. Isochron maps Kecamp-Tpal (Figure 2.11) and Tpal-Tolig (Figure 2.12) show that the northwestward located Kecamp-Tpal sediment thick migrated to the central portions of the study area by Tpal-Toligtime. The Tpal-Tolig thickness map shows two distinct thicks (Figure 2.12). These two are located on the western area and central area of the dataset. The central thick and the western thick on the Tpal-Tolig thickness map (Figure 2.12) are linked with the central canyon and western depocenter also seen on the Kecamp-Tpal thickness map (Figure 2.11), respectively.

Four sweetness attribute extractions through the Tpal-Tolig interval, map the evolution of gully systems through this time. Slope gullies prograde from southeast to northwest through time (Figure 4.2, 4.5, 4.7, 4.10). This transition is mirrored in the

migration of the afore mentioned, isopach thicks located near the interpreted paleo shelf edge. This thick, believed to be deposits of a paleo delta, moved northwestward from the southeast edge of the dataset at Kecamp-Tpal time to central portions of the study area during Tpal-Tolig time (Figure 2.11, 2.12). The gullied slope likewise migrates to the northwest over time. Gullies developed in southwest and central regions of the slope are wider and deeper than gullies developed in the northernmost regions of the slope. This contrast is likely a reflection of varying sediment volumes being supplied to the slope. Southwest and central slopes were fed by two simultaneously active sediment sources, in contrast to northeastern slopes which were fed by only a single sediment source.

5.2 Continental Slope Evolution

A basin margin's shelf edge trajectory is a record of a basin's changes in relative sea level and sediment supply (Henriksen et al. 2009). Relative sea level changes in tectonically quiescent basins such as the Browse are primarily due to accommodation changes caused by sedimentation driven subsidence, eustacy and sediment volumes building the shoreline. Margins prograde, aggrade or retrograde as the balance of accommodation and sediment supply vary. Shelf edge architecture and trajectory of the shelf edge (Sanchez et al., 2012) as interpreted from the Poseidon 3D seismic data were used to assess margin behavior in response to relative sea level and sediment supply.

Sediments during the Late Cretaceous and Paleogene and Neogene were supplied to the Browse Basin by the Kimberley Basin (Figure 1.4), located to the southeast of the Browse Basin(AGSO Browse Basin Project Team, 1997). During Early Cretaceous,

overall relative sea level transgression established open marine environments in the study area. Shoreline reached its highest (most eastward) level in Late Cenomanian. Following this maximum transgression, the study area experienced frequent fluctuations in sea level from Campanian to Late Maastrichtian, which led to repeated exposure and incision of the margin (AGSO Browse Basin Project Team, 1997) and resulted in development of the Tbase unconformity, the basal surface of the section of study in this research. It was at this time that the major canyon/valley, in the central portions off the study area formed. The margin then underwent a slight relative sea level rise during Neogene, as indicated by the flat to slightly rising shelf edge trajectories seen on seismic profiles (Figure 3.2, 3.3, 3.4). Sediment delivered to the study area exceeds the available space resulting in development of wedge-shaped progradational clinoform packages. A brief period of accelerated subsidence from Middle Oligocene to Middle Miocene, resulted in the increase of accommodation and a thickening of these prograding wedges. This prograding sequence is dominated by bioclastic carbonate and calcareous shale (AGSO Browse Basin Project Team, 1997). This brief period of increased subsidence is believed to be driven by regional tectonics (ConocoPhillips, 2011). Although tectonic subsidence adds to the accommodation increase during this time, the clinoform trajectory still show a rising style in western and central region, reflecting the long-lived and strong sediment supply during this time (Figure 3.2B, 3.3B). Rising sea levels initiate reef buildups on in the southwestern and central portions of this margin which also contributes to the rise of the trajectory. In contrast, the northern margins do not experience the stabilizing growth of reefs, and sea level rise and

regional decreases in sediment after the Early Miocene, result in a backstepping margin trajectory (Figure 3.4B).

5.3 Slope Gully Complexes

Slope gully complexes developed and behavior (ie., lateral and vertical migration) during Eocene and Early Oligocene record a valuable history of sediment supply and marine processes for the Browse Basin. In addition, the excellent imaging of these gullies offers opportunity to compare and contrast the morphology of slope gully elements with, submarine channel elements and fluvial channel elements. In this study, gullies evolve and laterally migrate as unconfined slope systems. This behavior can be seen in attribute maps and seismic cross-sections (Figure 4.2, 4.4, 4.5, 4.7, 4.9, 4.10, 4.12). Lateral migration direction is southwest to northeast over time and examination through time shows a significantly progradation of the Tpal-Tolig slope.

Global research from a variety of ages and tectonic settings suggests that submarine channel belt architecture is dominated by aggradation more than lateral migration (Kolla et al., 2007; Jobe et al., 2016; Deptuck et al., 2007). In contrast, fluvial channel behavior is dominated by lateral accretion (Kolla et al., 2007; Jobe et al, 2016). However, very little work has been published on the morphology and behavior of slope gully channels. A few recent and notable exceptions are Shumaker et al. (2016) and Rinke-Hardekopf et al.(2018). Gully width (W) and thickness (L), gully complex width (W_c) and gully complex thickness (L_c) were measured from 21 gully systems within the study area (Figure 5.1). In addition, calculation of ratio of gully complex width, gully width (W_c/W), the ratio of gully complex thickness and gully thickness (L_c/L) as well as the gully aspect ratio (W/L) and gully complex aspect ratio (W_c/L_c) were completed

(Figure 5.2, Table 5.1). These data were used in comparison to published morphometrics from 297 submarine and fluvial channels belts (see Jobe et al., 2016 for locations) to examine the morphologic similarities and differences in these channel types. Measures and associated nomenclature used by Jobe include channel width (B) and thickness (H), channel belt width (B_{cb}) and channel belt thickness (H_{cb}) are applied in this comparison, as well as the normalized channel belt width (B_{cb}/B), normalized channel belt thickness (H_{cb}/H) and the channel belt aspect ratio (B_{cb}/H_{cb}). Data for this comparison are integrated in Figure 5.2.

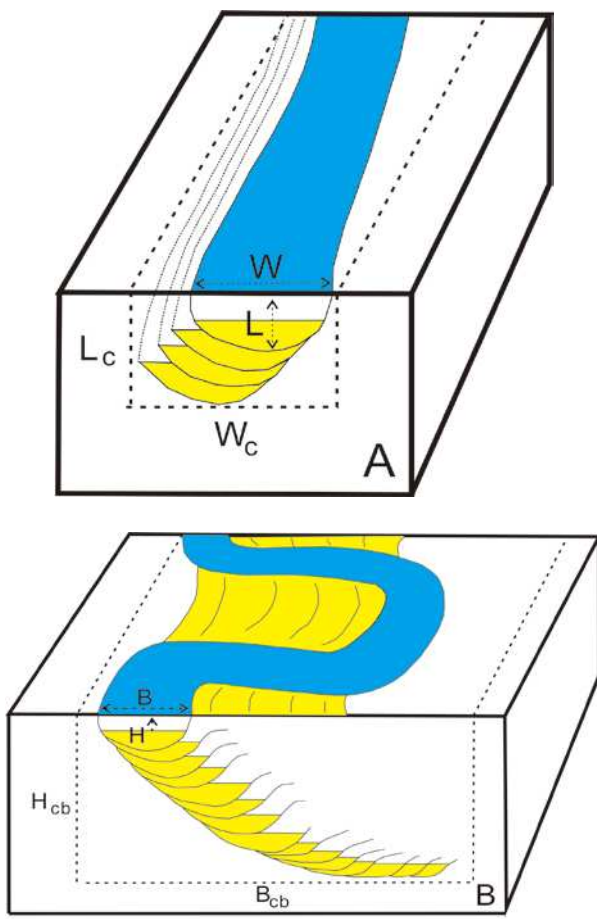


Figure 5.1 Schematic of A) Slope gully systems and measured parameters from this study, and B) channel belt measures and nomenclature used by Jobe et al. (2016). Figure modified from Jobe et al., 2016.

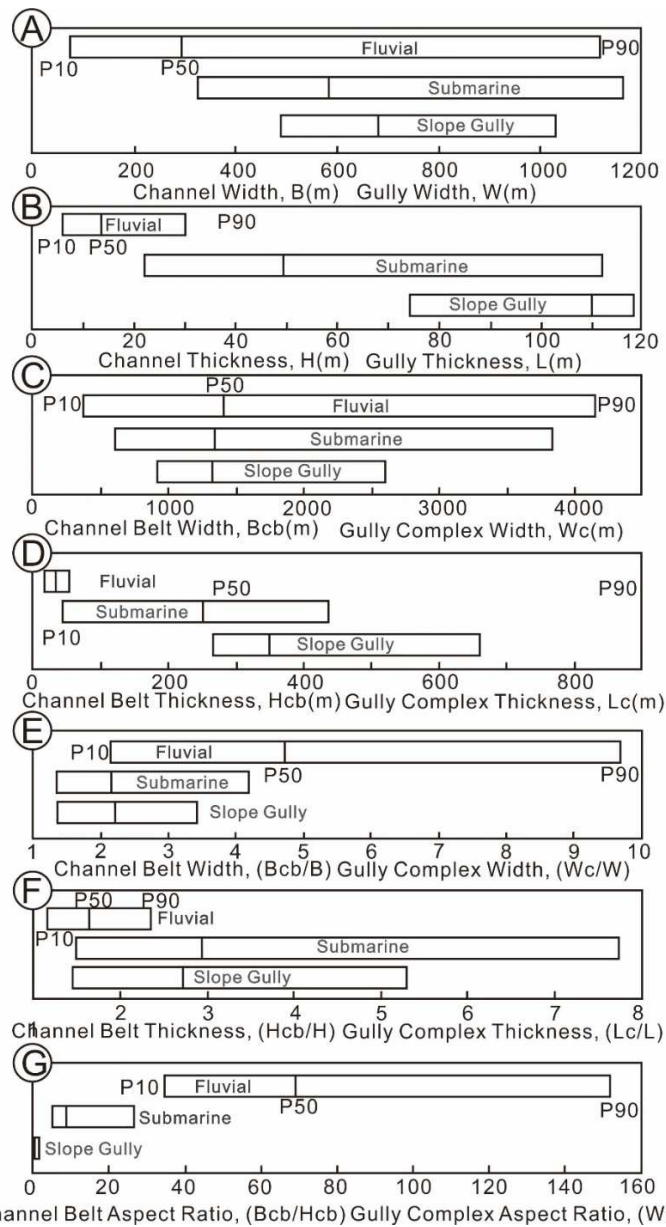


Figure 5.2 Series of graphs showing absolute measures in meters along the Y-axis and the 10%, 50% and 90% probability measures (P=probability) for A. fluvial, submarine and slope gully channel widths, B. fluvial, submarine and slope gully channel thicknesses, C. fluvial and submarine channel belts and gully complex widths, D. fluvial and submarine channel belt and gully complex thicknesses, E. ratio of fluvial and submarine channel to channel belt widths, and the ratio of gully to gully complex widths, F. the ratio of fluvial and submarine channel to channel belt thicknesses, and the ratio of gully to gully complex thicknesses, and G. the aspect ratio of fluvial and submarine channel belt width to thickness and the aspect ratio of gully complex width to thickness. (Figure modified after Jobe et al., 2016).

Table 5.1 Slope gully dimensions for each sub-interval of Sequence Set 2 Tpal-Tolig.

attribute map	Vavg. (m/s)	gully number	gully width (W) (m)	gully complex width (Wc)(m)	gully thickness (L)(ms)	gully thickness (L)(m)	gully complex thickness (Lc)(ms)	gully complex thickness (Lc)(m)	Wc/W	Lc/L	W/L	Wc/Lc
B	4781.6	1	755	1989	53	126.7	177	423	2.6	3.3	6.0	11.2
		2	841	2264	56	133.9	216	516	2.7	3.9	6.3	10.5
		3	840	2546	61	145.8	278	665	3.0	4.6	5.8	9.2
		4	744	2530	56	133.9	240	574	3.4	4.3	5.6	10.5
C	4169.8	1	664	2247	46	95.9	202	421	3.4	4.4	6.9	11.1
		2	803	1814	53	110.5	195	407	2.3	3.7	7.3	9.3
		4	793	2597	55	114.7	223	465	3.3	4.1	6.9	11.6
		8	580	1654	47	98.0	164	342	2.9	3.5	5.9	10.1
		9	580	1215	41	85.5	219	457	2.1	5.3	6.8	5.5
		10	592	1338	43	89.7	173	361	2.3	4.0	6.6	7.7
		11	546	973	48	100.1	180	375	1.8	3.8	5.5	5.4
		12	485	1132	35	73.0	177	369	2.3	5.1	6.6	6.4
		14	520	999	48	100.1	157	327	1.9	3.3	5.2	6.4
D	4169.8	2	795	2337	64	133.4	195	407	2.9	3.0	6.0	12.0
		3	818	2147	62	129.3	168	350	2.6	2.7	6.3	12.8
		4	679	1781	49	102.2	123	256	2.6	2.5	6.6	14.5
		5	746	1290	51	106.3	123	256	1.7	2.4	7.0	10.5
		6	1014	1356	91	189.7	264	550	1.3	2.9	5.3	5.1
		7	1008	1314	95	198.1	295	615	1.3	3.1	5.1	4.5
		8	582	856	47	98.0	154	321	1.5	3.3	5.9	5.6
		10	820	1114	76	158.5	124	259	1.4	1.6	5.2	9.0

Dimensions show that individual gully widths (W : 485-1014 m) in this study are similar in width to individual submarine channels but show a narrower range of widths than submarine channels (B : ~300-1200 m) or fluvial channels (B : ~100-1100 m). Likewise gully systems are similar in their amalgamated and shingled widths but do show a narrower range of widths than submarine channel belts (W_c : 856-2546 m versus B_{cb} : ~500-3800 m, respectively), or fluvial channel belts (B_{cb} : ~400-4000 m) (Figure 5.2A, 5.2C) (Jobe et al., 2016). Gullies and gully complex thickness (L : 90-200 m; L_c : 240-660 m) are on average larger than submarine channel and channel belt (H : 20-115 m; H_{cb} : 50-430 m). Slope channels are up to five times thicker than individual fluvial channels and fluvial channel belts (H , H_{cb} : ~8-30 m, ~10-50 m, respectively) (Figure 5.2B, 5.2D) (Jobe et al., 2016). The normalized dimensions, which is more useful in the evaluation of differences in lateral and vertical channel migration at channel belt scale, were also calculated in this study (Figure 5.2E-G) (Jobe et al., 2016). These data indicate that the median value for normalized gully complex width (W_c/W) is 2.1, which is similar to the normalized channel belt width of submarine channels (B_{cb}/B) but much smaller than the 4.7 calculated for fluvial channel systems (Figure 5.2E) (Jobe et al., 2016). Normalized gully complex thickness (L_c/L) values have the opposite relationship, with median values for gully complex thickness (2.7) being similar to submarine channel belt thickness (2.9), but almost twice that of fluvial systems (1.6) (Figure 5.2F) (Jobe et al., 2016). The aspect ratios for gully complexes (W_c/L_c) and submarine channel belts (B_{cb}/H_{cb}) are much smaller than fluvial channel belt aspect ratios (B_{cb}/H_{cb}). This supports the concept that slope gully systems and submarine channel systems are

dominated by vertical aggradation rather than dominated by lateral migration, as are fluvial channel systems (Figure 5.2G) (Jobe et al., 2016).

Figure 5.3 illustrates the accretion style for slope gully systems, fluvial channel systems and submarine channel systems. This figure (Figure 5.3) is divided into two parts by a diagonal line. The upper part of the figure represents the vertical accretion dominant system, while the data below this line indicates that the system is dominated by lateral accretion. On Figure 5.3, all fluvial systems plot below the line which indicates the domination of lateral accretion. However, most of the submarine channel belts and 80% of gully complexes in this Browse Basin study plot above this line. The slope gully complexes in this study exhibit both lateral migration and vertical aggradation, however, the data and comparison of this study and previous studies suggest that, vertical accretion is dominant in slope gully system in the Browse Basin area. These similarities to submarine channels suggests a similarity of suspensional flow processes active in both submarine and slope gully channels, rather than more tractional flow processes as in fluvial systems.

Slope gullies migrate persistently over time from southwest to northeast along the seismic profiles (Figures 4.4, 4.9 and 4.12). There are several possibilities for this consistent migration direction, including 1. Sediment factories along the shelf edge were continually shifting to the northeast. Interpretations indicate possibly two sediment sources located to the south of the study area. There is some suggestion from the changing trajectories that sediment source directions shifted to the southeast overtime. However there is no indication that sediment supplies were shifting over the Tpal to Tolig time.2. Changes in marine current conditions encouraged migration of gullies to

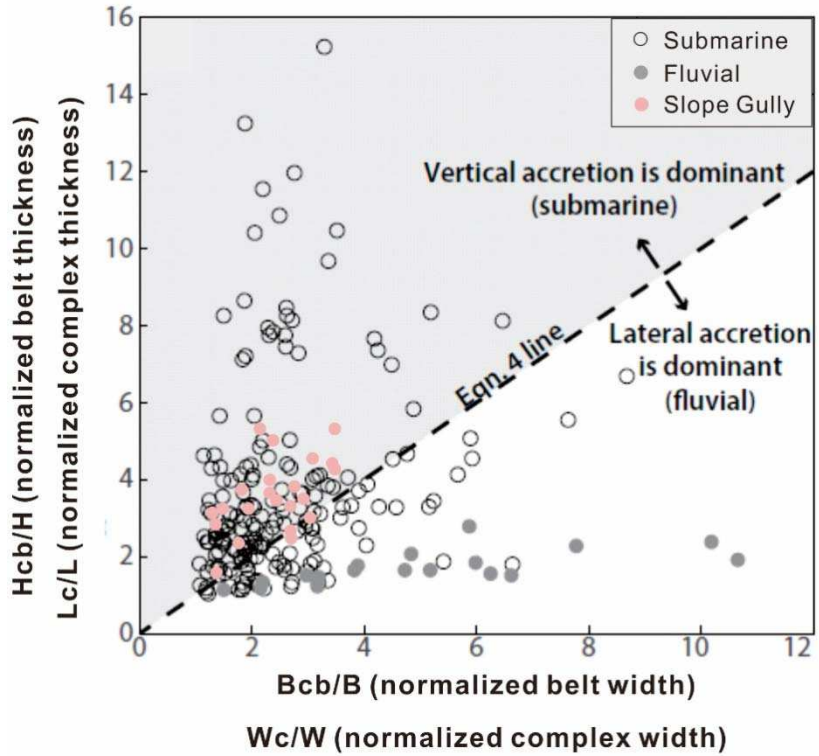


Figure 5.3 Normalized channel belt and gully complex dimension cross-plot. The cross-plot is divided into two parts by a diagonal line. The upper part of the figure represents the vertical accretion dominant systems, while the data below this line indicates that the systems are dominated by lateral accretion.

the northeast over time. Work by Zhu et al., (2010) in the South China Sea document the persistent uni-directional northeastward migration of slope channels due to the northeastward directed bottom currents. The authors observed the northeastward migration of submarine canyons from seismic profiles and borehole information, and suggests the migrating submarine canyons reveal the persistence of northeast-oriented bottom currents in their study area. The northeastward lateral migration of slope gullies in the Browse Basin during Tpal-Tolig time could be the result of a similarly persistent marine current moving from southwest to northeast. These currents could be affecting both the location of shoreline sediment inputs as they force deltaic migration to the north, and the submarine distribution of suspensional flows further northward over time. The

West Australian current has been documented to be a strong influence on modern day sediment dispersal along the Browse Basin margin (Jones, 1973). Currents in this region today are dominately north to south. However, the early Neogene separation of western Australia and Antarctica, resulted in development of a strong clockwise current circulating Antarctica, and a north to south current along the western Australia margin (Association for Canadian Educational Resources, 2012)(Figure 5.4). These ideas are beyond the scope of this study but bear additional research.

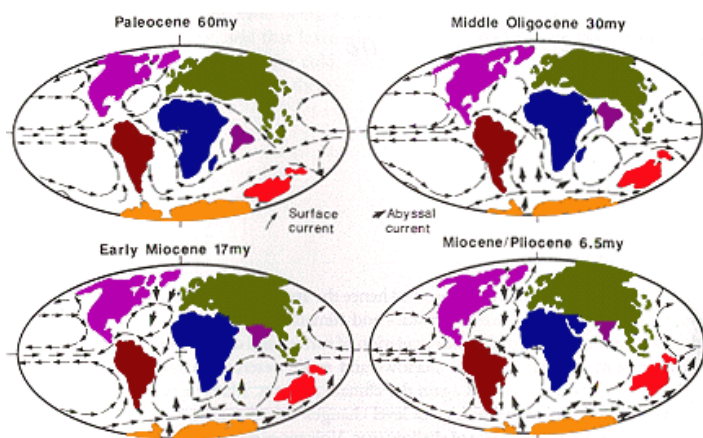


Figure 5.4 Series of paleogeographic renderings showing a strong south to north current along the western margin of Australia throughout the Neogene (<http://www.acer-acre.ca/the-components-of-the-earth-system>).

5.4 Conclusions

The northwestward trending Browse Basin continental margin has experienced a long tectonic and sedimentologic evolution. It was developed during the second phase of thermal subsidence occurring from Late Cretaceous to late Neogene during the continental margin's evolution and has evolved from a clastic-dominated margin to a modern carbonate-dominated margin. This evolution and the proliferation of data from industry hydrocarbon exploration offers an excellent opportunity to document changes in morphology of a continental margin as it evolves through such change.

Six time structure maps have been generated on six horizons mapped throughout a 5000 sq km study area in the Browse Basin margin. These unconformities (sequence boundaries) within the late Cretaceous to late Miocene bound three sequence sets (SS), which document specific evolution phases of the margin. SS1, bounded by Kecamp and Tpal, documents the early clastic-dominated continental margin evolution. The deposition within this sequence set is dominated by a shelf incised canyon which is filled with multiple phases of channelized fill. SS2 is bounded by Tpal and Tolig, and is dominated by a series of northwestward prograding siliciclastic clinoforms. SS3 which is bounded by Tolig and Tmmio , shows a strong northwestward shift of the shoreline and is dominated by a rimmed carbonate reef and a carbonate rich prograding shelf system. Throughout Tpal to Tolig time, water depth of siliciclastic margin is greater than 1000 m. The margin exhibits a high rate of aggradation and low rate of progradation. In contrast, the Tolig to Tmmio time margin is dominated by carbonate deposition. Carbonate slopes are much steeper, exhibit a concave profile.

Slope gullies are well developed from Eocene to Middle Oligocene time. Four sweetness attribute maps extracted from the Tpal-Tolig interval show the evolution of the slope gullies in the study area. The gullied slope migrates over time to the northwest. Gully complexes show lateral migration from southwest to northeast along the slope. Gullies developed on the western slope and central slope are wider and deeper than the gullies on the northeast region of the slope. Although the gully size differences are likely a function of sediment volumes supplied along the slope, the influenced by marine currents are likely responsible for gully migration initiating in the Neogene, and directions of migration from southwest to northeast.

REFERENCES

- Adams, E.W., and J. A. Kenter. 2014, So different, yet so similar: comparing and contrasting siliciclastic and carbonate slopes. Deposits, architecture and controls of carbonate margin, slope and basinal settings: SEPM Special Publication, no. 105, p. 14-25.
- Adams E.W., and W. Schlager, 2000, Basic Types of Submarine Slope Curvature: *Journal of Sedimentary Research*, v. 70, no. 4, p. 814–828.
- Adams E.W, W. Schlager, and E. Wattel, 1998, Submarine Slopes with an Exponential Curvature: *Sedimentary Geology*, v. 117, no. 3, p. 135–141.
- Arnott, R. W. C., 2010, Deep-marine sediments and sedimentary systems: Facies models 4, p. 295-322.
- Australia Geological Survey Organization, 1993, Deep Structure of the Browse Basin Region, North West Shelf, Australia, Project 121.28.
- AGSO Browse Basin Project Team, 1997, Browse Basin High Resolution Study, Interpretation Report. Australian Geological Survey Organisation, Record 1997/38.
- Bridge, J.S., and R. S. Tye, 2000, Interpreting the dimensions of ancient fluvial channel bars, channels, and channel belts from wireline-logs and cores: *AAPG bulletin*, v. 84, no. 8, p. 1205-1228.
- Brincat, M.P., M. Lisk, J. M. Kennard, W. R. Bailey, and P. J. Eadington, 2003, Evaluating the oil potential of the Caswell Sub-basin: insights from fluid inclusion studies: *Proceedings Timor Sea Petroleum Geoscience, Proceedings of the Timor Sea Symposium*, Darwin, Northern Territory, p. 19-20.
- Cardenas, M. B, 2009, A model for lateral hyporheic flow based on valley slope and channel sinuosity: *Water Resources Research*, v. 45, no. 1.
- Carvajal, C., R. Steel, and A. Petter, 2009, Sediment Supply: The Main Driver of Shelf-margin Growth: *Earth-Science Reviews*, v. 96, no. 4, p. 221-248.
- Carvajal, C., and R. Steel, 2006, Thick Turbidite Successions from Supply-dominated Shelves During Sea-level Highstand: *Geology*, v. 34, no. 8, p. 665-668.
- Chiocci, F. L., and W. R. Normark, 1992, Effect of sea-level variation on upper-slope depositional processes offshore of Tiber delta, Tyrrhenian Sea, Italy: *Marine Geology*, v. 104, no. 1-4, p. 109-122.
- ConocoPhillips (Browse Basin) Pty Ltd, 2011, Kronos-1 Well Completion Report Volume 2: interpretation data, Document no: KRON-1/002.

- Courp, T., and A. Monaco, 1990, Sediment Dispersal and Accumulation on the Continental Margin of the Gulf of Lions: Sedimentary Budget: *Continental Shelf Research* v. 10, no. 9-11, p. 1063-1087.
- Deptuck, M.E., Z. Sylvester, C. Pirmez, and C. O'Byrne, 2007, Migration-aggradation history and 3-D seismic geomorphology of submarine channels in the Pleistocene Benin-major Canyon, western Niger Delta slope: *Marine and Petroleum Geology*, v. 24, no. 6, p. 406-433.
- Field, M.E., J. V. Gardner, and D. B. Prior, 1999, Geometry and significance of stacked gullies on the northern California slope: *Marine Geology*, v.154, no. 1, p. 271-286.
- Fulthorpe, C. S., and J. A. Austin Jr, 1998, Anatomy of Rapid Margin Progradation: Three-dimensional Geometries of Miocene Clinoforms, New Jersey Margin: *AAPG bulletin*, v. 82, no. 2, p. 251-273.
- Garrison, T. S., 2012, *Essentials of Oceanography*: Cengage Learning.
- Greenlee, S. M., and P. J. Lehmann, 1993, Stratigraphic Framework of Productive Carbonate Buildups: Carbonate sequence stratigraphy: recent developments and applications: *AAPG Memoir*, v. 57, p. 43-62.
- Haq, B. U., J. Hardenbol, and P. R. Vail, 1998, Mesozoic and Cenozoic chronostratigraphy and cycles of sea-level change.
- Henriksen, S., J. R. Hampson, W. Helland-Hansen, E. P. Johannessen, and R. J. Steel, 2009, Shelf edge and shoreline trajectories, a dynamic approach to stratigraphic analysis: *Basin Research*, v. 21, no. 5, p. 445–453.
- Hine, A. C., and H. T. Mullins, 1983, Modern carbonate shelf-slope breaks.
- James, N. P., and C. Christopher, 1991, Carbonate shelf edge off southern Australia: a prograding open-platform margin: *Geology*, v. 19, no. 10, p. 1005-1008.
- Jobe, Z. R., N. C. Howes, and N. C. Auchter, 2016, Comparing submarine and fluvial channel kinematics: Implications for stratigraphic architecture: *Geology*, v. 44, no. 11, p. 931-934.
- Johannessen, E. P., and R. J. Steel, 2005, Shelf-margin clinoforms and prediction of deepwater sands: *Basin Research*, v. 17, no.4, p. 521–550.
- Jones, H. A., 1973, Marine geology of the northwest Australian continental shelf.: Bureau of Mineral Resources, Geology and Geophysics, v. 136.
- Kenter, J. A., P. M. Harris, and G. Della Porta, 2005, Steep microbial boundstone-dominated platform margins—examples and implications: *Sedimentary Geology*, v. 178, no. 1, p. 5-30.

- Kenyon, P. M., and D. L. Turcotte, 1985, Morphology of a delta prograding by bulk sediment transport: Geological Society of America Bulletin, v. 96, no. 11, p. 1457-1465.
- Kolla, V., H. W. Posamentier, and L. J. Wood, 2007, Deep-water and fluvial sinuous channels—Characteristics, similarities and dissimilarities, and modes of formation: Marine and Petroleum Geology, v. 24, no. 6, p. 388-405.
- Lairakull, K., P. Weimer, and R. Bouroullec, 2011, Sequence Stratigraphic Interpretation of the Cretaceous through Miocene Section, Barcoo Sub-basin, Browse Basin, Northwest Shelf, Australia, in International Petroleum Technology Conference.
- Lonergan, L., N. H. Jamin, C. A. L. Jackson, and H. D. Johnson, 2013, U-shaped slope gully systems and sediment waves on the passive margin of Gabon (West Africa): Marine Geology, v. 337, p. 80-97.
- Marshall, N. G., and S. C. Lang, 2013, A new sequence stratigraphic framework for the North West Shelf, Australia: The Sedimentary Basins of Western Australia 4: Proceedings PESA Symposium. Perth: p. 1-32
- Micallef, A., and J. J. Mountjoy, 2011, A topographic signature of a hydrodynamic origin for submarine gullies: Geology, v. 39, no. 2, p. 115-118.
- Mitchum Jr, R. M., and J. C. Van Wagoner, 1991, High-frequency sequences and their stacking patterns: sequence-stratigraphic evidence of high-frequency eustatic cycles: Sedimentary Geology v. 70, no. 2-4, p. 131-160.
- Mitchum Jr, R. M., 1977, Seismic stratigraphy and global changes of sea level: Part 11. Glossary of terms used in seismic stratigraphy: Section 2. Application of seismic reflection configuration to stratigraphic interpretation, p. 205-212
- Neal, J., and V. Abreu, 2009, Sequence stratigraphy hierarchy and the accommodation succession method: Geology, v. 37, no. 9, p. 779-782.
- Normark, W.R., and P. R., Carlson, 2003, Giant submarine canyons: Is size any clue to their importance in the rock record: Special Papers-Geological Society of America, p.175-190.
- Posamentier, H. W., and V. Kolla, 2003, Seismic geomorphology and stratigraphy of depositional elements in deep-water settings: Journal of sedimentary research, v. 73, no. 3, p. 367-388.
- Read, J. F., 1982, Carbonate platforms of passive (extensional) continental margins: types, characteristics and evolution: Tectonophysics, v. 81, no. 3, p. 195-212.
- Read, J. F., 1985, Carbonate platform facies models: AAPG bulletin, v. 69, no. 1, p. 1-21.

Riedel, M., S. Mair, T. S. Collett, P. Kumar, and A. V. Sathe, 2008, SEISMIC MAPPING OF GAS HYDRATE DEPOSITS IN THE KRISHNA-GODHAVARI BASIN OFFSHORE INDIA: Proceedings of the 6th international conference on gas hydrates (ICGH 2008), Vancouver, British Columbia.

Rinke-Hardekopf, L., L. Reuning, J. Bourget, S. Back, 2018, Syn-sedimentary deformation as a mechanism for the initiation of submarine gullies on a carbonate platform to slope transition, Browse Basin, Australian North West Shelf: Marine and Petroleum Geology, doi: 10.1016/j.marpetgeo.2017.12.034.

Sanchez, C. M., C. S. Fulthorpe, and R. J. Steel, 2012, Miocene shelf-edge deltas and their impact on deepwater slope progradation and morphology, Northwest Shelf of Australia: Basin Research, v. 24, no. 6, p. 683-698.

Schlager W., and E. W. Adams, 2001, Model for the sigmoidal curvature of submarine slopes: Geology, v. 29, no. 10, p. 883–886.

Schlager, W., 2003, Benthic carbonate factories of the Phanerozoic: International Journal of Earth Sciences, v. 92, no. 4, p. 445-464.

Shepard, F.P., and K. O. Emery, 1973, Congo submarine canyon and fan valley: AAPG Bulletin, v. 57, no. 9, p.1679-1691.

Shepard, F. P., 1981, Submarine canyons: multiple causes and long-time persistence: AAPG Bulletin, v. 65, no. 6, p. 1062-1077.

Shumaker, L. E., Z. R. Jobe, and S. A. Graham, 2016, Evolution of submarine gullies on a prograding slope: Insights from 3D seismic reflection data: Marine Geology, v. 393, p. 35-46.

Steel, R. J., S. J. Porebski, P. Plink-Bjorklund, D. Mellere, and M. Schellpeper, 2003, Shelf-edge delta types and their sequence-stratigraphic relationships: Shelf Margin Deltas and Linked Down Slope Petroleum Systems, p. 205-230.

Struckmeyer, H. I., J. E. Blevin, J. Sayers, J. M. Totterdell, K. Baxter, D. L. Cathro, P. G. Purcell, and R. R. Purcell, 1998, Structural evolution of the Browse Basin. North West Shelf. new concepts from deep seismic data, p. 345-367.

Symonds, P. A., C. D. N. Collins, J. Bradshaw, P. G. Purcell, and R. R. Purcell, 1994, Deep structure of the Browse Basin: implications for basin development and petroleum exploration, p. 315-331.

Syvitski, J.P., C. R. Alexander, M. E. Field, J. V. Gardner, D. L. Orange, and J. W. Yun, 1996, Continental slope sedimentation: The view from northern California: Oceanography, v. 9, no. 3. p. 163–167.

Vail, P. R., and W. Wornardt Jr, 1991, An integrated approach to exploration and development in the 90s: well log-seismic sequence stratigraphy analysis.

Van Wagoner, J. C., H. W. Posamentier, R. M. J. Mitchum, P. R. Vail, J. F. Sarg, T. S. Loutit, and J. Hardenbol, 1998, An overview of the fundamentals of sequence stratigraphy and key definitions.

WEBB 2012. Oceans Circulation in Cenozoic. Association for Canadian Educational Resources. <http://www.acer-acre.ca/the-components-of-the-earth-system>

Young, G. C., and J. R. Laurie, editos, 1996, An Australian Phanerozoic Timescale: Oxford University Press, V. 6.

Zhu, M., S. Graham, X. Pang, T. McHargue, 2010, Characteristics of migrating submarine canyons from the middle Miocene to present: implications for paleoceanographic circulation, northern South China Sea: Marine and Petroleum Geology, v. 27, no. 1, p. 307-319

APPENDIX A

CHECK-SHOTS DATA OF KRONOS-1 WELL

Table A.1 List showing relationship between measured depth, true vertical depth, two-way time and interval velocity from Kronos-1 well. The list is sorted from shallowest depth to deepest depth within the target interval in this study (ConocoPhillips , 2011).

Measured Depth	True Vertical Depth From SRD [m]	Two-way Vertical Time [s]	Interval Velocity [m/s]
1513.1	1491.1	1.5012	
			3204.2
1528.2	1506.2	1.5106	
			3230.5
1543.3	1521.4	1.5200	
			3256.0
1558.4	1536.5	1.5293	
			3327.9
1573.6	1551.6	1.5384	
			3374.1
1588.7	1566.7	1.5473	
			3402.3
1603.8	1581.8	1.5562	
			3451.3
1618.9	1597.0	1.5650	
			3468.1
1634.0	1612.1	1.5737	
			3468.1
1649.2	1627.2	1.5824	
			3465.4
1664.3	1642.3	1.5911	
			3467.1
1679.4	1657.5	1.5999	
			3429.5
1694.4	1672.5	1.6086	
			3467.4
1709.5	1687.6	1.6173	
			3476.1
1724.7	1702.7	1.6260	
			3535.1
1739.8	1717.8	1.6346	
			3610.4
1755.0	1733.0	1.6430	
			3655.1

Table A.1 Continued

1770.1	1748.2	1.6513	
			3703.7
1785.2	1763.3	1.6595	
			3742.4
1800.4	1778.4	1.6675	
			3755.4
1815.5	1793.5	1.6756	
			3759.2
1830.6	1808.6	1.6836	
			3762.9
1845.7	1823.7	1.6917	
			3763.3
1860.8	1838.9	1.6997	
			3747.5
1875.9	1853.9	1.7077	
			3763.5
1891.0	1869.0	1.7158	
			3760.8
1906.1	1884.1	1.7238	
			3751.5
1921.2	1899.3	1.7319	
			3763.8
1936.4	1914.4	1.7399	
			3755.9
1951.5	1929.5	1.7480	
			3747.3
1966.6	1944.6	1.7560	
			3755.4
1981.8	1959.7	1.7641	
			3755.2
1996.9	1974.9	1.7721	
			3756.6
2012.0	1990.0	1.7802	
			3758.8
2027.1	2005.1	1.7882	
			3765.8
2042.3	2020.2	1.7962	
			3748.0
2057.2	2035.2	1.8042	
			3842.3
2072.3	2050.3	1.8121	
			3863.9
2087.5	2065.4	1.8199	
			3910.6

Table A.1 Continued

2102.6	2080.5	1.8276	
			4006.3
2117.9	2095.8	1.8353	
			3979.9
2133.0	2110.9	1.8429	
			3977.6
2148.1	2126.0	1.8505	
			4005.2
2163.2	2141.1	1.8580	
			3994.3
2178.3	2156.2	1.8656	
			3965.6
2193.4	2171.3	1.8732	
			3930.5
2208.6	2186.4	1.8809	
			3893.9
2223.7	2201.6	1.8886	
			3847.5
2238.8	2216.7	1.8965	
			3787.0
2253.9	2231.8	1.9045	
			3762.7
2269.0	2246.9	1.9125	
			3730.4
2284.2	2262.0	1.9206	
			3703.7
2299.3	2277.2	1.9288	
			3682.5
2314.4	2292.3	1.9370	
			3678.7
2329.5	2307.4	1.9452	
			3678.9
2344.7	2322.5	1.9534	
			3687.6
2359.8	2337.6	1.9617	
			3682.7
2364.2	2342.0	1.9640	
			3683.4
2374.9	2352.8	1.9699	
			3686.0
2379.3	2357.1	1.9722	
			3685.3
2390.0	2367.9	1.9781	
			3702.2

Table A.1 Continued

2394.4	2372.3	1.9804	
			3697.7
2405.2	2383.0	1.9862	
			3684.2
2409.5	2387.4	1.9886	
			3684.7
2420.2	2398.1	1.9944	
			3717.1
2435.4	2413.2	2.0026	
			3731.3
2450.5	2428.3	2.0107	
			3772.5
2465.6	2443.4	2.0187	
			3831.9
2480.7	2458.6	2.0266	
			3879.0
2495.9	2473.7	2.0344	
			3941.8
2511.0	2488.8	2.0420	
			4024.1
2526.1	2503.9	2.0496	
			4095.8
2541.2	2519.1	2.0570	
			4137.2
2556.3	2534.2	2.0643	
			4179.4
2571.5	2549.3	2.0715	
			4199.6
2586.6	2564.4	2.0787	
			4189.4
2601.7	2579.5	2.0859	
			4180.5
2616.8	2594.6	2.0931	
			4158.8
2631.9	2609.7	2.1004	
			4158.5
2647.0	2624.9	2.1077	
			4157.7
2662.1	2640.0	2.1149	
			4158.6
2677.2	2655.1	2.1222	
			4159.2
2692.4	2670.2	2.1295	
			4156.3

Table A.1 Continued

2707.5	2685.3	2.1367	
			4296.8
2722.7	2700.5	2.1438	
			4299.6
2737.8	2715.6	2.1508	
			4210.8
2752.9	2730.7	2.1580	
			4430.3
2768.0	2745.8	2.1648	
			4431.5
2783.1	2760.9	2.1717	
			4507.7
2798.2	2776.0	2.1784	
			4431.2
2813.4	2791.1	2.1852	
			4433.0
2828.5	2806.3	2.1920	
			4432.0
2843.6	2821.4	2.1988	
			4433.3
2858.7	2836.5	2.2056	
			4429.7
2873.8	2851.6	2.2125	
			4432.9
2888.9	2866.7	2.2193	
			4433.9
2904.1	2881.9	2.2261	
			4433.0
2919.2	2897.0	2.2329	
			4433.8
2934.4	2912.1	2.2398	
			4625.1
2949.5	2927.2	2.2463	
			4732.4
2964.6	2942.3	2.2527	
			4657.4
2979.7	2957.4	2.2592	
			4706.7
2994.8	2972.6	2.2656	
			4769.6
3009.9	2987.7	2.2719	
			5047.5
3025.1	3002.8	2.2779	
			4998.8

Table A.1 Continued

3040.2	3017.9	2.2840	
			4703.9
3055.3	3033.0	2.2904	
			4631.1
3070.4	3048.2	2.2969	
			4777.9
3085.6	3063.3	2.3033	
			5113.9
3100.7	3078.4	2.3092	
			5002.4
3115.8	3093.5	2.3152	
			4961.0
3130.9	3108.6	2.3213	
			4762.6
3146.0	3123.7	2.3276	
			4974.7
3161.1	3138.8	2.3337	
			4867.2
3176.2	3154.0	2.3399	
			5097.7
3191.4	3169.1	2.3459	
			5099.3
3206.5	3184.2	2.3518	
			5099.2
3221.6	3199.3	2.3577	
			4848.7
3236.7	3214.4	2.3640	
			4855.9
3251.8	3229.5	2.3702	
			5039.0
3267.0	3244.7	2.3762	
			5046.5
3282.1	3259.8	2.3822	
			5054.9
3297.2	3274.9	2.3882	
			5078.9
3312.3	3290.0	2.3941	
			4605.7
3327.5	3305.2	2.4007	
			5147.6
3342.6	3320.3	2.4066	
			4982.1
3357.7	3335.4	2.4126	
			5045.1

Table A.1 Continued

3372.8	3350.5	2.4186	
			5148.7
3387.9	3365.6	2.4245	
			5068.2
3403.0	3380.7	2.4305	
			4624.8
3418.2	3395.8	2.4370	
			4505.1
3433.3	3411.0	2.4437	
			4383.2
3448.4	3426.0	2.4506	
			4189.1
3463.5	3441.2	2.4578	
			4416.4
3478.6	3456.3	2.4647	
			4187.1
3493.7	3471.4	2.4719	
			4283.8
3508.9	3486.6	2.4790	
			4543.0
3524.0	3501.7	2.4856	
			4534.0
3539.2	3516.8	2.4923	
			4222.5
3554.3	3531.9	2.4994	
			4656.7
3569.3	3547.0	2.5059	
			4283.6
3584.5	3562.1	2.5130	
			4316.6
3599.6	3577.2	2.5200	
			4087.0
3614.7	3592.3	2.5274	
			4347.2
3629.9	3607.5	2.5344	
			3731.9
3645.0	3622.6	2.5425	
			3826.1
3660.1	3637.8	2.5504	
			3920.9
3675.2	3652.9	2.5581	
			4205.0
3690.3	3667.9	2.5652	
			4829.7

Table A.1 Continued

3705.4	3683.1	2.5715	
			4359.1
3714.1	3691.8	2.5755	
			4497.3
3720.5	3698.2	2.5783	
			4411.6
3729.3	3706.9	2.5823	
			4329.1
3735.7	3713.3	2.5853	
			4343.2
3744.4	3722.0	2.5893	
			4721.4
3750.9	3728.5	2.5920	
			4346.5
3759.5	3737.1	2.5960	
			4311.2
3766.0	3743.6	2.5990	
			4608.1
3781.1	3758.8	2.6056	
			4175.9
3796.2	3773.9	2.6128	
			3897.4
3811.3	3788.9	2.6205	
			3941.3
3826.4	3804.1	2.6282	
			3806.0
3841.5	3819.2	2.6362	
			3804.3
3856.7	3834.3	2.6441	
			3804.7
3871.8	3849.4	2.6521	
			3875.3
3886.9	3864.5	2.6599	
			4022.9
3902.1	3879.7	2.6674	
			4046.3
3917.2	3894.8	2.6748	
			4140.6
3932.3	3909.8	2.6821	
			4011.3
3947.4	3925.0	2.6897	
			4041.6
3962.5	3940.1	2.6971	
			4007.0

Table A.1 Continued

3977.6	3955.2	2.7047	
			4167.7
3992.8	3970.3	2.7119	
			4135.8
4007.9	3985.4	2.7192	
			4154.9
4023.0	4000.5	2.7265	
			3926.3
4038.1	4015.6	2.7342	
			3235.4
4053.2	4030.7	2.7435	
			3385.9
4068.3	4045.8	2.7525	
			3330.0
4083.4	4060.9	2.7615	
			3109.9
4098.6	4076.0	2.7712	
			3013.8
4113.7	4091.2	2.7813	
			3092.1
4128.8	4106.3	2.7911	
			3068.6
4144.0	4121.4	2.8009	
			3132.4
4159.1	4136.5	2.8106	
			3142.2
4174.2	4151.6	2.8202	
			3209.3
4189.3	4166.7	2.8296	
			3067.8
4204.4	4181.8	2.8394	
			3108.2
4219.5	4196.9	2.8492	
			3222.8
4234.7	4212.1	2.8586	
			3254.3
4249.8	4227.2	2.8679	
			3241.2
4264.9	4242.3	2.8772	
			3213.0
4280.1	4257.4	2.8866	
			3183.0
4295.2	4272.5	2.8961	
			3342.9

Table A.1 Continued

4310.3	4287.6	2.9051	
			3326.7
4325.4	4302.7	2.9142	
			3461.5
4340.5	4317.8	2.9229	
			3630.8
4355.6	4332.9	2.9312	
			3673.2
4370.7	4348.0	2.9394	
			3756.6
4385.8	4363.1	2.9475	
			3652.7
4401.0	4378.2	2.9558	
			4078.8
4416.1	4393.4	2.9632	
			3891.5
4431.2	4408.5	2.9709	
			3664.9
4446.4	4423.6	2.9792	
			3565.3
4461.5	4438.7	2.9877	
			4008.8
4476.5	4453.7	2.9952	
			3805.8
4491.7	4468.8	3.0031	
			3997.6
4506.8	4483.9	3.0107	
			4057.2
4521.9	4499.0	3.0181	
			4104.5
4537.0	4514.2	3.0255	
			4048.1
4552.2	4529.3	3.0330	
			3919.1
4567.3	4544.4	3.0407	
			4169.6
4582.4	4559.5	3.0479	
			4297.3
4597.5	4574.6	3.0549	
			4605.1
4612.7	4589.7	3.0615	
			4874.0
4627.8	4604.9	3.0677	
			4142.9

Table A.1 Continued

4642.9	4619.9	3.0750	
			4395.9
4658.1	4635.1	3.0819	
			3656.6
4673.1	4650.1	3.0901	
			3467.8
4688.3	4665.2	3.0988	
			3582.3
4703.4	4680.3	3.1073	
			4188.9
4718.5	4695.4	3.1145	
			4298.5
4733.6	4710.6	3.1215	
			4329.9
4748.7	4725.7	3.1285	
			4391.5
4763.9	4740.8	3.1354	
			4671.9
4779.0	4755.9	3.1418	
			5041.9
4794.1	4770.9	3.1478	
			4809.8
4809.2	4786.0	3.1541	
			4202.3
4824.3	4801.1	3.1613	
			4411.6
4839.4	4816.2	3.1681	
			3815.9
4854.4	4831.2	3.1759	
			3768.3
4869.5	4846.3	3.1840	
			4179.0
4884.6	4861.4	3.1912	
			4496.6
4899.8	4876.4	3.1979	
			4211.1
4915.1	4891.7	3.2051	